UNIVERSITA' DEGLI STUDI DI PADOVA

Sede Amministrativa: Università degli Studi di Padova
Sede Consorziata: Università degli Studi di Genova

Dipartimento di Ingegneria delle Costruzioni, dell'Ambiente e del Territorio

SCUOLA DI DOTTORATO DI RICERCA IN SCIENZE
DELL'INGEGNERIA CIVILE E AMBIENTALE

INDIRIZZO IDRODINAMICA E MODELLISTICA AMBIENTALE

CICLO XX

An analytical non linear model for river meandering

Direttore della Scuola: Ch.mo Prof. Andrea Rinaldo
Supervisore: Ch.mo Prof. Giovanni Seminara

Dottorando: Giampiero Nobile

DATA CONSEGNA TESI
31 gennaio 2008

A mamma e papà

Contents

Riassunto

Nella presente tesi è stata sviluppata una teoria asintotica non lineare per l'idrodinamica e per la topografia di alvei meandriformi, in grado di descrivere perturbazioni del fondo di ampiezza finita e tenere in conto variazioni arbitrarie, seppur lente, della curvatura dell'asse del canale. Tale approccio ha permesso di formulare una teoria non lineare di stabilità planimetrica in grado di predire molti aspetti caratteristici dei processi di meandrizzazione e di estendere i risultati ottenuti dalle classiche teorie lineari. In particolare, in accordo con i precedenti risultati forniti dalla teoria debolmente non lineare ed in accordo con le evidenze di campo, il coefficiente di amplificazione del meandro mostra un picco per un particolare numero d'onda prossimo al valore risonante fornito dalla teoria lineare. Inoltre emerge un'altra caratteristica tipica delle onde non lineari: il numero d'onda selezionato dipende dall'ampiezza della perturbazione iniziale (per dati valori dei rilevanti parametri adimensionali) ed, in particolare, lunghezze d'onda maggiori sono associate ad ampiezze più grandi. I meandri risultano migrare prevalentemente verso valle, sebbene una migrazione verso monte risulti possibile per valori relativamente grandi del rapporto tra semilarghezza e profondità del canale, un risultato in accordo con il quadro fornito dalla teoria lineare. La celerità di migrazione diminuisce all'incrementare dell'ampiezza della perturbazione, nuovamente una caratteristica tipica delle onde non lineari, governata nel caso in questione dall'idrodinamica piuttosto che dalle non linearità geometriche. Il modello è infine validato confrontandone le previsioni con misure di campo rilevate sul fiume Cecina, recentemente soggetto ad un monitoraggio dettagliato dell'evoluzione planimetrica.

Abstract

We develop a non linear asymptotic theory of flow and bed topography in meandering channels able to describe finite amplitude perturbations of bottom topography and account for arbitrary, yet slow, variations of channel curvature. This approach then allows us to formulate a non linear bend instability theory, which predicts several characteristic features of the actual meandering process and extends results obtained by classical linear bend theories. In particular, in agreement with previous weakly non linear findings and consistently with field observations, the bend growth rate is found to peak at some value of the meander wavenumber, reminiscent of the resonant value of linear stability theory. Moreover, a feature typical of non linear waves arises: the selected wavenumber depends on the amplitude of the initial perturbation (for given values of the relevant dimensionless parameters) and, in particular, larger wavelengths are associated with larger amplitudes. Meanders are found to migrate preferentially downstream, though upstream migration is found possible for relatively large values of the aspect ratio of the channel, a finding in agreement with the picture provided by linear theory. Meanders are found to slow down as their amplitude increases, again a feature typical of non linear waves, driven in the present case by flow rather than geometric nonlinearities. The model is substantiated by comparing predictions with field observations obtained for a test case, a reach of a river recently subjected to detailed monitoring of its plan form evolution.

Acknowledgments

I wish to thank first of all and most of all my supervisor, Giovanni Seminara, who has been an enthusiastic source of inspiration and made this work richer in contents and in form. I am deeply grateful to Marco Colombini for his advices and his human support. Thanks are also due to Guido Zolezzi for his agreement to read this work.

A special thank to Michele who, with his constant and brilliant advices, hard working side by side with me, has shared successes and failures in the drafting of this thesis.

My sincere thanks go to Giovannino and Alessandro for making these years full of fun and pleasure.

I also thank Nunzio, Valeria and Nicoletta and all the people working in the Department of Environmental Engineering of the University of Genova.

Massimo Rinaldi is kindly acknowledged for providing the aerial pictures and the data of the Cecina River.

A special thank goes to Floriana who, in any moments of discouragement, has never stopped supporting me.

Finally, I am grateful to my great friends Gabriele, Alessio, Fabio, Simone, Fulvio and Tiziano for their crucial, unconditional and costant support.

This thesis is dedicated to my mother Milena and my father Noemio, who have constantly encouraged me and made all this possible.

Introduction

River meandering is a major topic in the field of morphodynamics. It has been the subject of extensive investigations in the recent past. The review paper of Seminara (2006), to which the reader is referred to for a broad overview of the subject, has outlined the main steps whereby progress has been made in this field.

Let us briefly recall them. The attention was initially focused on understanding the mechanism of meander formation starting from a straight channel configuration. Linear stability analyses (so called 'bend' theories) were employed, hence *linear models* were developed to determine flow and bed topography in weakly curved channels. The physical implications of the linearity assumption can be appreciated recalling the main ingredients of the process whereby the pattern of bed topography develops in a sinuous channel. The first feature is the establishment of a *centrifugal* secondary flow directed outwards close to the free surface and inward close to the bed: it arises because the lateral pressure gradient driven by the lateral slope of the free surface established in a bend is unable to provide the centripetal force required for fluid particles to move along purely longitudinal trajectories. If the bed is non erodible, a 'free vortex' effect prevails initially, longitudinal trajectories in the inner part of the bend being shorter than in the outer part. As a result, flow at the inner bend accelerates relative to the outer bend. This is a purely metric effect which is accounted for also in linear models. Proceeding downstream, a *net transfer of momentum towards the outer bend* is driven by the secondary flow (the outward transfer occurring in the upper layer prevailing on the inward transfer occurring in the lower layer), hence the thread of high velocity progressively moves from the inner to the outer bend. In the context of theories of stability where the basic flow is laterally uniform, this is a second order effect. The picture changes considerably when the bed is erodible. Under the latter conditions, secondary flow also affects the motion of grain particles: they deviate from the longitudinal direction, hence sediments are transported towards the inner bends where a sequence of so called *point bars* are built up while *pools* develop at the outer bends. The bar-pool pattern then drives a *topographical* component of the secondary flow and an additional contribution to sediment transport which further modifies the bed topography.

Linear theories are indeed able to generate this topographical effect, though the important role of the lateral transfer of momentum driven by the topographical secondary flow is again neglected, formally appearing still at second order.

The need to relax the linear constraint was recognized in the engineering literature, where a large effort was made to construct a rational framework, amenable to numerical treatment, in order to predict flow and bed topography in meandering channels with *finite curvature and arbitrary width variations*. These models serve the interests of river engineering, being fairly successful when applied to relatively short reaches of alluvial rivers and fairly short events.

However, a more general interest towards the construction of sound analytical non linear models arises in the context of the fundamental research on the subject.

In fact, linear theories display the occurrence of a resonance mechanism which controls the selection of the preferred wavelength for bend instability (Blondeaux & Seminara (1985)). Resonance is obviously damped by non linear effects, as shown by the weakly non linear theory of Seminara & Tubino (1992). No fully non linear theory has been proposed so far, though the role of non linearity is known to affect the flow field, hence the selection mechanism, considerably. In the present work, it is our principal objective to develop a non linear theory of bend instability, based on a non linear asymptotic solution of flow and bed topography in meandering rivers.

The availability of such a model is also potentially suitable to investigate a number of important processes observed in meander evolution, which still await to be understood. Though we will not discuss these processes in the present paper, however it may be of interest to outline the issues raised by field observations.

An inspection of the patterns of meandering rivers (e.g. figure 1) reveals that the river width, defined as the width of the stream free surface, undergoes typically spatial oscillations which display a distinct correlation with channel curvature. The river width may peak at bend apexes, reaching a minimum at inflection points (figure 1a) or vice versa (figure 1b). Note that this issue bears both a conceptual and a practical relevance. In fact, we know from the seminal contributions of Parker (1978a), Parker (1978b), that the average width of straight channels in equilibrium is ultimately controlled by requirements of bank stability. We also know that meandering does not alter such equilibrium in the mean.

Figure 1: Meander bends showing the dependence of river width on curvature and stage. (a) Maximum widths experienced at bend apexes (Eel River, California) (from Google Earth); (b) minimum widths at bend apexes, and local widening in straight reach (tributary of the Amazon River, Brazil) (from Google Earth).

Figure 2: A meander showing the formation of an island close to the bend apex (Finke River, Australia, courtesy of Aberdeen University, Geoff Pickup)

However, provided the river is free to erode and deposit, i.e. it is able to choose its own width, then curvature makes the stream unable to keep a constant width. Why? And to what extent channel widening at the bend apexes modifies the scour pattern typically observed at the outer banks, thus affecting the lateral migration of meanders?

A further reason of interest is related to a second observation: it is not uncommon to detect the formation of an island at bends of meandering channels (figure 2). The presence of the island then forces the stream to bifurcate into an outer and an inner branch.

In natural settings this is not a stable configuration: sooner or later, the stream will cut through and abandon the outer branch. The latter well known process is described as *chute cut-off* and occurs typically in wide bends with fairly large curvatures, high discharges, poorly cohesive unvegetated banks and high slope (Howard & Knutson (1984)). Though some recent numerical investigations (Jager (2003), and references therein) have attempted to model the latter process, it is not unfair to state that the occurrence of chute cutoff is a problem yet awaiting to be understood. The availability of an analytical non linear model of river meanders would allow to approach the latter problem. In fact, the process of widening is known (Repetto *et al.* (2002)) to promote the formation of steady central bars in straight channels: it is then natural to wonder whether the formation of bend islands is similarly related to a bottom instability driven by widening of a curved channel. The next step would then consist of modeling the tendency of the central bar to force the stream to bifurcate into an outer and an inner branch leading to the occurrence of chute cutoff.

A third motivation to develop an analytical approach to non linear meanders involving a sufficiently modest computational effort, is related to investigations of long term meander evolution, a topic which has attracted the attention of both geomorphologists (Sun *et al.* (1996)) and engineers (Camporeale & Ridolfi (2006)). For such applications numerical models are not appropriate tools as the computational effort they require would be prohibitive. Researchers have then been forced to employ analytical linear models for flow and bed topography, allowing only for geometric nonlinearities arising from plan form evolution. The present model removes the latter restriction.

This idea is pursued by resorting to the use of perturbation methods. We set up an appropriate perturbation expansion for the solution of the problem of morphodynamics, valid in the general case of rivers with arbitrary distributions of channel curvature, the only constraint being that flow and bottom topography must be 'slowly varying' in both longitudinal and lateral directions and channel curvature must be 'sufficiently small'. The former assumption requires the channel to be 'wide' with channel alignment varying on a longitudinal scale much larger than channel width, while the latter assumption is satisfied provided the radius of curvature of channel axis is large compared with channel width. Both conditions are typically met in actual rivers but, in spite of the popularity enjoyed by linear models, neither of them implies that perturbations of bottom topography are necessarily 'small'. Taking advantage of the slowly varying assumption, a suitable extension of the approach developed by Seminara & Solari (1998) to investigate bed deformations in constant curvature channels with constant width can be developed.

The latter approach allows for slow, yet finite, perturbations of flow and bed topography relative to a basic state consisting of a *locally and instantaneously* uniform flow, slowly varying in both the lateral and longitudinal directions. The only unknowns left for numerical computation are then flow depth, a slow function of longitudinal and lateral coordinates, and variation of the longitudinal free surface slope satisfying a strongly non linear differential equation subject to continuity constraints.

The present work is then organized as follows. In chapter 1 we formulate the 3D problem of flow in sinuous alluvial channels with a non cohesive bed. In the analysis, the direct effect of secondary flow on the transverse distribution of the main flow, leading to lateral transfer of longitudinal momentum is accounted for. This effect, which has been argued to be important by many authors (e.g. Nelson & Smith (1989), Imran & Parker (1999)), appears at the first order of approximation in the present scheme. Chapter 3 is then devoted to ascertaining the role of flow nonlinearity on 'bend instability theory' by coupling the morphodynamic model with a bank erosion law, expressing the dependence of erosion intensity on the flow field. We are then able to predict the wavelength selected by bend instability as well as the meander wave speed in a non linear context. In chapter 4 the model predictions are then tested by a direct application to a test case (a reach of the Cecina River, Italy) for which accurate data obtained by recent detailed monitoring are available. Predictions of both the equilibrium configuration and of the wavenumber selected in the meandering process do support the soundness of the present nonlinear approach.

Chapter 1

Non linear theory of slowly varying meanders: mathematical formulation

River morphodynamics deals with the turbulent free surface flow of a low concentration two phase mixture of water and sediment particles bounded by a granular medium consisting of still sediment particles packed at their highest concentration: in river morphodynamics one ultimately wishes to determine the configuration of the bed interface. In other words, the mathematical problem of river morphodynamics is essentially a *free boundary problem*. Let us formulate it.

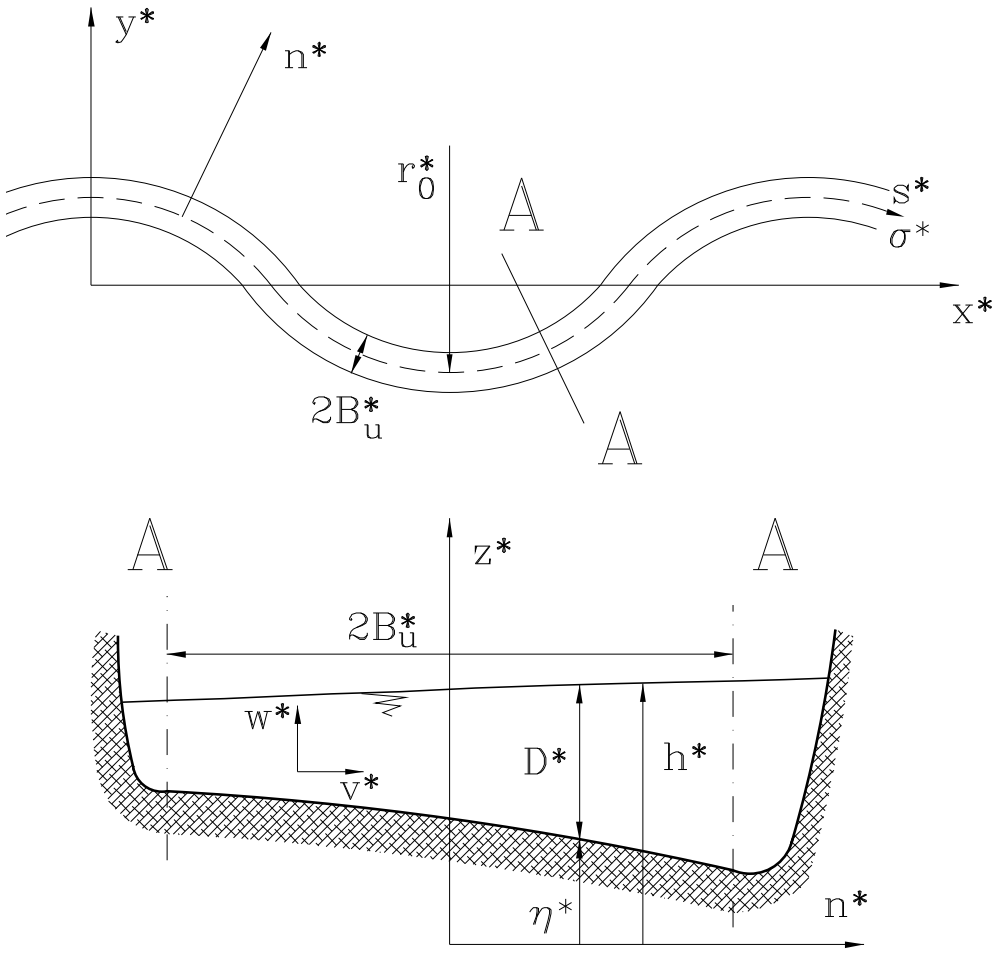

Figure 1.1: Sketch illustrating the meandering channel and notations

1.1 Formulation of the problem

Let us consider a sinuous alluvial channel with a non cohesive bed and refer it to the intrinsic coordinates sketched in figure 1.1 (s^*, n^* and z^*). Notice that s^* denotes a longitudinal coordinate defined along the channel axis, n^* is a transverse coordinate spanning the entire cross section and z^* is a nearly vertical coordinate orthogonal to the plane (s^*, n^*) and pointing upwards.

Furthermore let us assume:

$$\cos\ \theta_s \simeq 1 \tag{1.1}$$

where θ_s is the angle the tangent to the axis forms with a horizontal plane. Let us then consider the flow of a constant discharge Q^* in the meandering reach. In the case of channels with constant width, say $2B_u^*$, the appropriate scaling for the intrinsic coordinates, the local mean velocity averaged over turbulence $\mathbf{u}^*=(u^*, v^*, w^*)^T$, the flow depth D^*, the free surface elevation h^*, the eddy viscosity ν_T^* and the sediment flux per unit width $(q_s^*, q_n^*)^T$ reads:

$$(s^*, n^*) = B_u^*(s, n) \tag{1.2a}$$

$$(z^*, D^*, h^*) = D_u^*(z, D, F_u^2 h) \tag{1.2b}$$

$$\mathbf{u} = (u^*, v^*, w^*) = U_u^*(u, v, \frac{w}{\beta_u}) \tag{1.2c}$$

$$\nu_T^* = (\sqrt{C_{fu}} U_u^* D_u^*)\nu_T \tag{1.2d}$$

$$\mathbf{q} = (q_s^*, q_n^*) = \sqrt{(s_p - 1) g d^{*3}}(q_s, q_n) \tag{1.2e}$$

where a star denotes dimensional quantities. Moreover, s_p is the relative particle density ($= \rho_s/\rho$) with ρ and ρ_s water and particle density respectively, d^* is the particle diameter taken to be uniform. The index $_u$ refers to reference quantities consisting of the properties of uniform flow in a straight channel with the same flow discharge Q^* and the average channel slope S_u. In particular C_{fu} is the friction coefficient, β_u is the aspect ratio of the channel, F_u is the Froude number.

These parameters read:

$$\beta_u = \frac{B_u^*}{D_u^*} \tag{1.3a}$$

$$F_u^2 = \frac{U_u^{*2}}{gD_u^*} \tag{1.3b}$$

$$C_{fu} = 6 \ + \ 2.5 \ \ln \ \frac{D_u^*}{2.5 \ d^*} \tag{1.4}$$

having estimated the absolute bottom roughness as $2.5d^*$.
We then take advantage of the hydrostatic approximation which applies when the spatial scale of the relevant hydrodynamic processes largely exceeds the flow depth. The steady turbulent flow of water in a channel characterized by a slowly varying spatial distribution of channel curvature $\mathcal{C}^*(s)$, is then governed by the longitudinal and lateral components of Reynolds equations, along with the continuity equations for the fluid and solid phases. In dimensionless form, they read:

$$Nu_{,s} + \left[N\nu_0 \mathcal{C} + \frac{\partial}{\partial n} \right] v + w_{,z} = 0 \tag{1.5}$$

$$\begin{aligned} N\left(u^2\right)_{,s} + (uv)_{,n} + (uw)_{,z} + 2\nu_0 N\mathcal{C}uv = \\ -Nh_{,s} + N\beta_u C_{fu} + \beta_u \sqrt{C_{fu}} \left(\nu_T u_{,z}\right)_{,z} \end{aligned} \tag{1.6}$$

$$N\left(uv\right)_{,s}+\left(v^2\right)_{,n}+\left(vw\right)_{,z}+N\nu_0\mathcal{C}\left(v^2-u^2\right)= -h_{,n}+\beta_u\sqrt{C_{fu}}\left(\nu_T v_{,z}\right)_{,z} \tag{1.7}$$

$$P_{,z}=-\frac{1}{F_u^2} \tag{1.8}$$

$$Nq_{s,s}+q_{n,n}=-N\nu_0\mathcal{C}(s)q_n\ , \tag{1.9}$$

Moreover ν_0 is a curvature parameter, $\mathcal{C}(s)$ is dimensionless curvature and N is a metric coefficient of the orthogonal curvilinear coordinates:

$$\nu_0=\frac{B_u^*}{r_0^*} \tag{1.10a}$$

$$\mathcal{C}(s)=r_0^*\mathcal{C}^*(s) \tag{1.10b}$$

$$N=\frac{1}{1+\nu_0 n\mathcal{C}(s)} \tag{1.10c}$$

where r_0^* is some typical radius of curvature of the channel axis.
In the following we will assume the channel to be *wide* and *weakly curved*. Hence we write:

$$\beta_u\gg 1 \tag{1.11a}$$

$$\nu_0\ll 1 \tag{1.11b}$$

Note that the assumption (1.11a) allows one to ignore the role of the side walls, concentrating the attention on the central region of the flow. The latter does not interact with the side wall boundary layers at least under natural conditions due to the relatively low slope of natural banks. The assumption (1.11b) implies that the flow field is slightly perturbed with respect to that in a straight channel. The equations (1.5-1.9) must be solved subject to boundary conditions which may be written in the dimensionless form:

$$u = v = w = 0 \qquad (z = z_0) \tag{1.12}$$

$$P = u_{,z} = v_{,z} = w - h_s^{-1} u F_u^2 h_{,s} - v F_u^2 h_{,n} = 0 \quad (z = F_u^2 h) \tag{1.13}$$

$$\int_{z_0}^{F_u^2 h} v \, dz = q_n = 0 \qquad (n = \pm 1) \tag{1.14}$$

The equations (1.12) impose no slip at the conventional reference level z_0; the equations (1.13) impose the conditions of no stress at the free surface and the requirement that the latter must be a material surface; finally, the condition (1.14) imposes the constraint that both the water and the sediment flux must vanish at the banks.

Closure relationships are then needed for the sediment flux per unit width $\mathbf{q}$ and for the eddy viscosity ν_T. We now take advantage of the *slowly varying* character of flow field and bed topography to assume that the turbulent structure is in *quasi* equilibrium with the local conditions, i.e. it is only slightly perturbed by weak curvature effects. Hence we write:

$$\nu_T = \left(\frac{|\boldsymbol{\tau}^*|}{\rho C_{fu} U_u^{*2}} \right)^{1/2} D(n,s) \mathcal{N}(\xi) \tag{1.15}$$

where $\boldsymbol{\tau}^*$ is the local value of the bottom stress, $D(n,s)$ is the local dimensionless value of the flow depth and $\mathcal{N}(\xi)$ is the vertical distribution of the eddy viscosity in a plane uniform free surface flow. Note that ξ is a normalized vertical coordinate which reads:

$$\xi = \frac{z - [F_u^2 h(n,s) - D(n,s)]}{D(n,s)} \tag{1.16}$$

Hence, ξ maps the actual cross section into the rectangle:

$$\xi_0 \leq \xi \leq 1 \qquad -1 \leq n \leq 1 \tag{1.17}$$

with ξ_0 normalized reference level, a weakly dependent function of the longitudinal and lateral coordinates, here assumed to be constant and equal to:

$$\xi_0 \simeq \exp(-\frac{k}{\sqrt{C_{fu}}} - 0.777) \tag{1.18}$$

with $k = 0.41$ the von Karman's constant. The distribution $\mathcal{N}(\xi)$ is taken to coincide with the classical parabolic distribution characteristic of uniform flows corrected by Dean's wake function (1974):

$$\mathcal{N}(\xi) = \frac{k\xi(1-\xi)}{1 + 2A\xi^2 + 3B\xi^3}, \qquad A = 1.84 \qquad B = -1.56 \tag{1.19}$$

The closure for the sediment flux per unit width $\mathbf{q}$ derives from a well established approach of semi empirical nature. In uniform open channel flow over a homogeneous non cohesive plane bed no significant sediment transport occurs below some *critical value* θ_c of a dimensionless form θ of the average shear stress $\boldsymbol{\tau}^*$ acting on the bed, depending on the *particle Reynolds number* R_p. With ν_f kinematic viscosity of the fluid, the Shields stress (Shields (1936)) and R_p read:

$$\theta = \frac{|\boldsymbol{\tau}^*|}{(\varrho_s - \varrho)\mathrm{g}d^*} \tag{1.20a}$$

$$R_p = \frac{\sqrt{(s_p - 1)\mathrm{g}d^{*3}}}{\nu_f} \tag{1.20b}$$

For values of θ exceeding θ_c but lower than a second threshold value θ_s, particles are transported as bedload with a distinct dynamics driven by, but different from, the dynamics of fluid particles. In the following, sediment transport will be assumed to occur dominantly as bedload and its direction deviates from the direction of bottom stress because of the effect of gravity. Under these conditions, on pure dimensional ground, the average bedload flux per unit width on a weakly sloping bottom may be given the general form:

$$\mathbf{q} = \Phi(\theta - \theta_c; R_p)\left(\frac{\boldsymbol{\tau}^*}{|\boldsymbol{\tau}^*|} + \mathbf{G}\cdot\nabla_h\eta\right) \tag{1.21}$$

where η $(= F_u^2 h - D)$ is the dimensionless bed elevation.
Furthermore ∇_h is $(h_s^{-1}\partial/\partial s, \partial/\partial n)$, Φ is a monotonically increasing function of the excess Shields stress $(\theta - \theta_c)$ for given particle Reynolds number R_p, while $\mathbf{G}$ is a (2 x 2) matrix dependent on θ, θ_c and the angle of repose of the sediment. The function Φ can be estimated through well known empirical of semi empirical relationships: in the following we use the relation proposed by Parker (1990).

Moreover we only account for the prevailing lateral effect of gravity on the particle motion and write (Parker (1984)):

$$G_{ss} = G_{sn} = G_{ns} = 0 \tag{1.22a}$$

$$G_{nn} = -R \tag{1.22b}$$

with R a typically small parameter which reads:

$$R = \frac{r_c}{\beta_u \sqrt{\theta}} \tag{1.23}$$

r_c being an empirical constant ranging about 0.56 (Talmon *et al.* (1995)). The reader should note that (1.21) fails close to sharp fronts (for the case of *arbitrarily sloping beds*, see Kovacs & Parker (1994) and Seminara *et al.* (2003)).

At last, the problem formulated above is subject to two integral constraints stipulating that flow and sediment supply must be constant at any cross section, hence:

$$\int_{-1}^{+1} D \int_{\xi_0}^{+1} u(\xi, n, s)\, d\xi\, dn = constant \tag{1.24}$$

$$\int_{-1}^{+1} \Phi\left[\theta(n, s)\right]\, dn = constant \tag{1.25}$$

1.2 Solution for channels with slowly varying distribution of curvature

Let us consider a sinuous channel characterized by a *slowly varying* distribution of curvature of the channel axis. Flow and bottom topography are then assumed to be *slowly varying* in both longitudinal and lateral directions. It's important to note that the above assumptions do not imply that perturbations of flow and bottom topography are necessarily small. It is then appropriate to rescale the longitudinal coordinate s introducing a *slowly varying coordinate* σ as follows:

$$\sigma = \frac{s^*}{r_0^*} = \nu_0 s \tag{1.26}$$

It is now useful to employ the new system of coordinates (σ, n, ξ). Using the relations (1.26) and (1.16) the chain rule gives:

$$(s, n, z) \qquad \rightarrow \qquad (\sigma, n, \xi)$$

$$\begin{cases} \frac{\partial}{\partial s} & \rightarrow & \nu_0 \frac{\partial}{\partial \sigma} + \nu_0 \left[\frac{(1-\xi) D_{,\sigma} - F_u^2 h_{,\sigma}}{D} \right] \frac{\partial}{\partial \xi} \\ \frac{\partial}{\partial n} & \rightarrow & \frac{\partial}{\partial n} + \left[\frac{(1-\xi) D_{,n} - F_u^2 h_{,n}}{D} \right] \frac{\partial}{\partial \xi} \\ \frac{\partial}{\partial z} & \rightarrow & \frac{1}{D} \frac{\partial}{\partial \xi} \end{cases} \tag{1.27}$$

and the system (1.5 - 1.9) can be rewritten in the form:

$$
\begin{aligned}
N\nu_0 u_{,\sigma} + N\nu_0 \left[\frac{(1-\xi)D_{,\sigma} - F_u^2 h_{,\sigma}}{D}\right] u_{,\xi} + v_{,n} \\
+ \left[\frac{(1-\xi)D_{,n} - F_u^2 h_{,n}}{D}\right] v_{,\xi} \\
+ \nu_0 N\mathcal{C} v \\
= -\frac{w_{,\xi}}{D}
\end{aligned}
\tag{1.28}
$$

$$
\begin{aligned}
N\nu_0 (u^2)_{,\sigma} + N\nu_0 \left[\frac{(1-\xi)D_{,\sigma} - F_u^2 h_{,\sigma}}{D}\right] (u^2)_{,\xi} + (uv)_{,n} \\
+ \left[\frac{(1-\xi)D_{,n} - F_u^2 h_{,n}}{D}\right] (uv)_{,\xi} + \frac{(uw)_{,\xi}}{D} \\
+ 2\nu_0 N\mathcal{C} uv \\
= \\
-N\nu_0 h_{,\sigma} + N\beta_u C_{fu} + \frac{\beta_u \sqrt{C_{fu}}}{D^2} (\nu_T u_{,\xi})_{,\xi}
\end{aligned}
\tag{1.29}
$$

$$
\begin{aligned}
N\nu_0 (uv)_{,\sigma} + N\nu_0 \left[\frac{(1-\xi)D_{,\sigma} - F_u^2 h_{,\sigma}}{D}\right] (uv)_{,\xi} + (v^2)_{,n} \\
+ \left[\frac{(1-\xi)D_{,n} - F_u^2 h_{,n}}{D}\right] (v^2)_{,\xi} + \frac{(vw)_{,\xi}}{D} \\
+ \nu_0 N\mathcal{C}(v^2 - u^2) \\
= \\
-h_{,n} + \frac{\beta_u \sqrt{C_{fu}}}{D^2} (\nu_T v_{,\xi})_{,\xi}
\end{aligned}
\tag{1.30}
$$

$$
\frac{P_{,\xi}}{D} = -\frac{1}{F_u^2} \tag{1.31}
$$

$$
N\nu_0 q_{\sigma,\sigma} + q_{n,n} + N\mathcal{C}\nu_0 q_n = 0 \tag{1.32}
$$

To simplify further the system (1.28-1.32) we can use the continuity equation for the liquid phase (1.28) and perform simple algebra, to obtain:

$$\begin{aligned} N\nu_0 uu_{,\sigma} + N\nu_0 \left[\frac{(1-\xi)D_{,\sigma} - F_u^2 h_{,\sigma}}{D}\right] uu_{,\xi} + vu_{,n} \\ + \left[\frac{(1-\xi)D_{,n} - F_u^2 h_{,n}}{D}\right] vu_{,\xi} + \frac{wu_{,\xi}}{D} \\ + N\nu_0 \mathcal{C} uv \\ = \\ -N\nu_o h_{,\sigma} + N\beta_u C_{fu} + \frac{\beta_u\sqrt{C_{fu}}}{D^2}(\nu_T u_{,\xi})_{,\xi} \end{aligned} \tag{1.33}$$

$$\begin{aligned} N\nu_0 uv_{,\sigma} + N\nu_0 \left[\frac{(1-\xi)D_{,\sigma} - F_u^2 h_{,\sigma}}{D}\right] uv_{,\xi} + vv_{,n} \\ + \left[\frac{(1-\xi)D_{,n} - F_u^2 h_{,n}}{D}\right] vv_{,\xi} + \frac{wv_{,\xi}}{D} \\ - N\nu_0 \mathcal{C} u^2 \\ = \\ -h_{,n} + \frac{\beta_u\sqrt{C_{fu}}}{D^2}(\nu_T v_{,\xi})_{,\xi} \end{aligned} \tag{1.34}$$

The differential problem (1.33-1.34) will be solved with the following boundary conditions:

$$u = v = w = 0 \qquad (\xi = \xi_0) \tag{1.35}$$

$$P = u_{,\xi} = v_{,\xi} = 0 \quad (\xi = 1) \tag{1.36}$$

$$w - \nu_0 N u F_u^2 h_{,\sigma} - v F_u^2 h_{,n} = 0 \quad (\xi = 1) \tag{1.37}$$

$$\int_{\xi_0}^{1} v \; d\xi = q_n = 0 \qquad (n = \pm 1) \tag{1.38}$$

Integrating the continuity equation of the liquid phase (1.28) in the vertical direction we get a relation for the vertical component of velocity in the form:

$$\begin{aligned} w = -N\nu_0 \frac{\partial}{\partial \sigma}\left[D \int_{\xi_0}^{\xi} u \; d\xi\right] - \frac{\partial}{\partial n}\left[D \int_{\xi_0}^{\xi} v \; d\xi\right] \\ -\nu_0 N \mathcal{C} D \left[\int_{\xi_0}^{\xi} v \; d\xi\right] - N\nu_0 U \left[(1-\xi) D_{,\sigma} - F_u^2 h_{,\sigma}\right] \\ -V \left[(1-\xi) D_{,n} - F_u^2 h_{,n}\right] \end{aligned} \tag{1.39}$$

Evaluating (1.39) at the free surface ($\xi = 1$) and using the kinematic boundary condition (1.37) we obtain the *depth-averaged form of the continuity equation for the liquid phase*:

$$N\nu_0 \frac{\partial}{\partial \sigma}\left[D \int_{\xi_0}^{1} u \; d\xi\right] + \frac{\partial}{\partial n}\left[D \int_{\xi_0}^{1} v \; d\xi\right] + \nu_0 N \mathcal{C}\left[D \int_{\xi_0}^{1} v \; d\xi\right] = 0 \tag{1.40}$$

Substituting from (1.39) and (1.28) into (1.29-1.30), dividing by $\beta_u\sqrt{C_{fu}}$ we finally derive an integro-differential system, which reads:

$$\begin{aligned}\delta N u u_{,\sigma} + \frac{1}{\beta_u\sqrt{C_{fu}}} v u_{,n} - \delta \frac{N u_{,\xi}}{D}\frac{\partial}{\partial\sigma}\left[D\int_{\xi_0}^{\xi} u\, d\xi\right] \\ - \frac{1}{\beta_u\sqrt{C_{fu}}}\frac{u_{,\xi}}{D}\frac{\partial}{\partial n}\left[D\int_{\xi_0}^{\xi} v\, d\xi\right] - \delta\mathcal{C}N u_{,\xi}\int_{\xi_0}^{\xi} v\, d\xi \\ + \delta\mathcal{C}N u v \\ = \\ -\delta N h_{,\sigma} + N\sqrt{C_{fu}} + \frac{1}{D^2}\left(\nu_T u_{,\xi}\right)_{,\xi}\end{aligned} \tag{1.42}$$

$$\begin{aligned}\delta N u v_{,\sigma} + \frac{1}{\beta_u\sqrt{C_{fu}}} v v_{,n} - \delta \frac{N v_{,\xi}}{D}\frac{\partial}{\partial\sigma}\left[D\int_{\xi_0}^{\xi} u\, d\xi\right] \\ - \frac{1}{\beta_u\sqrt{C_{fu}}}\frac{v_{,\xi}}{D}\frac{\partial}{\partial n}\left[D\int_{\xi_0}^{\xi} v\, d\xi\right] - \delta\mathcal{C}N v_{,\xi}\int_{\xi_0}^{\xi} v\, d\xi \\ - \delta\mathcal{C}N u^2 \\ = \\ -\frac{h_{,n}}{\beta_u\sqrt{C_{fu}}} + \frac{1}{D^2}\left(\nu_T v_{,\xi}\right)_{,\xi}\end{aligned} \tag{1.43}$$

$$\delta N\frac{\partial}{\partial\sigma}\left[D\int_{\xi_0}^{1} u\, d\xi\right] + \frac{1}{\beta_u\sqrt{C_{fu}}}\frac{\partial}{\partial n}\left[D\int_{\xi_0}^{1} v\, d\xi\right] + \delta N\mathcal{C}\left[D\int_{\xi_0}^{1} v\, d\xi\right] = 0 \tag{1.44}$$

$$N\delta q_{\sigma,\sigma} + \frac{1}{\beta_u\sqrt{C_{fu}}} q_{n,n} + \delta N\mathcal{C} q_n = 0 \tag{1.45}$$

where δ is the small parameter:

$$\delta = \frac{\nu_0}{\beta_u\sqrt{C_{fu}}}$$

We may then expand the unknown functions in a neighborhood of the solution for uniform flow in a *straight channel with an unknown shape of the cross section and an unknown slope of the free surface*, the latters described by a slowly varying function $D_0(n,\sigma)$ of both the longitudinal and lateral coordinates and a slowly varying function $h_{00,\sigma}(\sigma)$ of the longitudinal coordinate only. Hence:

$$\begin{aligned}(u,v,w,D) = [u_0(\xi,n,\sigma),0,0,D_0(n,\sigma)] + \\ + \sum_{m=1}^{\infty}(u_m,v_m,w_m,D_m)\,(\delta)^m\end{aligned} \tag{1.46}$$

Note that, in order to account for the small variations of the longitudinal free surface slope associated with channel curvature, the free surface elevation must have distinct contributions, according to the following expansion:

$$h(\sigma,n) = \frac{h_{00}(\sigma)}{\delta} + \delta h_1(\sigma,n) + \sum_{m=1}^{\infty}\left[\left(\frac{h_{0m}}{\delta} + \delta h_{m+1}(\sigma,n)\right)\delta^m\right] \tag{1.47}$$

We may now substitute from (1.46, 1.47) into (1.42 - 1.45) and equate likewise powers of δ, to obtain a sequence of differential problems, to be solved in terms of the unknown functions D and $h_{,\sigma}$.

1.3 Leading order solution: uniform flow in a straight channel with unknown cross-sectional shape and unknown free surface slope

At the leading order of approximation $O(\delta^0)$, the longitudinal component of the Reynolds equations (1.42) reduces to a uniform balance between gravity and friction in a channel with unknown distribution of flow depth $D_0(n,\sigma)$ and free surface slope -$h_{00,\sigma}(\sigma)$ with relative boundary condition (1.35 - 1.36):

$$\begin{cases} \frac{1}{D_0^2}\left[\nu_{T0}u_{0,\xi}\right]_{,\xi} &= h_{00,\sigma} - \sqrt{C_{fu}} \\ u_{0,\xi}\mid_1 = 0 \\ u_0\mid_{\xi_0} = 0 \end{cases} \tag{1.48}$$

After setting:

$$u_0 = D_0^{1/2}(n,\sigma)R_0^{1/2}(\sigma)F_0(\xi,n,\sigma) \tag{1.49}$$

$$\nu_{T0} = D_0^{3/2}(n,\sigma)R_0^{1/2}(\sigma)\mathcal{N}(\xi) \tag{1.50}$$

with $R_0 = 1 - h_{00,\sigma}/\sqrt{C_{fu}}$, one finds:

$$\begin{cases} \left[\mathcal{N}(\xi)F_{0,\xi}\right]_{,\xi} &= -\sqrt{C_{fu}} \\ F_{0,\xi}\mid_1 = 0 \\ F_0\mid_{\xi_0} = 0 \end{cases} \tag{1.51}$$

The solution for F_0 is the classical logarithmic distribution corrected by a wake function:

$$F_0(\xi) = \frac{\sqrt{C_{fu}}}{k}\left[\ln\frac{\xi}{\xi_0} + A(\xi^2 - \xi_0^2) + B(\xi^3 - \xi_0^3)\right] \tag{1.52}$$

where ξ_0 is the normalized conventional reference level, here assumed to be constant. Also note that the function F_0 satisfies the following integral constraint:

$$\int_{\xi_0}^{1} F_0 \, d\xi = 1 - \xi_0 \tag{1.53}$$

1.4 First order: secondary flow induced by curvature and longitudinal variations

At first order $O(\delta^1)$, the transverse component of the Reynolds equations (1.43) reduces to a balance between lateral component of gravity, centripetal inertia and lateral friction in a channel with unknown, yet slowly varying, distributions of flow depth $D_0(n,\sigma)$ and free surface slope (-$h_{00,\sigma}$) as well as given slowly varying distribution of channel curvature $c(\sigma)$. We find:

$$\begin{cases} \frac{1}{D_0^2}\left[\nu_{T0} v_{1,\xi}\right]_{,\xi} &= \frac{h_{1,n}}{\beta_u\sqrt{C_{fu}}} - u_0^2\mathcal{C} \\ v_1|_{\xi_0} = 0 \\ v_{1,\xi}|_1 = 0 \end{cases} \tag{1.54}$$

We then set:

$$v_1 = D_0^{3/2}(n,\sigma) R_0^{1/2}(\sigma) G_1(\xi,n,\sigma)\mathcal{C}(\sigma) \tag{1.55}$$

$$\frac{\partial h_1}{\partial n} = \beta_u\sqrt{C_{fu}} D_0(n,\sigma) R_0(\sigma)\mathcal{C}(\sigma) a_1(n,\sigma) \tag{1.56}$$

where G_1 is the solution of the following ordinary differential problem:

$$\begin{cases} \left[\mathcal{N}(\xi) G_{1,\xi}\right]_{,\xi} &= a_1(n,\sigma) - F_0^2(\xi) \\ G_1|_{\xi_0} = 0 \\ G_{1,\xi}|_1 = 0 \end{cases} \tag{1.57}$$

Let us write the solution for G_1 in the form:

$$G_1 = a_1(n,\sigma)G_{11}(\xi) + G_{12}(\xi) \tag{1.58}$$

where:

$$G_{1j} = g_j(\xi) - \frac{g_j'|_{\xi=1}}{g_0'|_{\xi=1}} g_0(\xi) \qquad (j = 1,2) \tag{1.59}$$

and g_j $(j = 0,1,2)$ are solutions of ordinary differential systems:

$$\begin{cases} [\mathcal{N}(\xi) g_{j,\,\xi}]_{,\xi} &= \delta_i \\ g_j|_{\xi_0} = 0 \\ g_{j,\,\xi}|_{\xi_0} = 1 \end{cases} \tag{1.60}$$

where:

$$\delta_0 = 0 \qquad \delta_1 = 1 \qquad \delta_2 = -F_0^2(\xi,\sigma,n) \tag{1.61}$$

The solutions for the functions g_j are obtained in an analytical form, as shown in Appendix E and depend only on the normalized conventional reference level ξ_0. Also note that a relation between the functions F_0 (1.51) and G_1 (1.57) can be easily found in the form:

$$F_0 = -\sqrt{C_{fu}} G_{11} \tag{1.62}$$

We may then proceed to determine the function $a_1(n,\sigma)$ firstly expressing the *depth-averaged form of the continuity equation for the liquid phase* (1.40) at $O(\delta)$:

$$\frac{\partial}{\partial\sigma}\left[D_0\int_{\xi_0}^{1} u_0\ d\xi\right]+\frac{1}{\beta_u\sqrt{C_{fu}}}\frac{\partial}{\partial n}\left[D_0\int_{\xi_0}^{1} v_1\ d\xi\right]=0 \tag{1.63}$$

and secondly integrating the latter over the cross section, with the use of the boundary condition (1.38) written at $O(\delta)$:

$$\int_{\xi_0}^{1} v_1\ d\xi=0 \qquad (n=\pm1) \tag{1.64}$$

to obtain:

$$\frac{\partial}{\partial\sigma}\int_{1}^{n}\left[D_0\int_{\xi_0}^{1} u_0\ d\xi\right]dn+\frac{1}{\beta_u\sqrt{C_{fu}}}\left[D_0\int_{\xi_0}^{1} v_1\ d\xi\right]=0 \tag{1.65}$$

Substituting (1.49) and (1.55) into the latter equation we find:

$$a_1(n,\sigma)=a_{10}-\frac{a_{11}}{\mathcal{C}D_0^{5/2}R_0^{1/2}}\frac{\partial}{\partial\sigma}\left(\int_{-1}^{n} D_0^{3/2}R_0^{1/2}I_{F_0}dn\right) \tag{1.66}$$

where:

$$a_{10}=-\frac{I_{G_{12}}}{I_{G_{11}}} \qquad a_{11}=\frac{\beta_u\sqrt{C_{fu}}}{I_{G_{11}}} \tag{1.67}$$

and I_f is the integral ($\int_{\xi_0}^{1} f d\xi$).
It's important to note that the coefficients (1.67) are analytical and depend on the normalized conventional reference level ξ_0 only.

Furthermore we observe that the secondary flow expressed in (1.55) can be split in two different contributions: the former v_{10} is correlated to the curvature of the channel axis and has a vanishing depth average, the latter v_{11} is due to the longitudinal variations of the flow field. This can be easily shown rearranging the equation (1.55) using the relation (1.66):

$$v_1 = v_{10} + v_{11} \tag{1.68}$$

$$v_{10} = D_0^{3/2} R_0^{1/2} \mathcal{C} \left(a_{10} G_{11} + G_{12} \right) \tag{1.69}$$

$$v_{11} = -\frac{\beta_u \sqrt{C_{fu}}}{D_0} F_0 \frac{\partial}{\partial \sigma} \left(\int_{-1}^{n} D_0 U_0 dn \right) \tag{1.70}$$

where:

$$U_0 = \frac{1}{1-\xi_0} \int_{\xi_0}^{1} u_0 \, d\xi = \frac{1}{1-\xi_0} I_{u_0} \tag{1.71}$$

is the depth average of the longitudinal velocity.
Let us then calculate the depth average of the transversal velocity:

$$V_1 = \frac{1}{1-\xi_0} \int_{\xi_0}^{1} v_1 d\xi = \overline{v_{10}} + \overline{v_{11}} \tag{1.72}$$

Using the equations (1.53), (1.67) and (1.72) we can readily show that:

$$\overline{v_{10}} = 0 \tag{1.73}$$

$$\overline{v_{11}} = -\frac{\beta_u \sqrt{C_{fu}}}{D_0} \frac{\partial}{\partial \sigma} \left(\int_{-1}^{n} D_0 U_0 dn \right) = V_1 \tag{1.74}$$

Hence, comparing (1.74) with (1.70) and using (1.68) we can write:

$$v_1(\sigma, n, \xi) = v_{10}(\sigma, n, \xi) + F_0(\xi) V_1(\sigma, n) \tag{1.75}$$

Let us finally come to the sediment continuity equation. Firstly, the closure relationships (1.21 - 1.23) for the bedload flux $\mathbf{q}$, rewritten in terms of the rescaled coordinates, allow us to write:

$$q_\sigma = \Phi \tag{1.76}$$

$$q_n = q_\sigma \left[\frac{\tau_n}{|\boldsymbol{\tau}|} - \frac{R\sqrt{\theta_u}}{\sqrt{\theta}} (F_u^2 h - D)_{,n} \right] \tag{1.77}$$

The lateral component of the bedload flux q_n can also be written in the form:

$$q_n = q_\sigma \left[\frac{v_{,\xi}}{u_{,\xi}}|_{\xi_0} - \delta \frac{R'\sqrt{\theta_u}}{\sqrt{\theta}} (F_u^2 h - D)_{,n} \right] \tag{1.78}$$

Here, we have introduced the $O(1)$ parameter $R' = \frac{R}{\delta}$: in fact, the slowly varying character of the lateral distribution of flow depth is due to the quantity R being $O(\delta)$.

Expanding the equation (1.78) with the use of (1.76) at $O(\delta)$ we find:

$$q_{n_1} = q_{\sigma_0}\left[\frac{v_{1,\xi}}{u_{0,\xi}}|_{\xi_0} + \frac{R' D_{0,n}}{\sqrt{D_0 R_0}}\right] \tag{1.79}$$

having set $\theta_0 = \theta_u D_o R_0$.
Let us finally come to the sediment continuity equation (1.45) integrated over the cross section with the use of the boundary condition (1.38). At $O(\delta)$ we find:

$$\frac{\partial}{\partial\sigma}\int_1^n q_{\sigma_0}\, dn + \frac{1}{\beta_u\sqrt{C_{fu}}} q_{n_1} = 0 \tag{1.80}$$

Finally, substituting from (1.79) into (1.80), the latter equation can be reduced to the following non linear partial integro-differential equation for the unknown functions $D_0(n,\sigma)$ and $h_{00,\sigma}(\sigma)$:

$$D_{0,n} = -\frac{\sqrt{D_0 R_0}}{R'}\left[\frac{v_{1,\xi}}{u_{0,\xi}}|_{\xi_0} + \frac{\beta_u\sqrt{C_{fu}}}{q_{\sigma_0}}\frac{\partial}{\partial\sigma}\int_{-1}^n q_{\sigma_0}\, dn\right] \tag{1.81}$$

This equation has to be solved subject to the integral constraints (1.24) and (1.25) evaluated at the order $O(\delta^0)$:

$$\int_{-1}^{+1} D_0^{3/2} I_{F_0}\, dn = 2(1-\xi_u) \tag{1.82}$$

$$\int_{-1}^{+1} q_{\sigma_0}\, dn = 2\Phi_u \tag{1.83}$$

These constraints can be reinforced by choosing appropriately the quantity $h_{00,\sigma}$ and the boundary condition for $D_0(n,\sigma)$ at one of the banks. For a complete description of the numerical procedure employed to solve the latter equation the reader is referred to Appendix C.

1.5 First order: correction of longitudinal motion due to convective effects

Our leading-order solution for the longitudinal velocity was simply a uniform flow slowly varying in the longitudinal and lateral directions and characterized by a free surface slope corrected with respect to the average intrinsic slope. However, because of the effects of curvature and flow variations, longitudinal momentum is transported outward close to the free surface and inward close to the bed. As a result, a perturbation of longitudinal velocity is then produced. In fact, by perturbing (1.15) we obtain:

$$\nu_T = \nu_{T0}\left[1 + \delta\left(\frac{D_1}{D_0} + \frac{u_{1,\xi}}{u_{0,\xi}}|_{\xi_0}\right) + O(\delta^2)\right] \tag{1.84}$$

We refer to Appendix A.1 for a complete derivation of (1.84).
At first order $O(\delta^1)$, in the Reynolds equation (1.42) contributions due to lateral, vertical and longitudinal transport of momentum appear. Further effects are due to metric transverse variation of curvature, topographic effects, perturbation of flow depth and longitudinal free surface slope. After setting:

$$\frac{\nu_{T1}}{\nu_{T0}} = \frac{D_1}{D_0} + \frac{u_{1,\xi}}{u_{0,\xi}}|_{\xi_0} \tag{1.85}$$

and using the longitudinal differential problem at previous order (1.48) we find:

$$\left\{\begin{array}{rcl}
\frac{1}{D_0^2}\left[\nu_{T0}u_{1,\xi}\right]_{,\xi} & = & -\sqrt{C_{fu}}R_0\left(\frac{D_1}{D_0}-\frac{u_{1,\xi}}{u_{0,\xi}}|_{\xi_0}\right)+n\mathcal{C}R_0\beta_u C_{fu}+h_{01,\sigma} \\
 & & +u_0u_{0,\sigma} \\
 & & \frac{1}{\beta_u\sqrt{C_{fu}}}v_1u_{0,n} \\
 & & -\frac{u_{0,\xi}}{D_0}\frac{\partial}{\partial\sigma}\left[D_0\int_{-1}^{n}u_0\ dn\right] \\
 & & -\frac{1}{\beta_u\sqrt{C_{fu}}}\frac{u_{0,\xi}}{D_0}\frac{\partial}{\partial n}\left[D_0\int_{-1}^{n}v_1\ dn\right] \\
u_1|_{\xi_0}=0 & & \\
u_{1,\xi}|_1=0 & &
\end{array}\right. \tag{1.86}$$

Hence, defining:

$$u_1 = D_0^{1/2}(n,\sigma)R_0^{1/2}(\sigma)F_1(\xi,n,\sigma) \tag{1.87}$$

and using equations (1.49), (1.50), (1.55), some algebra allows us to derive the problem for F_1, which reads:

$$\left\{\begin{array}{rcl}
\left[\mathcal{N}(\xi)F_{1,\xi}\right]_{,\xi} & = & R_1 \\
 & & +\frac{1}{2}R_2\ \left[F_0^2\right] \\
 & & +\frac{1}{2}R_3\ \left[F_0\mathcal{C}G_1\right] \\
 & & -\frac{3}{2}R_{2b}\ \left[F_{0,\xi}\int_{\xi_0}^{\xi}F_0\ d\xi\right] \\
 & & -\frac{5}{2}R_3\ \left[F_{0,\xi}\int_{\xi_0}^{\xi}\mathcal{C}G_1\ d\xi\right] \\
F_1|_{\xi_0}=0 & & \\
F_{1,\xi}|_1=0 & &
\end{array}\right. \tag{1.88}$$

where:

$$\begin{array}{lcl} R_1 & = & -\sqrt{C_{fu}}R_0\left(\frac{D_1}{D_0}-\frac{u_{1,\xi}}{u_{0,\xi}}|_{\xi_0}\right)+n\mathcal{C}R_0\beta_u C_{fu}+\frac{h_{01,\sigma}}{R_0} \\ R_2 & = & D_{0,\sigma}+\frac{D_0}{R_0}R_{0,\sigma} \\ R_{2b} & = & D_{0,\sigma}+\frac{D_0}{3R_0}R_{0,\sigma} \\ R_3 & = & \frac{1}{\beta_u\sqrt{C_{fu}}}D_0D_{0,n} \end{array} \tag{1.89}$$

The solution for F_1 can be given the form:

$$F_1 = R_1F_{11}-\frac{1}{2}R_2F_{12}-\frac{1}{2}R_3F_{13}-\frac{3}{2}R_{2b}F_{14}-\frac{5}{2}R_3F_{15} \tag{1.90}$$

where:

$$F_{1j} = f_j(\xi)-\frac{f_j'|_{\xi=1}}{f_0'|_{\xi=1}}f_0(\xi) \qquad (j=1,5) \tag{1.91}$$

and f_j $(j=0,1,2,3,4,5)$ are solutions of the following ordinary differential systems:

$$\left\{\begin{array}{ll} \left[\mathcal{N}(\xi)f_{j,\ \xi}\right]_{,\xi} & = \ \delta_i \\ f_j|_{\xi_0}=0 & \\ f_{j,\ \xi}|_{\xi_0}=1 & \end{array}\right. \tag{1.92}$$

where:

$$\begin{aligned}
\delta_0 &= 0 \\
\delta_1 &= 1 \\
\delta_2 &= -F_0^2 \\
\delta_3 &= -F_0 \mathcal{C} G_1 \\
\delta_4 &= F_{0,\xi} \int_{\xi_0}^{\xi} F_0 \, d\xi \\
\delta_5 &= F_{0,\xi} \int_{\xi_0}^{\xi} \mathcal{C} G_1 \, d\xi
\end{aligned} \tag{1.93}$$

We note from (1.60) that $f_0 = g_0$, $f_1 = g_1$, $f_2 = g_2$.
It can be easily shown that previous forcing terms come from the following contributions due to convective effects and coordinate transformation (refer to 1.42 and 1.43). In particular:

$$\begin{aligned}
-F_0^2 \quad &\rightarrow \quad N u u_{,\sigma} \\
-F_0 \mathcal{C} G_1 \quad &\rightarrow \quad v u_{,n} \\
F_{0,\xi} \int_{\xi_0}^{\xi} F_0 \, d\xi \quad &\rightarrow \quad \frac{N u_{,\xi}}{D} \frac{\partial}{\partial \sigma} \left[D \int_{\xi_0}^{\xi} u \, d\xi \right] \\
F_{0,\xi} \int_{\xi_0}^{\xi} \mathcal{C} G_1 \, d\xi \quad &\rightarrow \quad \frac{u_{,\xi}}{D} \frac{\partial}{\partial n} \left[D \int_{\xi_0}^{\xi} v \, d\xi \right]
\end{aligned} \tag{1.94}$$

In the Appendix E it is shown that all the functions F_{1j} can be expressed as combinations of simpler contributions depending only on the normalized conventional reference level ξ_0.
To evaluate the coefficient R_1 a closure relationship for $\frac{u_{1,\xi}}{u_{0,\xi}}|_{\xi_0}$ is needed. The latter can be readily obtained starting from (1.49) and (1.87):

$$\frac{u_{1,\xi}}{u_{0,\xi}}|_{\xi_0} = \frac{F_{1,\xi}}{F_{0,\xi}}|_{\xi_0} \tag{1.95}$$

Then, using the relation (1.90) and solving (1.95) for $\frac{u_{1,\xi}}{u_{0,\xi}}|_{\xi_0}$ we find:

$$\frac{u_{1,\xi}}{u_{0,\xi}}|_{\xi_0} = \frac{1}{1-\sqrt{C_{fu}}\frac{F_{11,\xi}}{F_{0,\xi}}|_{\xi_0}}\left[\left(-\sqrt{C_{fu}}\frac{D_1}{D_0} + n\mathcal{C}\beta_u C_{fu} + \frac{h_{01,\sigma}}{R_0}\right)\frac{F_{11,\xi}}{F_{0,\xi}}|_{\xi_0}\right.$$
$$-\frac{1}{2}R_2\frac{F_{12,\xi}}{F_{0,\xi}}|_{\xi_0} - \frac{1}{2}R_3\frac{F_{13,\xi}}{F_{0,\xi}}|_{\xi_0}$$
$$\left.-\frac{3}{2}R_{2b}\frac{F_{14,\xi}}{F_{0,\xi}}|_{\xi_0} - \frac{5}{2}R_3\frac{F_{15,\xi}}{F_{0,\xi}}|_{\xi_0}\right] \tag{1.96}$$

1.6 Second order: correction of secondary flow due to convective effects

Many second-order effects arise in the equation governing the secondary flow. Indeed the $O(\delta^1)$ correction of longitudinal velocity affects the centrifugal term and further contributions are due to the lateral variations of the lateral component of momentum, to topographic effects and perturbations of the eddy viscosity forced by perturbations of flow depth and longitudinal velocity. The lateral component of Reynolds' equation at order $O(\delta^2)$, using the differential problem at previous order (1.54) and the perturbation of the eddy viscosity (1.85), is readily written in the form:

$$\begin{cases} \frac{1}{D_0^2}\left[\nu_{T0} v_{2,\xi}\right]_{,\xi} = \left(\frac{h_{1,n}}{\beta_u\sqrt{C_{fu}}} - \mathcal{C}u_0^2\right)\left(\frac{D_1}{D_0} - \frac{u_{1,\xi}}{u_{0,\xi}}|_{\xi_0}\right) \\ \qquad +\beta_u\sqrt{C_{fu}} n \mathcal{C}^2 u_0^2 + \frac{h_{2,n}}{\beta_u\sqrt{C_{fu}}} \\ \qquad +u_0 v_{1,\sigma} \\ \qquad \frac{1}{\beta_u\sqrt{C_{fu}}} v_1 v_{1,n} \\ \qquad -\frac{v_{1,\xi}}{D_0}\frac{\partial}{\partial\sigma}\left[D_0\int_{-1}^{n} u_0\, dn\right] \\ \qquad -\frac{1}{\beta_u\sqrt{C_{fu}}}\frac{v_{1,\xi}}{D_0}\frac{\partial}{\partial n}\left[D_0\int_{-1}^{n} v_1\, dn\right] \\ \qquad -2cu_0u_1 \\ v_2|_{\xi_0} = 0 \\ v_{2,\xi}|_1 = 0 \end{cases} \tag{1.97}$$

Hence, defining:

$$v_2 = D_0^{3/2}(n,\sigma) R_0^{1/2}(\sigma) G_2(\xi, n, \sigma)\mathcal{C}(\sigma) \tag{1.98}$$

$$\frac{\partial h_2}{\partial n} = \beta_u\sqrt{C_{fu}} D_0(n,\sigma) R_0(\sigma)\mathcal{C}(\sigma) a_2(n,\sigma) \tag{1.99}$$

and using equations (1.49), (1.50), (1.55), (1.56), (1.85), (1.87), some algebra allows us to derive the differential system for G_2:

$$\begin{cases} \left[\mathcal{N}(\xi)G_{2,\xi}\right]_{,\xi} = a_2 + R_5\ a_1 \\ \qquad\qquad +R_{4b}\ \left[F_0^2\right] \\ \qquad\qquad \frac{R_{6b}}{\mathcal{C}}\ \left[F_0\mathcal{C}G_1\right] \\ \qquad\qquad +\frac{3}{2}\frac{R_3}{\mathcal{C}}\ \left[(\mathcal{C}G_1)^2\right] \\ \qquad\qquad -2\ \left[F_0F_1\right] \\ \qquad\qquad -\frac{3}{2}\frac{R_{2b}}{\mathcal{C}}\ \left[\mathcal{C}G_{1,\xi}\int_{\xi_0}^{\xi} F_0\ d\xi\right] \\ \qquad\qquad -\frac{5}{2}\frac{R_3}{\mathcal{C}}\ \left[\mathcal{C}G_{1,\xi}\int_{\xi_0}^{\xi} \mathcal{C}G_1\ d\xi\right] \\ \qquad\qquad +\frac{R_7}{\mathcal{C}}\ \left[F_0\frac{\partial}{\partial\sigma}\left(\mathcal{C}G_1\right)\right] \\ G_2|_{\xi_0} = 0 \\ G_{2,\xi}|_1 = 0 \end{cases} \tag{1.100}$$

where:

$$\begin{aligned} R_{4b} &= -\left(\frac{D_1}{D_0} - \frac{u_{1,\xi}}{u_{0,\xi}}|_{\xi_0}\right) + n\mathcal{C}\beta_u\sqrt{C_{fu}} \\ R_5 &= \left(\frac{D_1}{D_0} - \frac{u_{1,\xi}}{u_{0,\xi}}|_{\xi_0}\right) \\ R_{6b} &= \frac{3}{2}R_{2b} \\ R_7 &= D_0 \end{aligned} \tag{1.101}$$

and the other coefficients are the same as shown in equations (1.89). In the previous analysis terms deriving from $G_{1,n}$ were neglected taking advantage of the slowly varying assumption.

The solution for G_2 can be given the form:

$$G_2 = a_2\ G_{21} + \tilde{G}_{22} \tag{1.102}$$

with:

$$\begin{aligned}\tilde{G}_2 = a_1 R_5 G_{21} - R_{4b} G_{22} - 2G_{23} - \frac{R_{6b}}{\mathcal{C}} G_{24} - \frac{3}{2}\frac{R_3}{\mathcal{C}} G_{25} \\ -\frac{3}{2}\frac{R_{2b}}{\mathcal{C}} G_{26} - \frac{5}{2}\frac{R_3}{\mathcal{C}} G_{27} - \frac{R_7}{\mathcal{C}} G_{28}\end{aligned} \tag{1.103}$$

where:

$$G_{2j} = g_j(\xi) - \frac{g_j'|_{\xi=1}}{g_0'|_{\xi=1}} g_0(\xi) \qquad (j = 1, 8) \tag{1.104}$$

and g_j $(j = 0..8)$ are solutions of the following ordinary differential systems:

$$\left\{ \begin{array}{rcl} \left[\mathcal{N}(\xi) g_{j,\ \xi}\right]_{,\xi} & = & \delta_i \\ g_j|_{\xi_0} = 0 & & \\ g_{j,\ \xi}|_{\xi_0} = 1 & & \end{array} \right. \tag{1.105}$$

where:

$$\begin{aligned}
\delta_0 &= 0 \\
\delta_1 &= 1 \\
\delta_2 &= -F_0^2 \\
\delta_3 &= F_0 F_1 \\
\delta_4 &= -F_0 \mathcal{C} G_1 \\
\delta_5 &= -(\mathcal{C} G_1)^2 \\
\delta_6 &= \mathcal{C} G_{1,\xi} \int_{\xi_0}^{\xi} F_0 \, d\xi \\
\delta_7 &= \mathcal{C} G_{1,\xi} \int_{\xi_0}^{\xi} \mathcal{C} G_1 \, d\xi \\
\delta_8 &= -F_0 \tfrac{\partial}{\partial \sigma} (\mathcal{C} G_1)
\end{aligned} \tag{1.106}$$

Obviously g_0, g_1 and g_2 are the same solutions found in (1.60), hence:

$$G_{21} = G_{11} \qquad\qquad G_{22} = G_{12} \tag{1.107}$$

Furthermore, we note that g_3 is the solution forced by perturbations of the centrifugal term driven by the longitudinal flow; the remaining terms represent the contributions of vertical and longitudinal variations of the secondary flow at order $O(\delta)$. Similarly to (1.94) it can be easily shown that terms come from following contributions:

$$\begin{aligned}
-F_0^2 \qquad &\rightarrow \qquad \mathcal{C} N u^2 \\
F_0 F_1 \qquad &\rightarrow \qquad \mathcal{C} N u^2 \\
-F_0 \mathcal{C} G_1 \qquad &\rightarrow \qquad N u v_{,\sigma} \\
-(\mathcal{C} G_1)^2 \qquad &\rightarrow \qquad v v_{,n} \\
\mathcal{C} G_{1,\xi} \int_{\xi_0}^{\xi} F_0 \, d\xi \qquad &\rightarrow \qquad \tfrac{N v_{,\xi}}{D} \tfrac{\partial}{\partial \sigma} \left[D \int_{\xi_0}^{\xi} u \, d\xi \right] \\
\mathcal{C} G_{1,\xi} \int_{\xi_0}^{\xi} \mathcal{C} G_1 \qquad &\rightarrow \qquad \tfrac{v_{,\xi}}{D} \tfrac{\partial}{\partial n} \left[D \int_{\xi_0}^{\xi} v \, d\xi \right] \\
-F_0 \tfrac{\partial}{\partial \sigma} (\mathcal{C} G_1) \qquad &\rightarrow \qquad N u v_{,\sigma}
\end{aligned} \tag{1.108}$$

We refer to Appendix E for a complete derivation of functions G_{2j}.

We proceed to determine the function $a_2(n,\sigma)$ in a quite similar way as done for (1.65). The *depth-averaged form of the continuity equation for the liquid phase* (1.40) at $O(\delta^2)$, after some algebra, takes the form:

$$\frac{\partial}{\partial\sigma}\left[D_1\int_{\xi_0}^{1}u_0\;d\xi\right]+\frac{\partial}{\partial\sigma}\left[D_0\int_{\xi_0}^{1}u_1\;d\xi\right]+\frac{1}{\beta_u\sqrt{C_{fu}}}\frac{\partial}{\partial n}\left[D_1\int_{\xi_0}^{1}v_1\;d\xi\right]$$
$$\frac{1}{\beta_u\sqrt{C_{fu}}}\frac{\partial}{\partial n}\left[D_0\int_{\xi_0}^{1}v_2\;d\xi\right]+\mathcal{C}D_0\int_{\xi_0}^{1}v_1\;d\xi$$
$$-n\mathcal{C}\beta_u\sqrt{C_{fu}}\frac{\partial}{\partial\sigma}\left[D_0\int_{\xi_0}^{1}u_0\;d\xi\right]=0 \tag{1.109}$$

We then integrate the latter equation over the cross section. With the use of the boundary condition (1.38) written at $O(\delta)$ (1.64) and at $O(\delta^2)$, namely:

$$\int_{\xi_0}^{1}v_2\;d\xi=0\qquad(n=\pm1) \tag{1.110}$$

we find:

$$+\frac{1}{\beta_u\sqrt{C_{fu}}}D_1\int_{\xi_0}^{1}v_1\;d\xi+\mathcal{C}\int_{-1}^{n}\left[D_0\int_{\xi_0}^{1}v_1\;d\xi\right]\;dn$$
$$+\frac{\partial}{\partial\sigma}\left[\int_{-1}^{n}\left(D_1\int_{\xi_0}^{1}u_0\;d\xi+D_0\int_{\xi_0}^{1}u_1\;d\xi\right)\;dn\right]$$
$$-\mathcal{C}\beta_u\sqrt{C_{fu}}\int_{-1}^{n}n\frac{\partial}{\partial\sigma}\left[D_0\int_{\xi_0}^{1}u_0\;d\xi\right]\;dn$$
$$+\frac{1}{\beta_u\sqrt{C_{fu}}}D_0\int_{\xi_0}^{1}v_2\;d\xi=0 \tag{1.111}$$

Now a useful relationship is obtained multiplying by $n\mathcal{C}\beta_u\sqrt{C_{fu}}$ the depth-averaged continuity equation (1.65) at $O(\delta)$ and integrating the latter in the lateral direction using (1.64):

$$-\mathcal{C}\beta_u\sqrt{C_{fu}}\int_{-1}^{n} n\frac{\partial}{\partial\sigma}\left[D_0\int_{\xi_0}^{1} u_0\ d\xi\right]\ dn = \mathcal{C}\left\{nD_0\int_{\xi_0}^{1} v_1\ d\xi - \int_{-1}^{n}\left(D_0\int_{\xi_0}^{1} v_1\ d\xi\right)\ dn\right\} \tag{1.112}$$

Substituting from (1.112) into (1.111) we find:

$$+\frac{1}{\beta_u\sqrt{C_{fu}}}\left[D_1\int_{\xi_0}^{1} v_1\ d\xi + D_0\int_{\xi_0}^{1} v_2\ d\xi\right] +\frac{\partial}{\partial\sigma}\left[\int_{-1}^{n}\left(D_1\int_{\xi_0}^{1} u_0\ d\xi + D_0\int_{\xi_0}^{1} u_1\ d\xi\right)\ dn\right] +\mathcal{C}nD_0\int_{\xi_0}^{1} v_1 d\xi = 0 \tag{1.113}$$

Finally, using (1.98) and (1.102), we end up with an expression for a_2:

$$a_2(n,\sigma) = a_{20} - \frac{a_{21}}{\mathcal{C}D_0^{5/2}R_0^{1/2}}\left\{+\frac{1}{\beta_u\sqrt{C_{fu}}}D_1\int_{\xi_0}^{1} v_1\ d\xi + \frac{\partial}{\partial\sigma}\left[\int_{-1}^{n}\left(D_1\int_{\xi_0}^{1} u_0\ d\xi + D_0\int_{\xi_0}^{1} u_1\ d\xi\right)\ dn\right] +\mathcal{C}nD_0\int_{\xi_0}^{1} v_1 d\xi\right\} \tag{1.114}$$

where:

$$a_{20} = -\frac{I_{\tilde{G}_{22}}}{I_{G_{21}}} \qquad a_{21} = \frac{\beta_u \sqrt{C_{fu}}}{I_{G_{21}}} \tag{1.115}$$

The second order correction of secondary flow can be split in a way similar to (1.75), with a first contribution characterized by vanishing vertical average and a second contribution providing the non zero part of the vertical average of the lateral velocity. This can be easily shown rearranging the equation (1.98) using the relations (1.53) and (1.107):

$$v_2 = v_{20} + v_{21} \tag{1.116}$$

$$v_{20} = D_0^{3/2} R_0^{1/2} \mathcal{C} \left(a_{20} G_{11} + \tilde{G}_{22} \right) \tag{1.117}$$

$$\begin{aligned} v_{21} = -\frac{\beta_u \sqrt{C_{fu}}}{D_0(1-\xi_0)} F_0 \Bigg\{ & \frac{1}{\beta_u \sqrt{C_{fu}}} D_1 \int_{\xi_0}^{1} v_1 \, d\xi \\ + \frac{\partial}{\partial \sigma} \left[\int_{-1}^{n} \left(D_1 \int_{\xi_0}^{1} u_0 \, d\xi + D_0 \int_{\xi_0}^{1} u_1 \, d\xi \right) \, dn \right] & \\ + \mathcal{C} n D_0 \int_{\xi_0}^{1} v_1 d\xi \Bigg\} & \end{aligned} \tag{1.118}$$

Let us then calculate the vertical average of the lateral velocity:

$$V_2 = \frac{1}{1-\xi_0} \int_{\xi_0}^{1} v_2 d\xi = \overline{v_{20}} + \overline{v_{21}} \tag{1.119}$$

Using the equations (1.53), (1.107), (1.115) and (1.119) we can readily show that:

$$\overline{v_{20}} = 0 \tag{1.120}$$

$$\overline{v_{21}} = V_2 \tag{1.121}$$

Hence, comparing (1.121) with (1.118) and using (1.116), we can finally express v_2 in the form:

$$v_2(\sigma, n, \xi) = v_{20}(\sigma, n, \xi) + F_0(\xi)V_2(\sigma, n) \tag{1.122}$$

Expanding the quantity q_n (see the equation 1.78) and using (1.76) and (1.79), at $O(\delta^2)$ we obtain:

$$q_{n_2} = q_{\sigma_0}\left[\frac{v_{2,\xi}}{u_{0,\xi}}|_{\xi_0} - \frac{u_{1,\xi}}{u_{0,\xi}}|_{\xi_0}\frac{q_{bn1}}{q_{\sigma_0}} - \frac{R'(D_{1,n} - F_u^2 h_{1,n})}{\sqrt{D_0 R_0}} - \frac{\Phi_1 q_{bn1}}{q_{\sigma_0}^2}\right] \tag{1.123}$$

having set $\frac{\theta_1}{\theta_0} = 2\frac{u_{1,\xi}}{u_{0,\xi}}|_{\xi_0}$.
We may finally come to the sediment continuity equation (1.45). Integrating the latter over the cross section, with the use of the boundary condition (1.38) at $O(\delta^2)$, it takes the form:

$$\frac{\partial}{\partial\sigma}\int_1^n q_{\sigma_1}\, dn + \frac{1}{\beta_u\sqrt{C_{fu}}}q_{n_2} + \mathcal{C}\int_1^n q_{n_1}\, dn - \mathcal{C}\beta_u\sqrt{C_{fu}}\int_1^n n q_{\sigma 0,\sigma}\, dn = 0 \tag{1.124}$$

Similarly to (1.112), multiplying by $n\mathcal{C}\beta_u\sqrt{C_{fu}}$ the sediment continuity equation (1.45) at $O(\delta)$ and integrating it in the lateral direction, we obtain the following useful relation:

$$-\mathcal{C}\beta_u\sqrt{C_{fu}}\int_{-1}^{n} nq_{\sigma 0,\sigma}\ dn = \mathcal{C}\left\{nq_{n_1} - \int_{-1}^{n} q_{n_1}\ dn\right\} \tag{1.125}$$

Finally, substituting from (1.123) into (1.124) the latter equation can be reduced to a non linear partial integro-differential equation for the unknown functions $D_1(n,\sigma)$ and $h_{01,\sigma}(\sigma)$. We find:

$$\begin{aligned} D_{1,n} = -\frac{\sqrt{D_0 R_0}}{R'}\Bigg\{ &+\frac{v_{2,\xi}}{u_{0,\xi}}|_{\xi_0} \\ &+\frac{\beta_u\sqrt{C_{fu}}}{q_{\sigma_0}}\frac{\partial}{\partial\sigma}\int_{-1}^{n} q_{\sigma_1}\ dn \\ &+\frac{\beta_u\sqrt{C_{fu}}}{q_{\sigma_0}}\mathcal{C}nq_{n_1} \\ &+\frac{\Phi_1 q_{n_1}}{q_{\sigma_0}^2} \\ &+\frac{u_{1,\xi}}{u_{0,\xi}}|_{\xi_0} q_{n_1}\Bigg\} + F_u^2 h_{1,n} \end{aligned} \tag{1.126}$$

Clearly this equation has to be solved subject to the integral constraints (1.24) and (1.25) evaluated at the order $O(\delta^1)$:

$$\int_{-1}^{+1}\left(D_0^{3/2} I_{F_1} + D_0^{1/2} D_1 I_{F_0}\right)\ dn = 0 \tag{1.127}$$

$$\int_{-1}^{+1} q_{\sigma_1}\ dn = 0 \tag{1.128}$$

Again we refer to Appendix C for a complete description of the numerical procedure employed to solve (1.126).

Chapter 2

Non linear theory of slowly varying meanders: results

In this chapter we briefly report the main results of the present non linear theory. In figure 2.1 we show two periodic sequences of sine generated meanders such that $c(s) = \cos(\lambda s)$ (Langbein & Leopold (1966)), characterized by different dimensionless wavenumbers λ (quite small in figure 2.1a, fairly large in figure 2.1b). As expected, the phase lag of bed topography relative to channel curvature is fairly small when convective effects play a negligible role, i.e. for small wavenumbers. As the latter increases, the location of maximum scour moves from downstream to upstream of the bend apex and the pattern of scour and deposits displays oscillations larger than those found for larger wavelengths.

The corresponding values of the vertically averaged longitudinal velocity predicted in the previous meander configurations are reported in figure 2.1c and 2.1d. In both cases, the thread of high velocity (greater for smaller wavelengths), which shifts from one side to the other side of the channel with distance through the meander, displays a peak just downstream the bend apex.

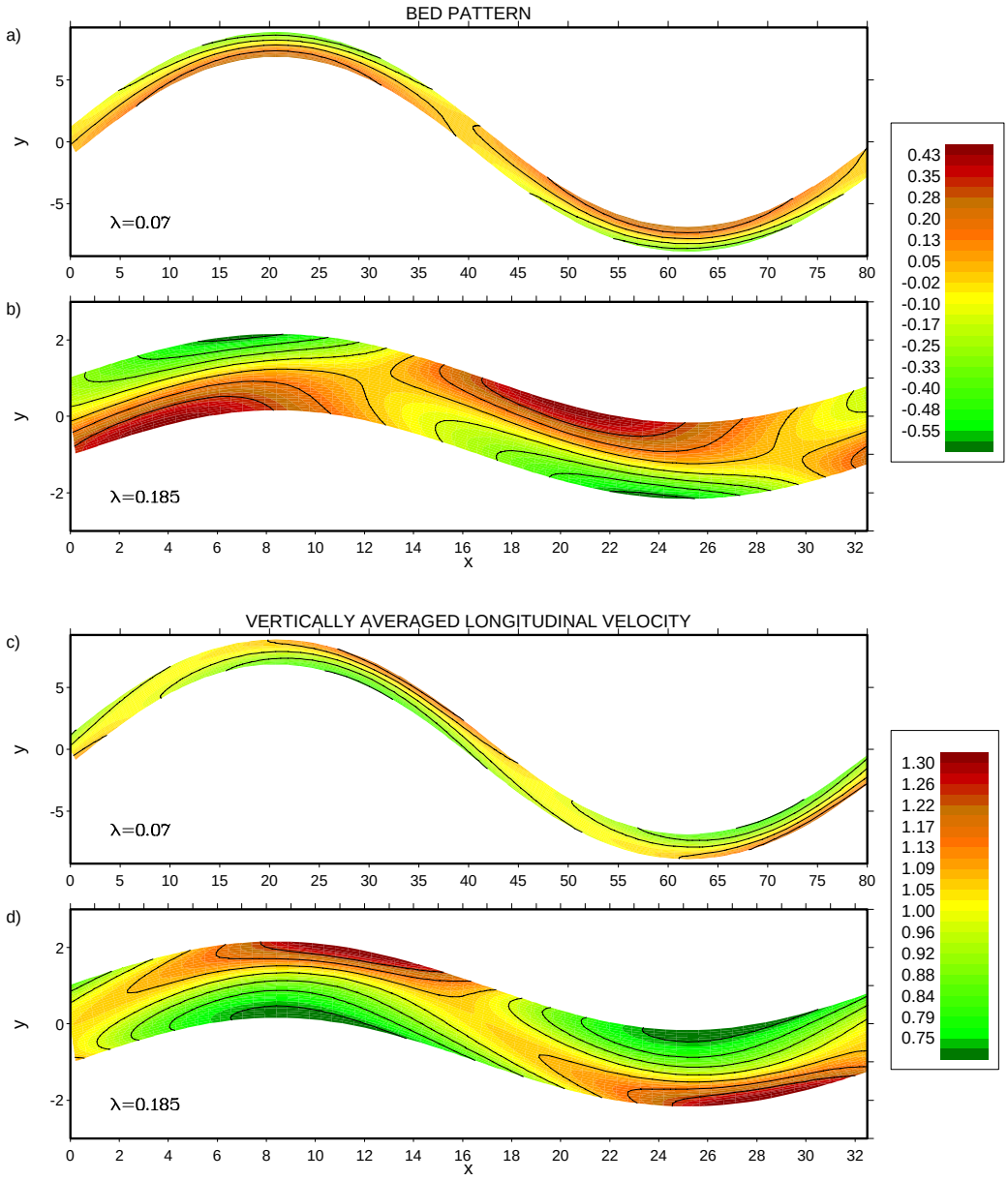

Figure 2.1: Dimensionless bed elevation (a, b) and dimensionless value of vertically averaged longitudinal velocity (c, d) predicted by the present theory for two periodic sequences of sine generated meanders, characterized by different dimensionless wavenumbers. ((a) λ=0.07; (b) λ=0.185; (c) λ=0.07; (d) λ=0.185). The values of the relevant dimensionless parameters are $d_s = 5 \cdot 10^{-3}$, $\nu_0 = 0.04$, $\vartheta_u = 0.1$, β_u=7. Flow is from left to right.

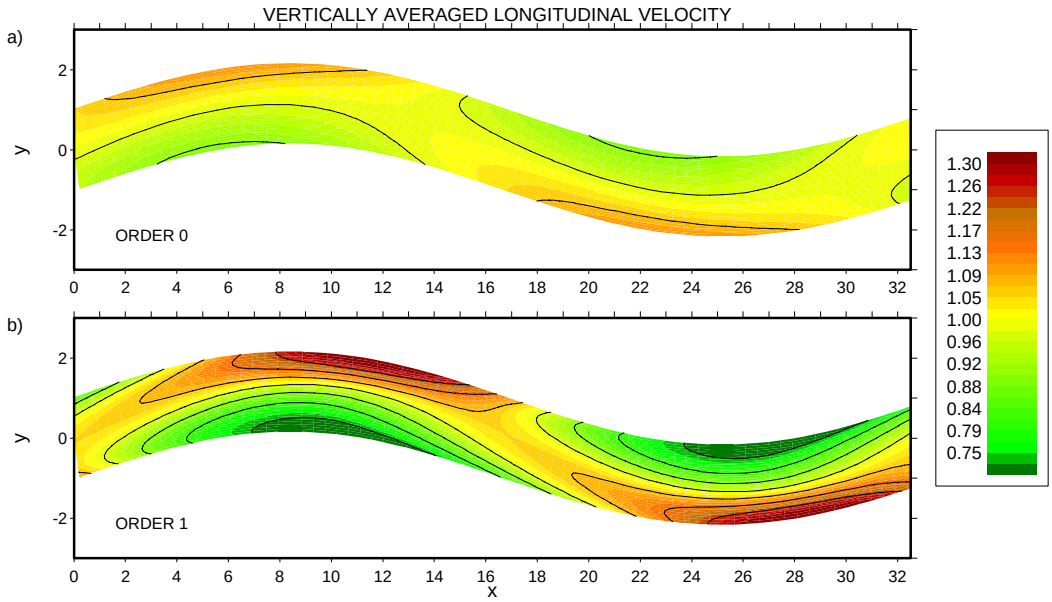

Figure 2.2: The dimensionless value of the vertically averaged longitudinal velocity at leading (a) and first (b) order predicted by the present theory for a periodic sequence of sine generated meanders, characterized by dimensionless wavenumber λ=0.185. The values of the relevant dimensionless parameters are $d_s = 5 \cdot 10^{-3}$, $\nu_0 = 0.04$, $\vartheta_u = 0.1$, β_u=7. Flow is from left to right.

In figure 2.2 we show a comparison between the leading and first order solution of the vertically averaged longitudinal velocity. Note that the first order contribution has the twofold effect of increasing the velocity magnitude and shifting the velocity peak downstream . This is due to the main role of convective effects. The complete flow field calculated in four cross sections located at different positions along the shorter meander (λ=0.185) are also reported in figure 2.3. Here the line contours represent the values of the dimensionless downstream velocity and are plotted together with the vectors showing the secondary flow and the projection of some streamlines on the cross section. At the inflection point (figure 2.3a) the secondary flow is nearly uniform in the cross section and is directed from the left to the right bank except for regions close to the sidewalls where a secondary flow cell is found.

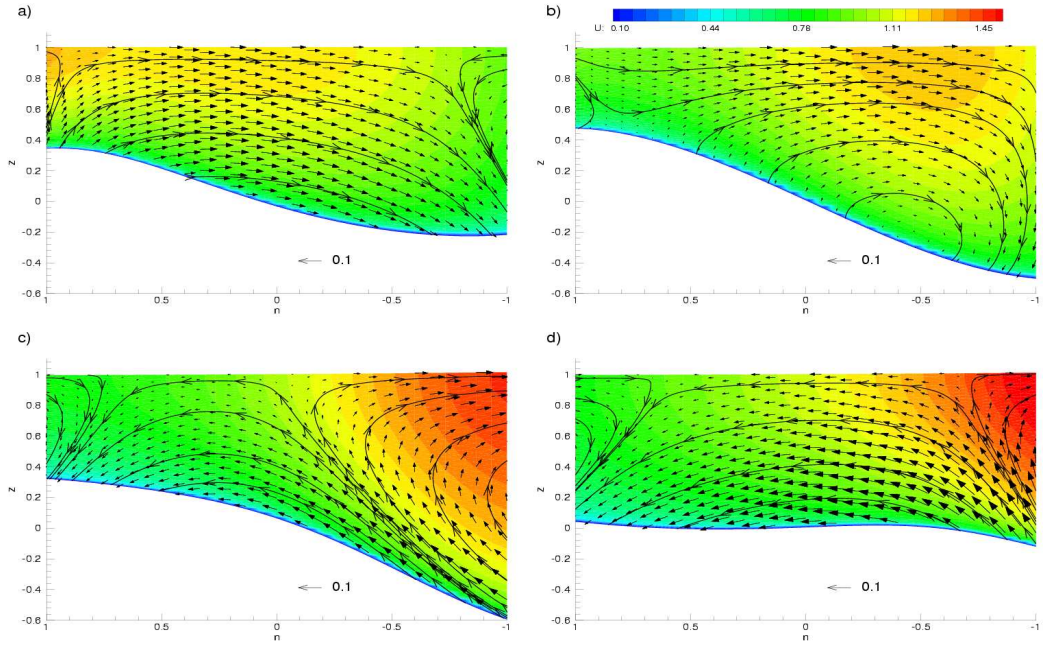

Figure 2.3: Isocontours of dimensionless downstream velocity at different cross sections of the sine generated meander of figure 2.1b (λ=0.185). Vectors showing the secondary motion and the projection of some streamlines on the cross section are also represented. ((a) $s\lambda/\pi$=0.5; (b) $s\lambda/\pi$=0.75; (c) $s\lambda/\pi$=1; (d)) $s\lambda/\pi$=1.25). The values of the relevant dimensionless parameters are $d_s = 5 \cdot 10^{-3}$, $\nu_0 = 0.04$, $\vartheta_u = 0.1$, β_u=7.

In the shallower portion of the cross section, flow is towards the left bank except for the region close to the sidewall where the secondary flow with vanishing depth average does again prevail. Downstream of the bend apex (figure 2.3d) the bed elevation is nearly uniform in the transverse direction and the secondary flow is driven by convective effects. Also note that the values of the secondary flow velocity are typically one order of magnitude smaller than those of the longitudinal motion. However note that, at the banks, the transverse flow rate has vanishing depth average as required by the boundary conditions. Moving downstream, the secondary flow driven by streamline curvature and topographic effects is initially enhanced near the bottom and close to the outer bank (figure 2.3b). Further downstream it occupies the outer part of the cross section (figure 2.3c).

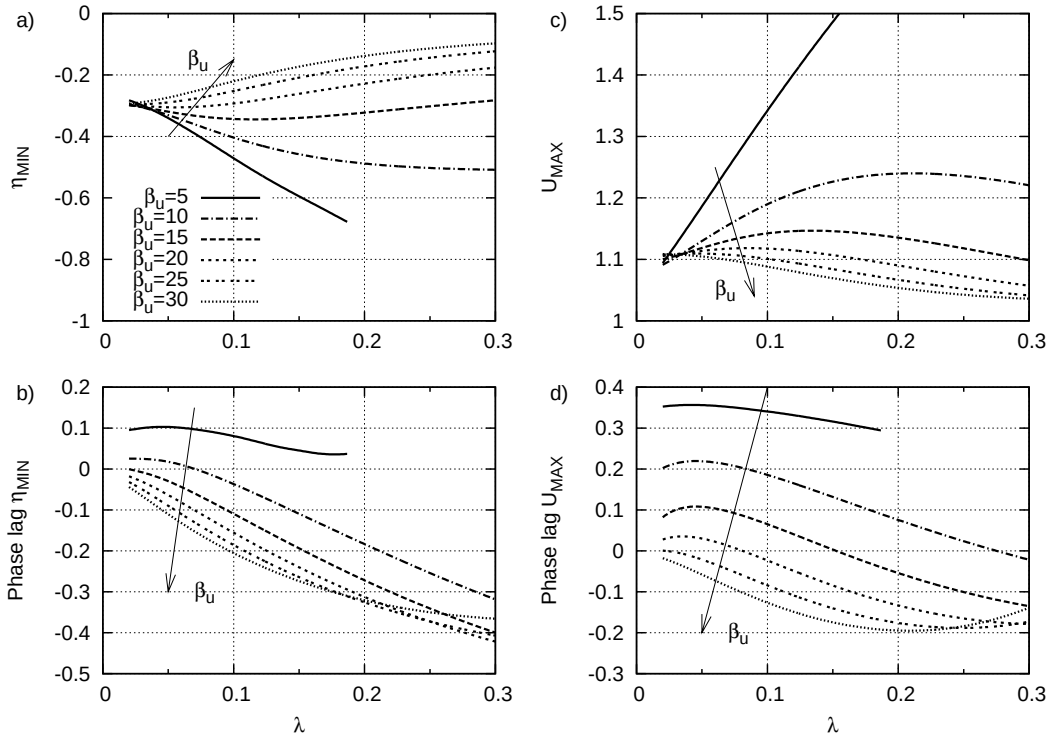

Figure 2.4: (a) Peak value and (b) relative phase lag ($\lambda s/\pi$) of the minimum bed level elevation with respect to the undisturbed bed for different values of β_u. (c) Peak values and (d) relative phase lag of vertically averaged velocity for different value of β_u ($d_s = 5 \cdot 10^{-3}$, $\nu_0 = 0.04$, $\vartheta_u = 0.1$).

The figure 2.4 reports the peak value (a) and relative phase lag (b) of the minimum bed elevation relative to the undisturbed bed calculated in a sine generated meander characterized by a given amplitude parameter ν_0 for different values of β_u. Note that, for increasing values of β_u, the curvature parameter ν_0 being kept constant, the perturbation parameter δ decreases, hence smaller values of the maximum scour (-η_{MIN}) are experienced.

Moreover, for small values of β_u, the location of the cross section where the maximum scour is experienced moves from downstream to upstream of the bend apex as the wavenumber increases. For larger values of β_u the trend is similar but the maximum scour is located upstream of the bend apex even for small wavenumbers.

The same tendency is shown by the phase lag of the peak value of velocity calculated along the meander (figure 2.4d).

Also note that, for given value of β_u, the curves representing the maximum value of velocity (figure 2.4c) are characterized by a peak. In the case of β_u=5, the curve is interrupted because the value of the Shields stress falls below the threshold of motion anywhere along the entire meander.

A comparison with the leading order solution is also reported in figure 2.5 where it is clear that the convective terms, appearing at first order, generally contribute to increasing the values of maximum scour and maximum velocity and to shifting the latter peaks downstream. These corrections are dominant as β_u decreases.

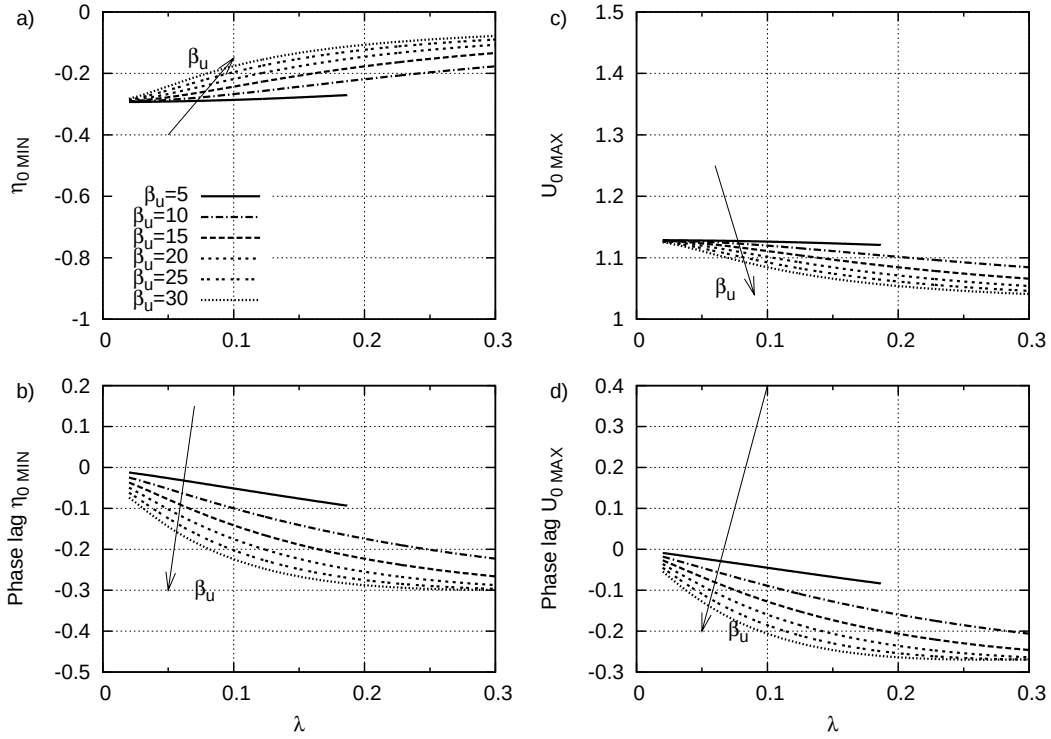

Figure 2.5: Same as figure 2.4 but at leading order.

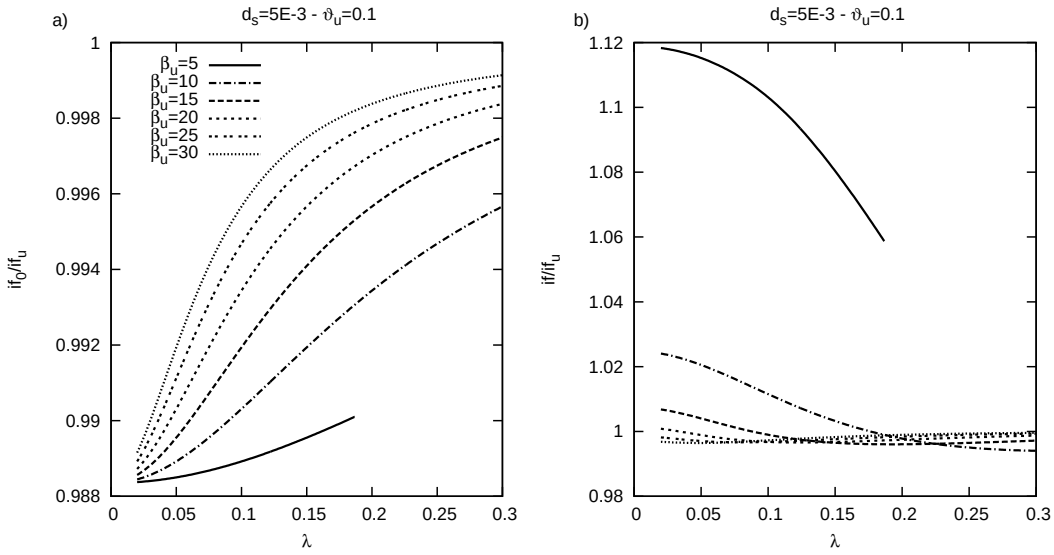

Figure 2.6: Ratio between the mean free surface slope i_f and the reference uniform flow slope i_{fu} at leading order (a) and at first order of approximation (b).

Furthermore, in figure 2.6 we report the ratio between the free surface slope i_f, averaged along the entire meander, and the reference uniform flow slope i_{fu}, at leading order (a) and at the first order of approximation (b). Note that, at leading order δ^0, the mean free surface slope is slightly different and invariably smaller than the reference uniform slope i_{fu}. In the Appendix D we show that the latter effect is strictly related to the perturbation of the shear stresses due to depth variations. On the contrary, at the first order of approximation δ^1, convective terms appear and, for small values of β_u, they lead to an increase of the mean free surface slope. The value of the correction diminishes as the aspect ratio β_u increases. In the Appendix D we show that the latter effect is strictly related to the perturbation of the shear stresses due to velocity variations induced by convective effects.

Chapter 3

Non linear bend instability theory for river meanders

The model presented in the previous chapters is suitable for the formulation of a non linear bend instability theory. In order to pursue the latter goal one needs to associate a bank erosion equation to the governing equation for flow and bed topography. As pointed out in Seminara (2006), the detailed mechanics of bank erosion, both the *continuous process* of particle removal of small particles from the bank surface and the *intermittent* process of bank collapse occurring typically during the decaying stage of flood events, depends on several factors, namely scour at the bank toe, bank cohesion, wetting and drying of banks, its rate being ultimately controlled by the ability of the stream to remove sediments accumulated at the bank foot. However, for long term investigations, rather than attempting to investigate in detail the mechanics of single events, it is more appropriate to resort to some integrated formulation: in other words, one simply locates the region of the outer bank where erosion is expected to occur on the basis of the knowledge of the hydrodynamic field and simply models the actual intermittent mechanism as effectively continuous and such to reproduce the averaged effects of the actual process.

3.1 Amplification and migration rate: the integral criterion for bank erosion

It appears to be physically more sensible to compare the evolution of meanders with given amplitudes as their wavelengths and curvatures vary. Thus we assume that the channel axis follows a sinusoidal curve in the (x^*, y^*) plane and denote by k^* its cartesian wavenumber and by ϵ^* its amplitude:

$$y_a^* = \epsilon^* \cos(k^* x^*) \tag{3.1}$$

Normalizing both k^* and ϵ^* by the half-width of the channel B_u^* we readily obtain, as sketched in figure 3.1:

$$y_a = \epsilon \cos(kx) \tag{3.2}$$

Consequently, as shown in the Appendix B, the following relation can be found:

$$\nu_0 = \epsilon k^2 \tag{3.3}$$

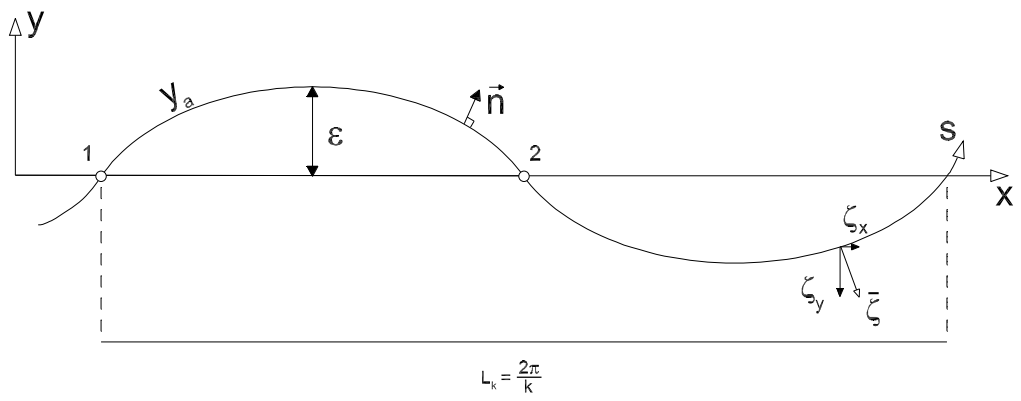

Figure 3.1: Sketch illustrating channel axis

We then follow the approach of Ikeda *et al.* (1981) and assume that bank erosion is linearly proportional to an excess flow speed at the outer bank while bank deposition is conversely linearly related to a defect of flow speed at the inner bank.
Hence we write:

$$\vec{\zeta}(s) = \vec{n}\ E\,(U|_{n=1} - U|_{n=-1}) \tag{3.4}$$

where both the lateral migration speed $\vec{\zeta}(s)$ and the depth averaged longitudinal velocity U are scaled by some reference speed U_u^* and E is a dimensionless long term *erosion coefficient*. Note that $\vec{n}$ represents the direction orthogonal to the banks. The suitability of the above linear rule has received some support (Pizzuto & Meckelnburg (1989)) from field observations on rivers with fairly uniform cohesive banks. Note that the rule (3.4) is such that channel width is preserved throughout the process of meander development.

We then define an average measure of the migration vector $(\bar{\zeta_x}, \bar{\zeta_y})$ integrating the local values of $\vec{\zeta}(s)$ given by the equation (3.4) along the intrinsic coordinate s, between two consecutive inflection points:

$$\bar{\zeta_x} = \int_{s_1}^{s_2} \zeta_x\ ds \tag{3.5}$$

$$\bar{\zeta_y} = \int_{s_1}^{s_2} \zeta_y\ ds \tag{3.6}$$

It can be shown (see the Appendix B) that the x and y cartesian components of the above vector provide measures of the meander wave speed and meander growth rate, respectively. In particular a positive (negative) value of $\bar{\zeta_x}$ corresponding to downstream (upstream) meander migration while positive (negative) values of $\bar{\zeta_y}$ correspond to meander amplification (attenuation).

The relation between the average migration vector $(\bar{\zeta}_x, \bar{\zeta}_y)$ and meander amplification $\frac{\epsilon_{,t}}{\epsilon}$ and migration c can be easily found to have the form:

$$c = \bar{\zeta}_x \frac{2}{\epsilon^2 k \lambda} \qquad \frac{\epsilon_{,t}}{\epsilon} = \bar{\zeta}_y \frac{\pi}{2\epsilon} \frac{k}{\lambda} \tag{3.7}$$

3.2 Comparison with linear theory

The figures 3.2a and 3.2b respectively show the meander growth rate and wave speed as functions of the wavenumber λ for different values of the amplitude ϵ. The values corresponding to the linear theory are also reported and it is evident that for small wavenumbers, i.e. for meanders characterized by very slow longitudinal variations, non linear terms are negligible, hence all the curves tend to collapse. On the contrary, as the wavenumber increases, the solution strongly depends on the amplitude of the perturbation ϵ due to the increasing importance of convective terms. The curves obtained by the present model are interrupted when the value of the Shields stress falls below the threshold of motion somewhere along the meander. Clearly, within the linear context, both amplification and migration rates are not affected by the value of the amplitude of the initial perturbation ϵ.

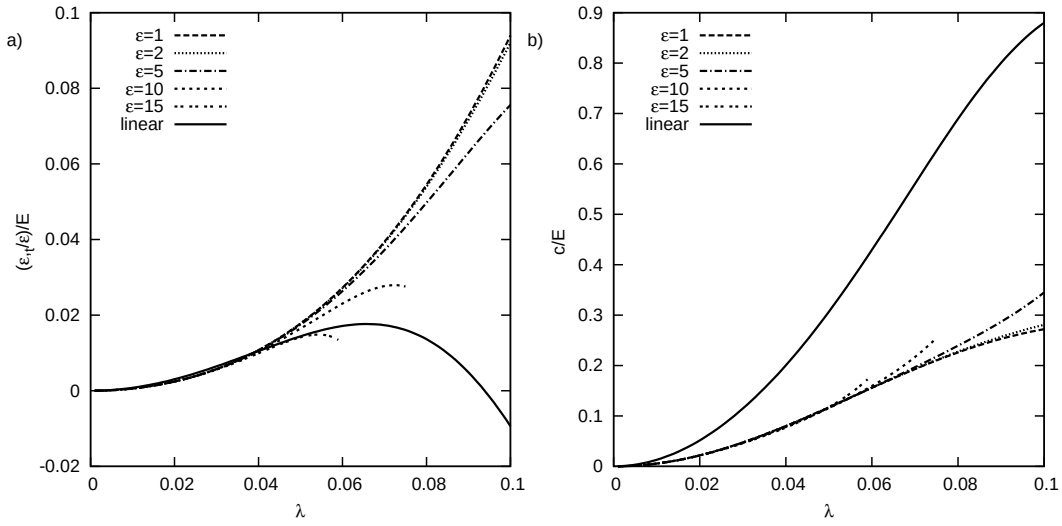

Figure 3.2: (a) Meander amplification $\epsilon_{,t}/\epsilon$ and (b) wave speed c divided by the erosion coefficient E versus the wavenumber are reported in the case of a meander following a sinusoidal planimetric pattern with different values of amplitude ϵ. Values corresponding to the linear theory are also reported. ($d_s = 5 \cdot 10^{-3}$, $\vartheta_u = 0.1$, $\beta_u = 10$)

However, note that the linear solution for flow field and bed topography depends on the value attained by the small parameter ν_0, related to both ϵ and λ through the equation 3.3. Hence, for example, in the case of $\epsilon = 15$ the bed emerges in the linear case for a value of $\lambda = 0.079$, the latter value increasing as ϵ decreases.

In figure 3.3 we compare the non linear (3.3a) and linear (3.3b) values of the meander amplification rate $\epsilon_{,t}/\epsilon$ (scaled by the erosion coefficient E) as a function of the meander wavenumber λ for a given value of the amplitude ϵ. Note that, for different values of β_u, the non linear solution is characterized by a peak which corresponds to the value of the critical wavenumber selected in the meandering process. The location of the peak, i.e. the wavenumber selected, increases monotonically as β_u increases. On the other hand, the linear solution is highly influenced by the fact that the amplification rate tends to infinite for values of β_u and λ close to the resonant values ($\beta_R = 18.25$, $\lambda_R = 0.123$). Close to resonance the linear solution is plotted with dotted lines when the bed emerges (figure 3.3b, $\beta_u = 20$).

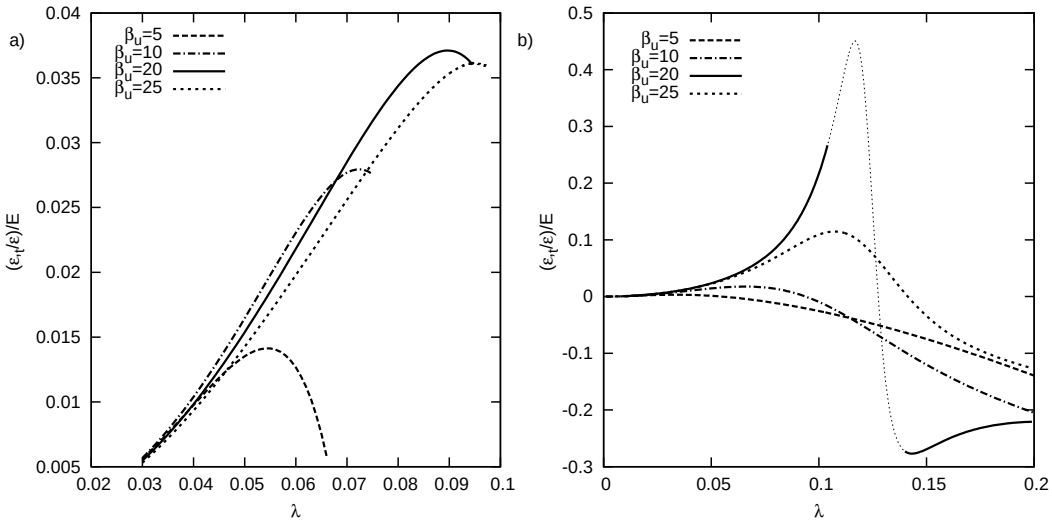

Figure 3.3: (a) Non linear and (b) linear solution for meander amplification rate $\epsilon_{,t}/\epsilon$ divided by the erosion coefficient E versus the wavenumber is reported for different values of β_u in the case of a meander following a sinusoidal planimetric pattern with amplitude ϵ =10. ($d_s = 5 \cdot 10^{-3}$, $\vartheta_u = 0.1$)

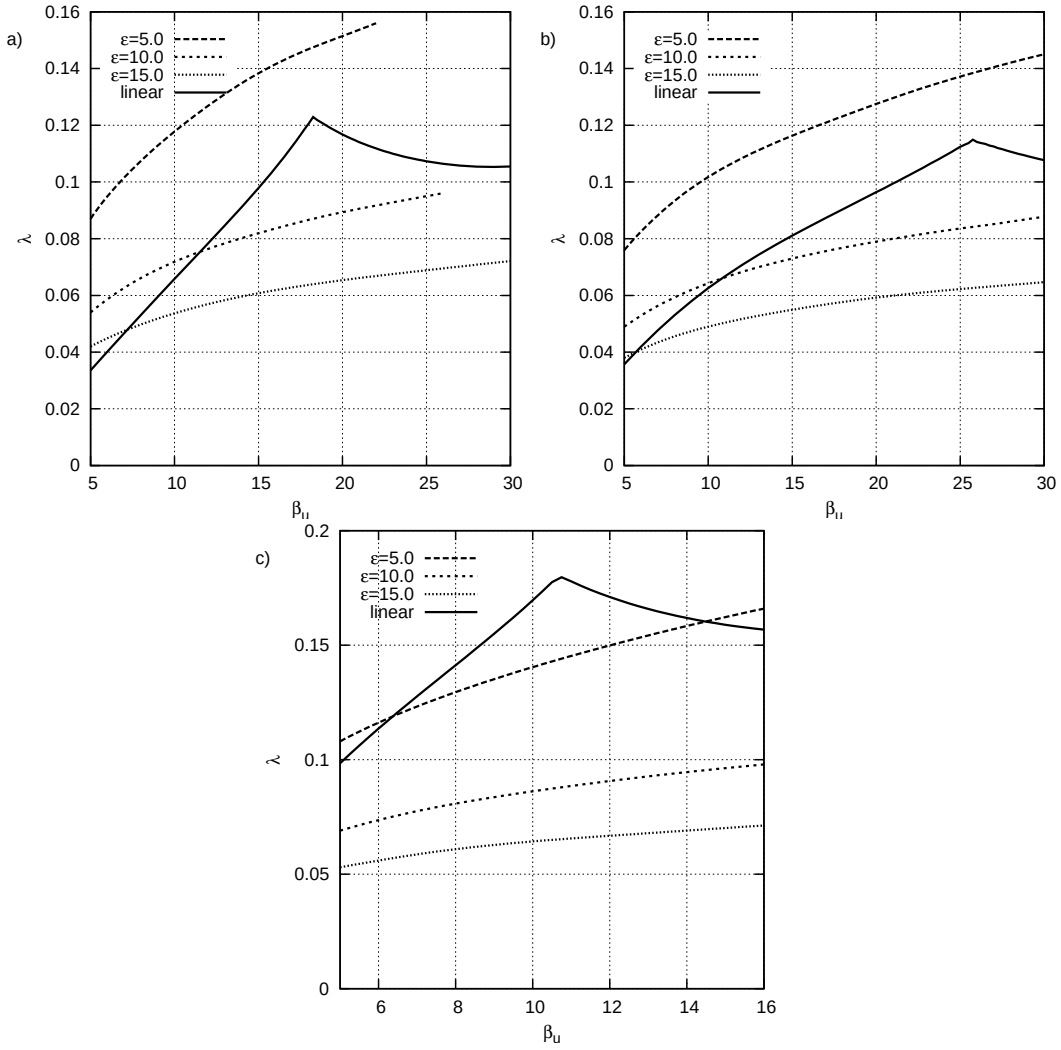

Figure 3.4: The selected wavenumbers for bend instability are reported for different values of the amplitude ϵ and compared with the linear theory. (a) $d_s = 5 \cdot 10^{-3}$, $\vartheta_u = 0.1$, (b) $d_s = 5 \cdot 10^{-3}$, $\vartheta_u = 0.2$), (c) $d_s = 0.1$, $\vartheta_u = 0.1$

In figure 3.4 the wavenumbers corresponding to the maximum bend amplification are plotted versus β_u for different values of the amplitude ϵ. Note that the selected wavenumber depends on the amplitude of the initial perturbation and in particular larger wavelengths (smaller wavenumbers) are associated with larger amplitudes ϵ. Increasing the reference Shields stress (compare figure 3.4a and figure 3.4b) and decreasing the relative roughness (compare figure 3.4c and figure 3.4a) also have a minor influence which leads to a decrease of the wavenumber selected. The values corresponding to the linear theory of Blondeaux & Seminara (1985) are also reported in the figures and show a peak close to the resonant values (β_R, λ_R). It turns out that, for small values of β_u, the non linear model typically selects a larger wavenumber, i.e. shorter wavelengths. The situation is reversed increasing bed friction (figure 3.4c), independently of the value attained by the aspect ratio β_u.

In figure 3.5 the values of the meander wave speed c, scaled by the erosion coefficient E, are plotted versus the aspect ratio β_u, for the values of meander wavenumbers selected by bend instability and different values of the amplitude ϵ. The wave speed corresponding to the linear theory are also reported and show the well-known feature of linear resonator (Kevorkian & Cole (1981)), i.e. that the phase of the response changes quadrant on crossing the resonant conditions.

Note that the wave speed is strongly affected by resonance for a wide range of β_u leading to results markedly different from the non linear case. However a common feature is still preserved in the present context: the resonant value still distinguishes between upstream and downstream migration (figure 3.5 a,b,c). Note also that the meander wave speed grows as the meander amplitude decreases (a well known feature, observed in the field, e.g. Nanson & Hickin (1983)), as Shield stress increases (compare figure 3.5a and 3.5b) and as friction decreases (compare figure 3.5c and 3.5a). Moreover, for each given meander amplitude ϵ, a threshold value of the aspect ratio β_u exists above which the model predicts upstream migration, a finding which confirms the picture obtained in the context of the linear model of Zolezzi & Seminara (2001). Meander amplification rates are finally reported in figure 3.6 for the values of meander wavenumbers selected by bend instability and different values of the amplitude ϵ. Unlike the linear model, amplification rates are only sligtly affected by the aspect ratio β_u for a given amplitude ϵ. Similarly to wave speed, the meander amplification rates grows as the meander amplitude decreases, as Shield stress increases (compare figure 3.6a and 3.6b) and as friction decreases (compare figure 3.6c and 3.6a).

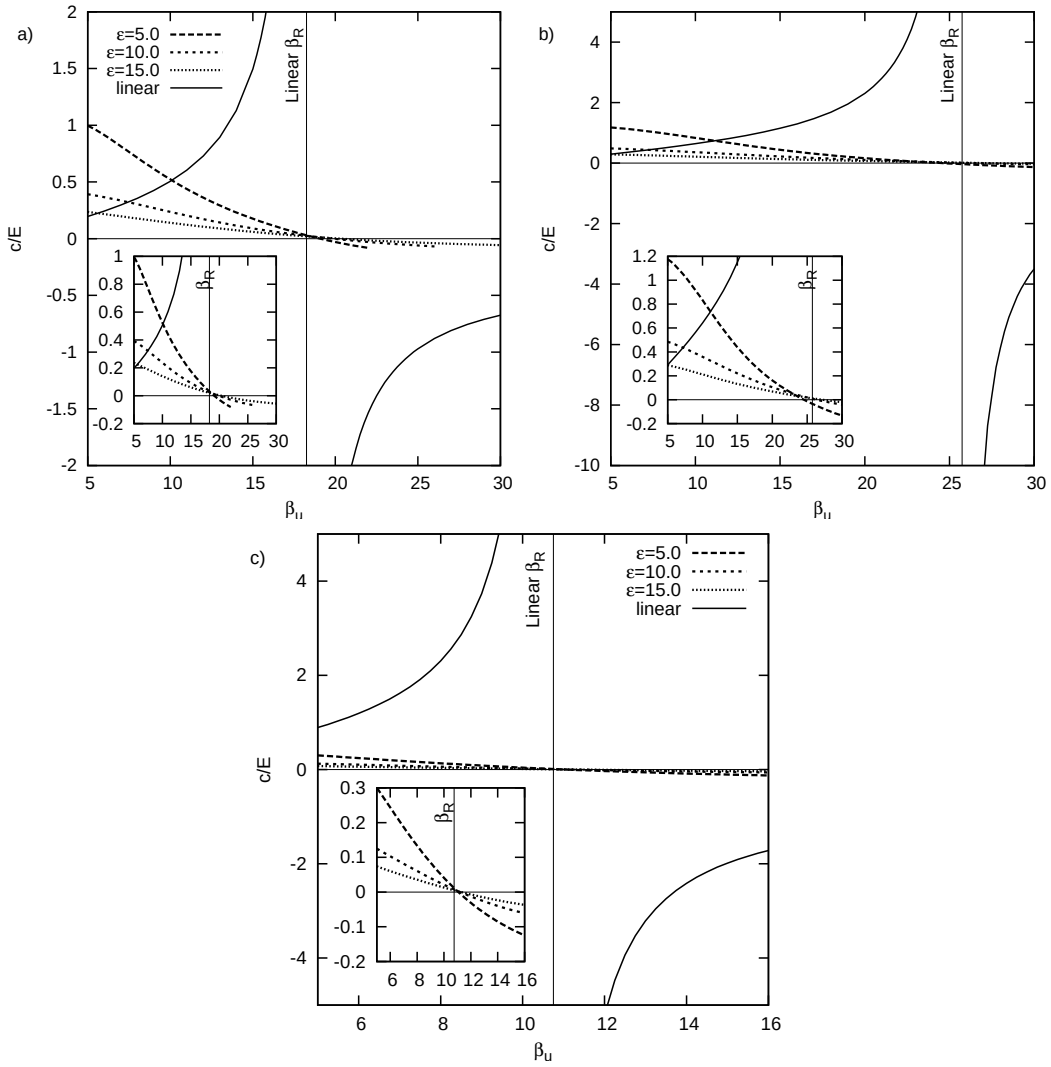

Figure 3.5: The values of meander wave speed c divided by the erosion coefficient E corresponding to the selected wavenumbers for bend instability are reported versus the aspect ratio β_u for different values of the amplitude ϵ and compared with the values obtained in the context of the linear theory. (a) $d_s = 5 \cdot 10^{-3}$, $\vartheta_u = 0.1$, (b) $d_s = 5 \cdot 10^{-3}$, $\vartheta_u = 0.2$, (c) $d_s = 0.1$, $\vartheta_u = 0.1$

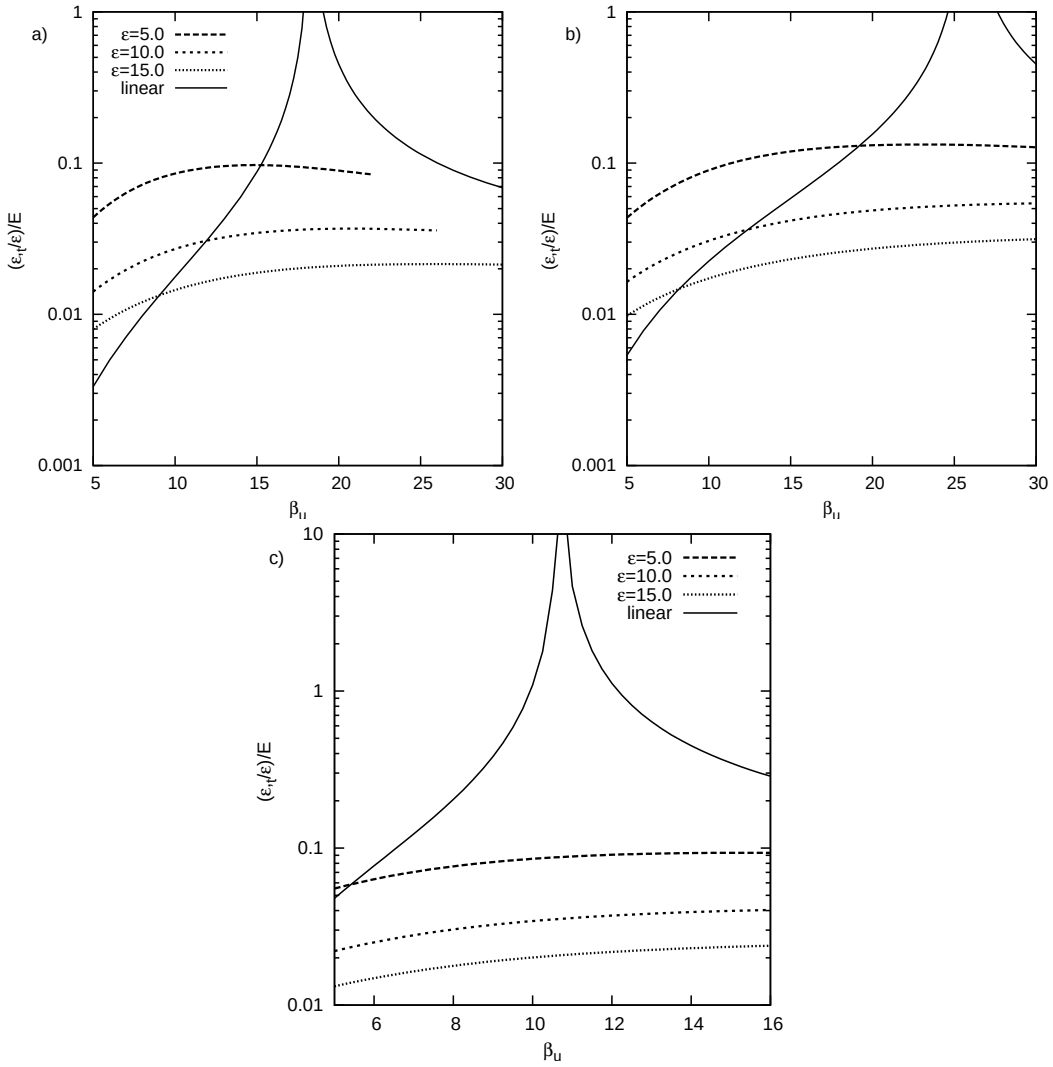

Figure 3.6: The values of meander amplification rate $\epsilon_{,t}/\epsilon$ divided by the erosion coefficient E corresponding to the selected wavenumbers for bend instability are reported versus the aspect ratio β_u for different values of the amplitude ϵ and compared with the values obtained in the context of the linear theory. (a) $d_s = 5 \cdot 10^{-3}$, $\vartheta_u = 0.1$, (b) $d_s = 5 \cdot 10^{-3}$, $\vartheta_u = 0.2$, (c) $d_s = 0.1$, $\vartheta_u = 0.1$

Chapter 4

Application to a case study

We now attempt to substantiate the soundness of the present non linear model by applying it to a short reach of the Cecina River (Tuscany, Italy), a gravel bed reach with actively migrating and growing outer banks (Romanelli *et al.* (2004)). We have compared the results with the linear model, simulating both the flow field and the bend stability. Furthermore we have performed a sensibility analysis varying the formative parameters.

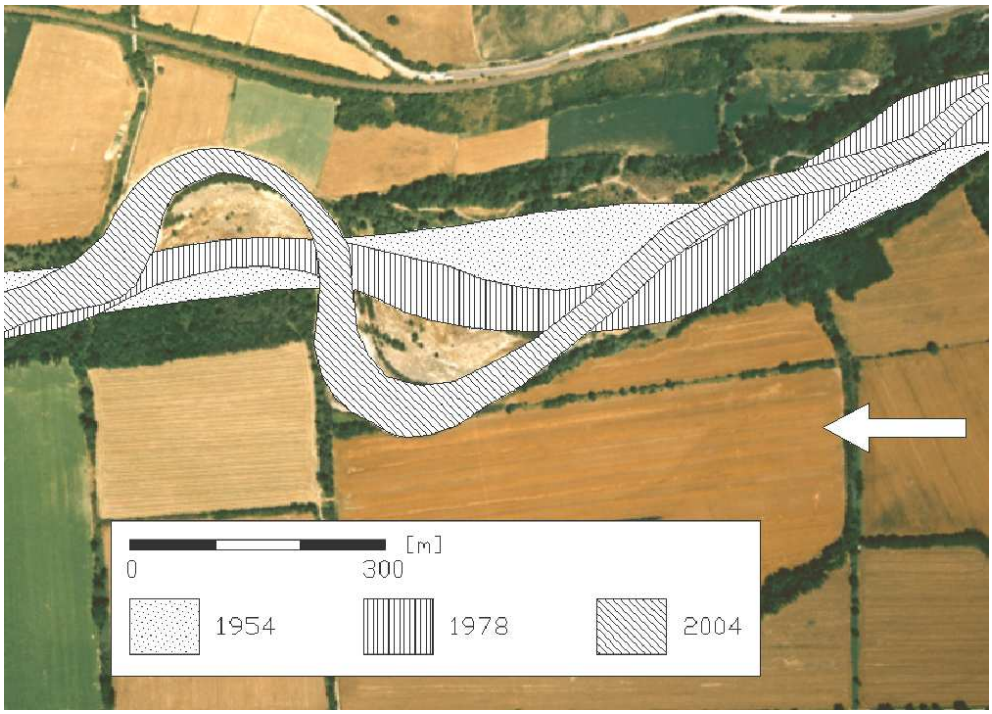

Figure 4.1: The reach of the Cecina River showing the formation of a meander from a nearly straight configuration. Flow is from right to left.

4.1 The Cecina River

The Cecina river basin is located in central Italy and comprises a basin surface area of approximately 900 km^2 with a total length of about 79 km. The study site is located a few kilometers upstream from the confluence between the tributary Sterza and the main course. The criteria guiding the selection of this site were the availability of aerial photographs taken at different years (1954, 1978, 1993, 2004) showing the formation of a meander from a nearly straight reach (Fig.4.1). The river evolution is described in the figures 4.2, 4.3, 4.4, 4.5. Data for the flow discharge were also available from a gauging station, located just downstream of the study site, at Ponte di Monterufoli. Grain size distributions were measured at the site and made available to the Authors (M. Rinaldi, personal communication). The study reach is about 1000 m long and is characterized by an average slope of about $i_{fu} = 0.002$.

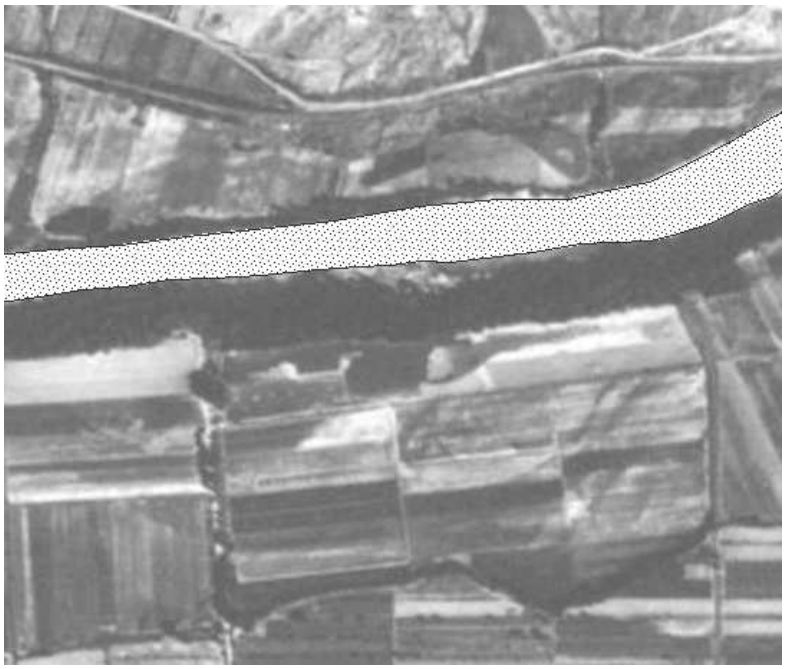

Figure 4.2: Cecina river in 1954

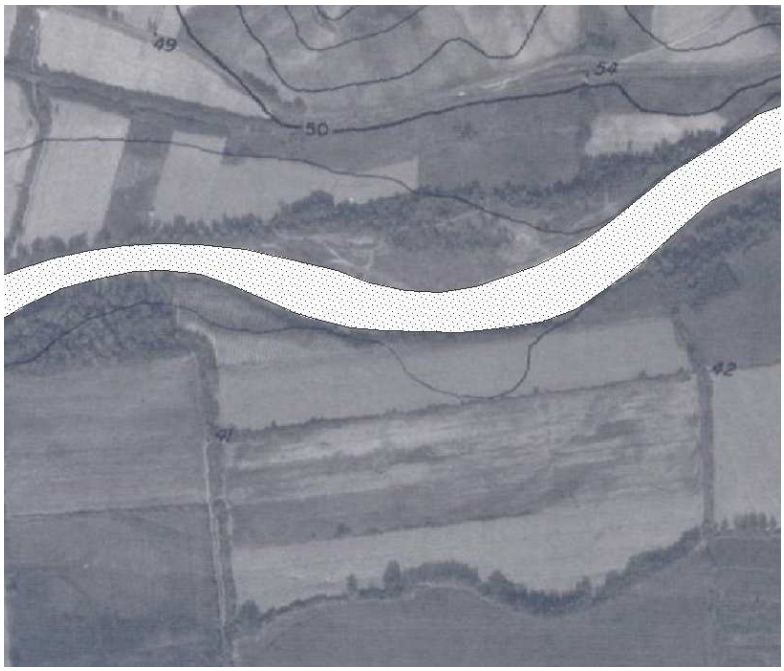

Figure 4.3: Cecina river in 1978

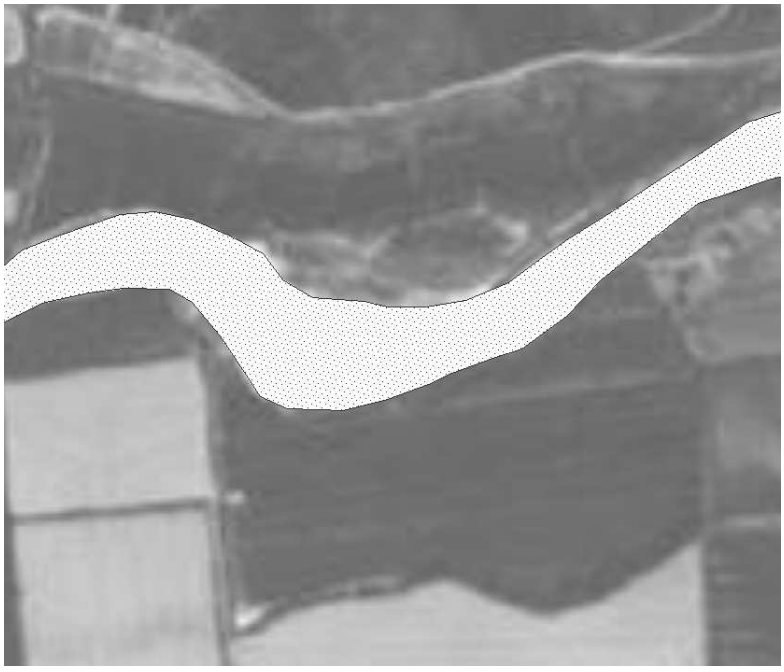

Figure 4.4: Cecina river in 1993

Figure 4.5: Cecina river in 2004

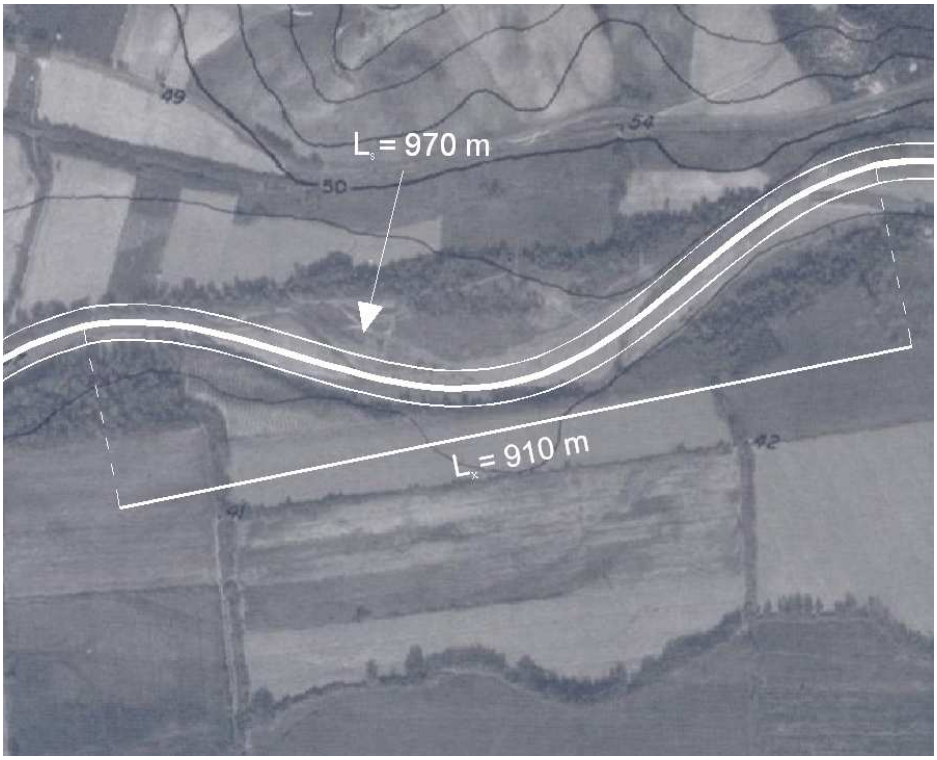

Figure 4.6: Cartesian and intrinsic wavelengths extrapolated from an aerial picture - 1978

The first group of numerical simulations was performed for a set of data obtained by extrapolating the plan form shape of the channel axis from a 1978 aerial picture. In that period Cecina channel left its straight set and began meandering, perhaps because of an antropogenic intervention. The shape turned out to follow closely a sine generated curve (Langbein & Leopold (1966)), characterized by a minimum radius of curvature $r_0^* \simeq 263$ m, a cartesian wavelength $L_x^* \simeq 910$ m, an intrinsic wavelength $L_s^* \simeq 970$ m and a channel width $2B_u^* \simeq 40$ m, taken to keep constant throughout the reach, as plotted in the figure 4.6. Sediments are modeled as uniform and characterized by $d^* = 7.4$ mm, characteristic value for the solid discharge and obtained by a volumetric sampling, and by $d^* = 19.5$ mm characteristic value for the bottom friction and obtained by a superficial bar sampling. The value of the effective water discharge $Q_u^* \simeq 110$ m^3/s (M. Rinaldi, personal communication) was used in the simulations, corresponding to a uniform flow depth of $D_u^* \simeq 1.3$ m.

4.2 Prediction of selected wave number: comparison between model and field observation

The values of the relevant parameters could then be calculated to give:

$$\begin{array}{lll} \beta_u \simeq 15.2 & \vartheta_u \simeq 0.216 & d_s \simeq 0.0056 \\ \nu_0 \simeq 0.076 & \lambda \simeq 0.129 & k \simeq 0.138 \\ i_{fu} \simeq 0.002 & & \end{array} \tag{4.1}$$

$$D_u^* \simeq 1.3\ m \quad B_u^* \simeq 20\ m \quad U_u^* \simeq 2.11\ m \tag{4.2}$$

From the 1954 aerial photo (figure 4.7) it is also possible to try and evaluate the magnitude of the initial perturbation of the channel axis. It can be easily noted that two parallel straight reaches, probably rectified by human intervention, are joined together by an oblique stretch. The distance between the two parallel straight reaches is roughly equal to two channel widths and finally let us estimate a value of $\epsilon = 4$. With the latter values, the model was then run to predict the equilibrium bed topography and the associated flow field.

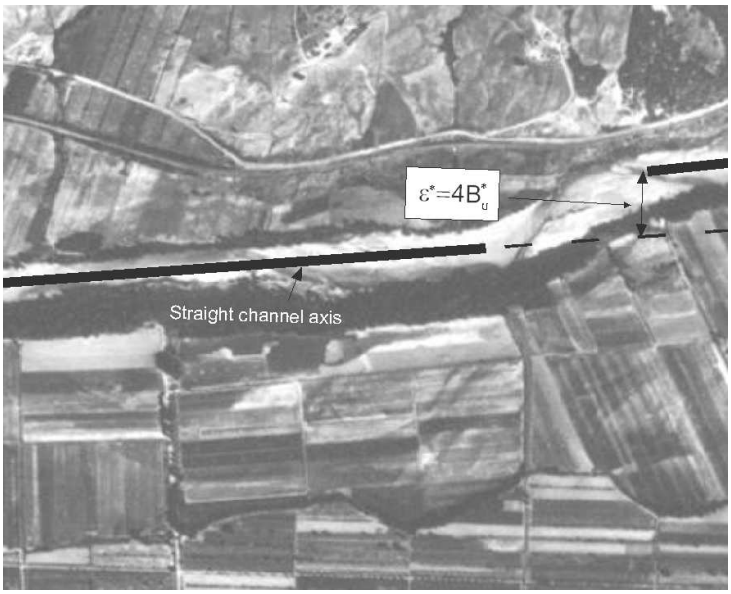

Figure 4.7: Initial perturbation of meandering process

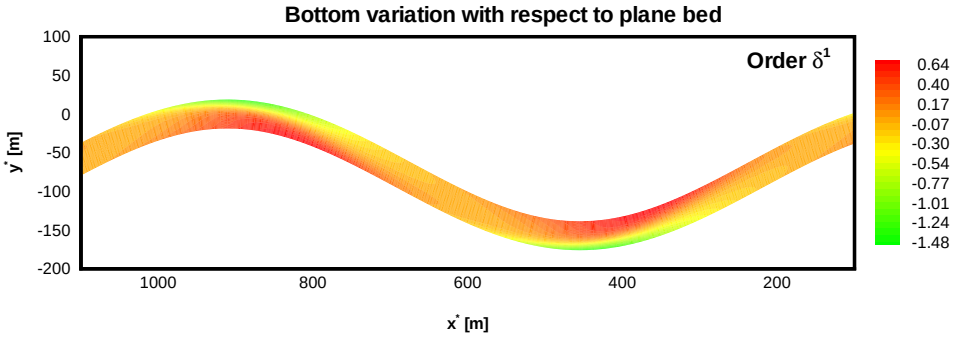

Figure 4.8: The equilibrium configuration of bed topography simulated in the Cecina river. Bed elevations (scaled by D_u^*) represent deviations from the averaged bottom associated with the mean longitudinal slope. Flow is from right to left.

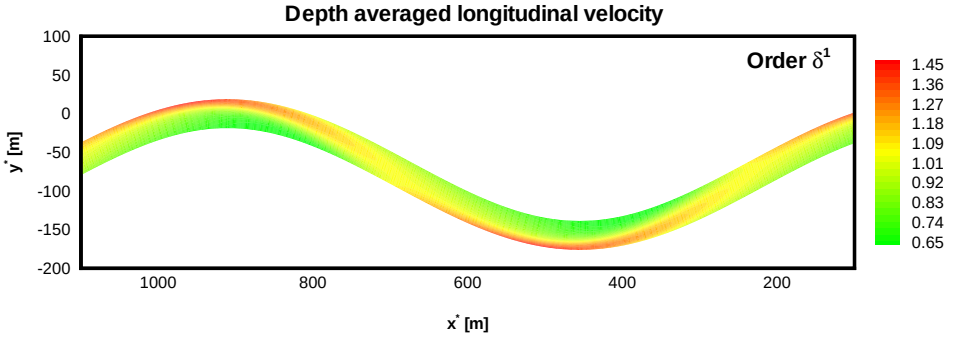

Figure 4.9: The pattern of longitudinal velocity (scaled by U_u^*) corresponding to the equilibrium configuration simulated in the Cecina river. Flow is from right to left.

The former is plotted in the figure 4.8 and shows that the value of the maximum scour depth relative to the mean bed elevation is slightly larger than the uniform flow depth and is roughly located at the bend apex. On the contrary, the position of the forced bars is upstream the bend apex and shows a value of bed elevation which does not lead to bar emergence. The corresponding values of the depth averaged longitudinal velocity predicted for this configuration are reported in the figure 4.9.

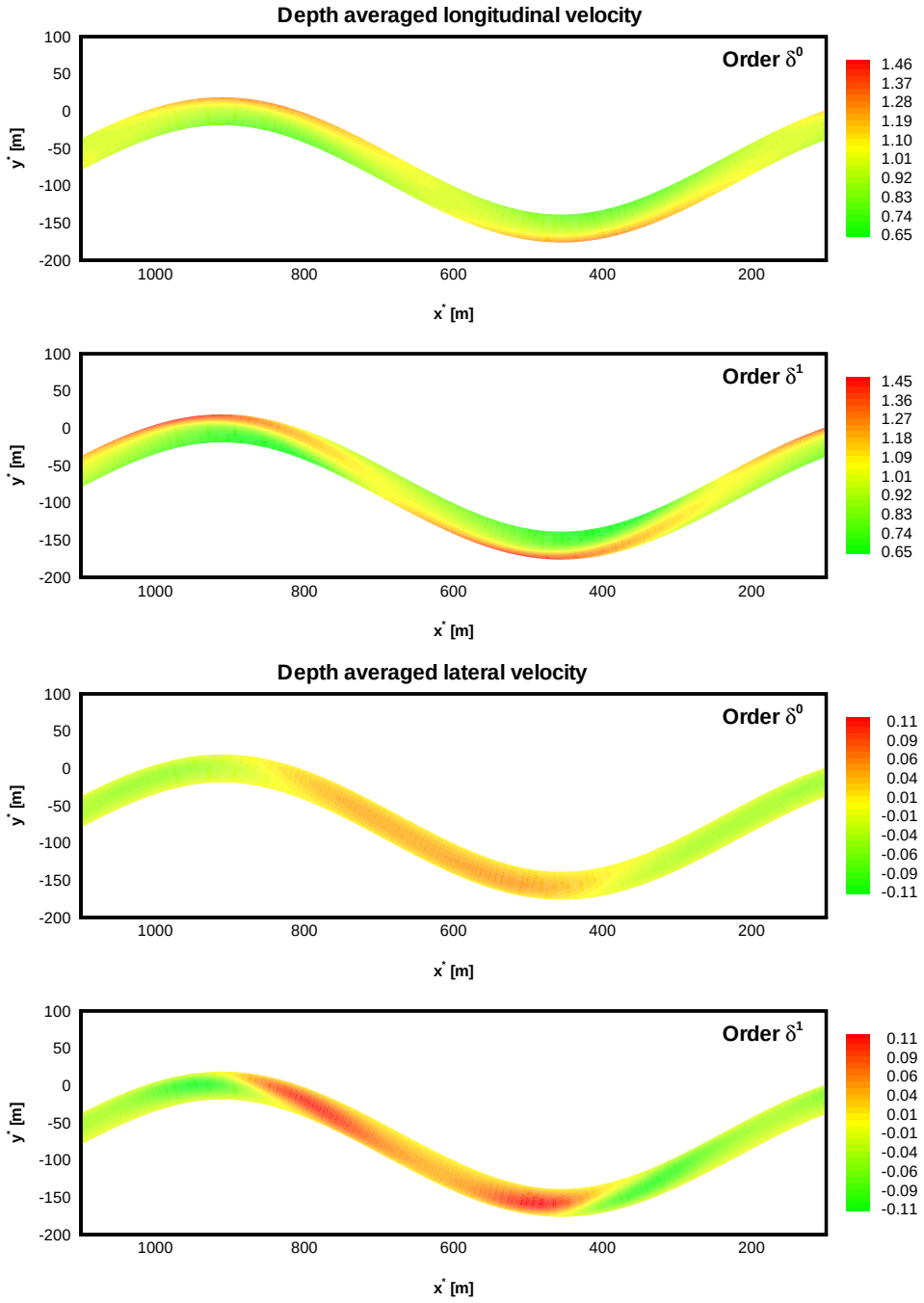

Figure 4.10: Effects of convective terms on the longitudinal and lateral velocity fields (values of speed scaled by U_u^*). Flow is from right to left.

Note that the thread of high velocity shifts from one side to the other side of the channel with distance along the meander, displaying a peak just downstream the bend apex. The value of the maximum velocity is slightly smaller than 3.1 m/s. It is also interesting to observe that the effect of convective terms increases the intensity of the flow fields and shifts the peak of maximum velocity from upstream to downstream of the bend apex (figures 4.10).

In figure 4.11 we have compared the non linear bottom topography with results obtained by the linear model. It is clear that the two configurations are significantly different: the linear topography has a pattern of scours and deposits symmetrical with respect to the channel axis, quite different from what observed in the field. Furthermore it is important to note that the linear model predicts a value for the dimensionless deposit of the forced bar greater than one: this implies that the bottom of the channel emerges. In figure 4.11 we have also compared the non linear longitudinal depth averaged velocity with respect to the linear model. We again observe that the flow field is symmetrical with respect to the channel axis. Although the intensity of the velocity is quite similar in the two models, the linear theory predicts a location of the velocity peak in the second quadrant, i.e. downstream of the bend apex, nearly at the inner bank. Finally, the comparison between the depth averaged lateral velocities reported in the figure 4.12, shows that the threads of high velocities in the linear and non linear solutions are significantly different in position along the meander, although not in absolute intensity.

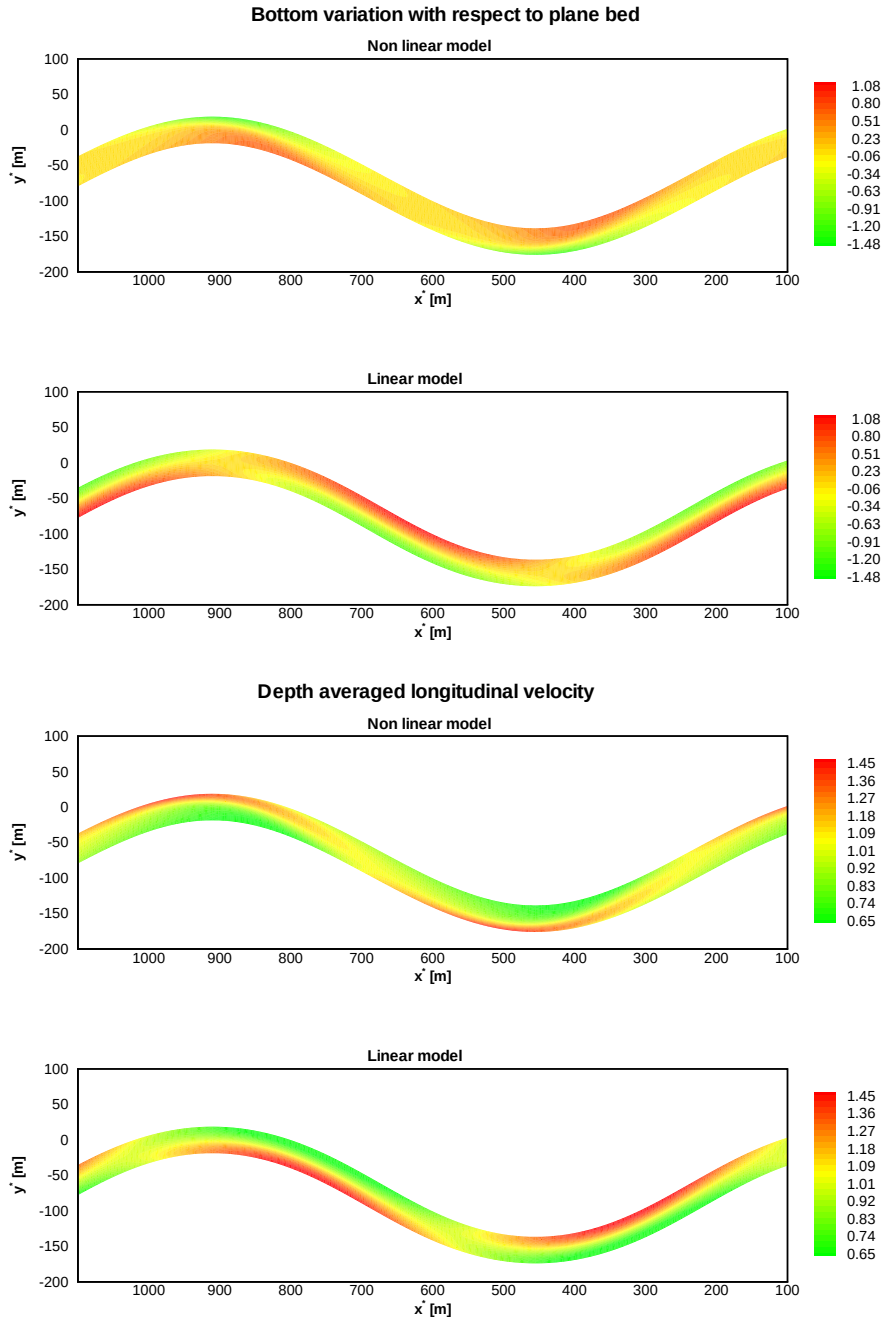

Figure 4.11: Comparison between non linear and linear model: perturbations of bed elevation (scaled by D_u^*) relative to the averaged bed elevation and pattern of depth averaged longitudinal velocity (scaled by U_u^*). Flow is from right to left.

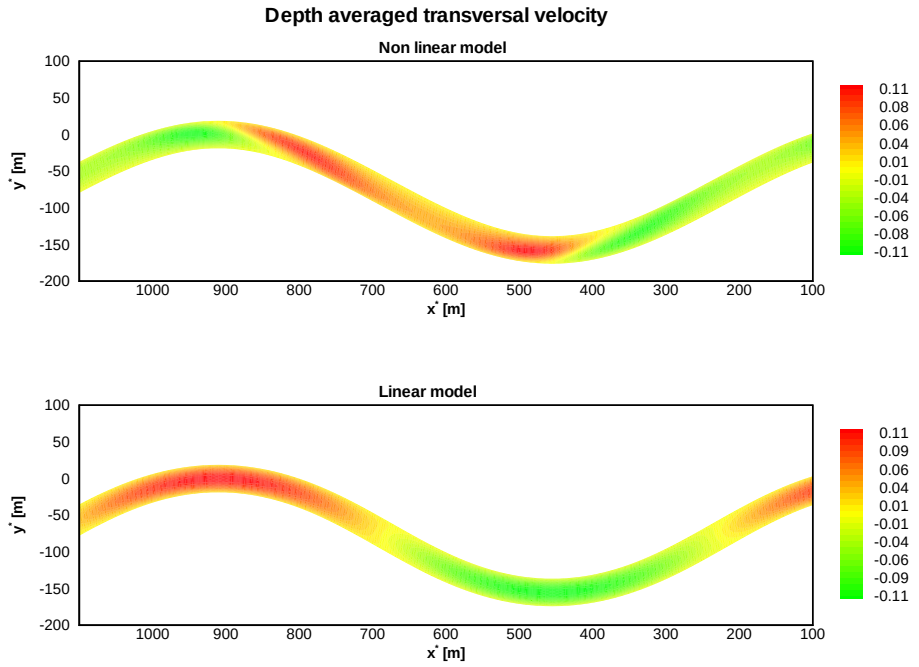

Figure 4.12: Comparison between non linear and linear model: pattern of depth averaged transversal velocity (scaled by U_u^*). Flow is from right to left.

A second simulation was performed in order to ascertain whether the model is able to predict the wavelength selected in the meandering process. The aerial picture of 1978 (figure 4.3) already shows evidence of a meandering process taking place downstream to the connection between the oblique and straight reaches. The intrinsic wavelength L_s^* of the incipient meander can be estimated at 970 m (corresponding to an intrinsic dimensionless wavenumber $\lambda = 0.129$) and the cartesian wavelength L_x^* can be estimated at 910 m (corresponding to a cartesian dimensionless wavenumber $k = 0.138$). The most recent pictures then clearly reveal the processes of meander amplification and downstream migration occurred from 1978 to 2004. In the figure 4.13 the meander amplification rate $\frac{\epsilon,t}{\epsilon}$ (scaled by the erosion coefficient E) is plotted versus the meander wavenumber for the values of the dimensionless parameters corresponding to the reach of the Cecina river considered as test case. The predicted value of the wavenumber selected by the non linear bend stability turns out to be $\lambda \simeq 0.134$ and corresponds to an intrinsic wavelength $L_s^* \simeq 938$ m, very close to the value estimated from the aerial pictures.

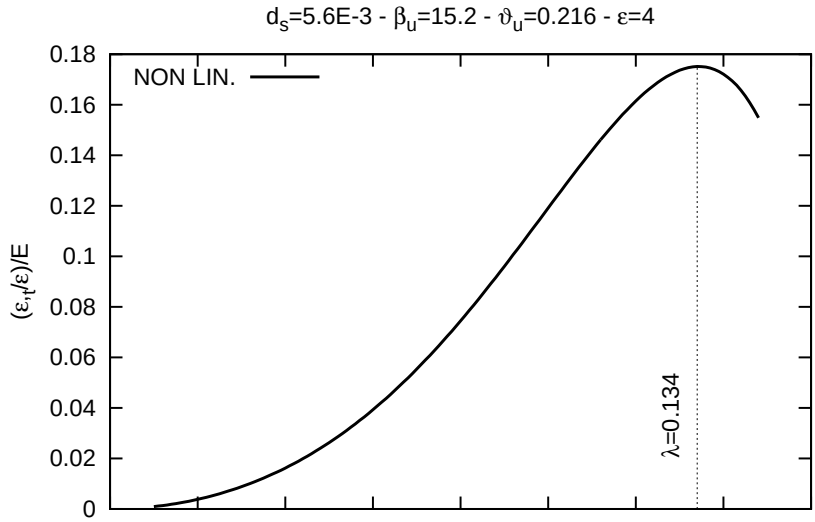

Figure 4.13: The meander amplification $\frac{\epsilon_{,t}}{\epsilon}$ scaled by the erosion coefficient E is plotted versus the intrinsic meander wavenumber for the Cecina River reach investigated. The wavenumber selected by the non linear bend instability turns out to be $\lambda \simeq 0.134$.

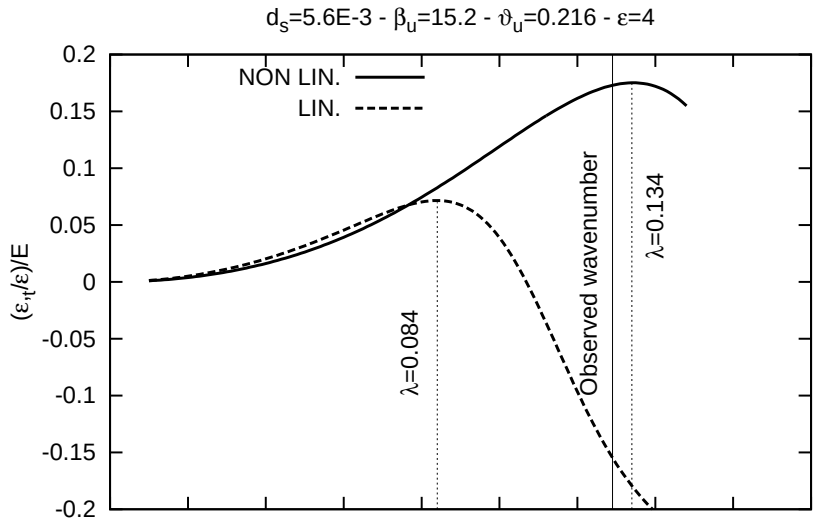

Figure 4.14: Comparison between results obtained by the non linear model and the linear model for the amplification coefficient. The intrinsic wavenumber selected by linear theory turns out to be $\lambda \simeq 0.084$, significantly smaller than the measured value.

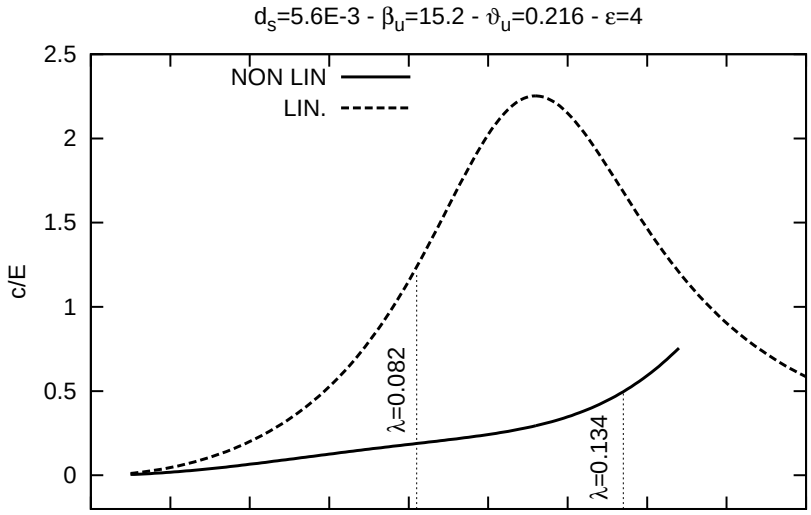

Figure 4.15: Comparison between results obtained by the non linear model and the linear model for the migration rate.

Furthermore in figure 4.14 and figure 4.15 we have compared results for the amplification rate $\frac{\epsilon_{,t}}{\epsilon}$ and for the migration speed c (both scaled by the erosion coefficient E) with results obtained by the linear theory. It turns out how the linear model tends to select meanders with a wavelength much longer than that estimated by aerial pictures. Furthermore in a a linear contest the observed wavelength $\lambda = 0.129$ would be dumped because the relative amplification rate is negative.

In order to verify the soundness of previous results we have performed a sensitivity analysis varying some of the formative parameters. In particular we have changed the most sensitive between the latters: the formative liquid discharge Q_E. In figure 4.16 we have reported the non linear amplification coefficient for different values of Q_E (in the range 50% Q_E - 150% Q_E). Comparison with the linear theory is reported in figure 4.17. We observe that results of the non linear model show that the selected wavenumber falls in the range $0.118 \leq \lambda \leq 0.165$, including the wavelength observed in the 1978 aerial picture. On the contrary, the linear theory underestimates the selected wavenumber which falls in the range between $0.062 \leq \lambda \leq 0.105$. Furthermore, the wavelength nearest to that observed corresponds to a bed topography such that part of cross section would emerge.

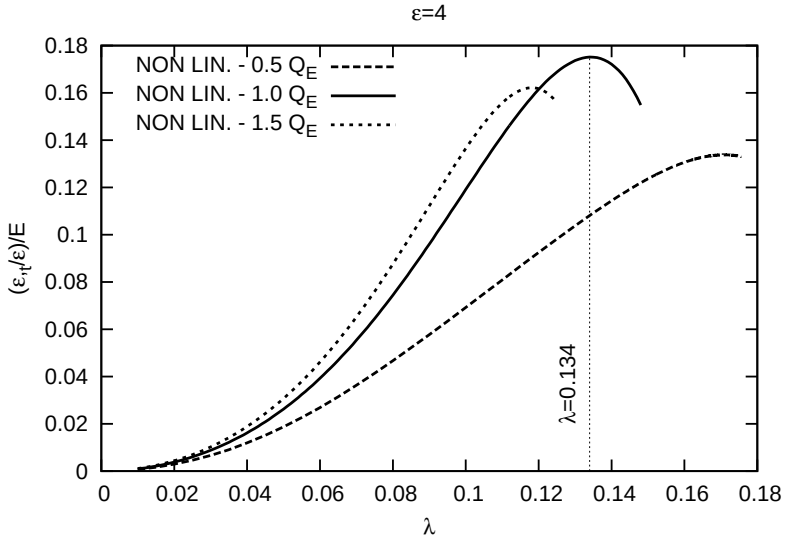

Figure 4.16: Variation of the amplification coefficient obtained by the non linear model in the range 50%Q_E - 150%Q_E.

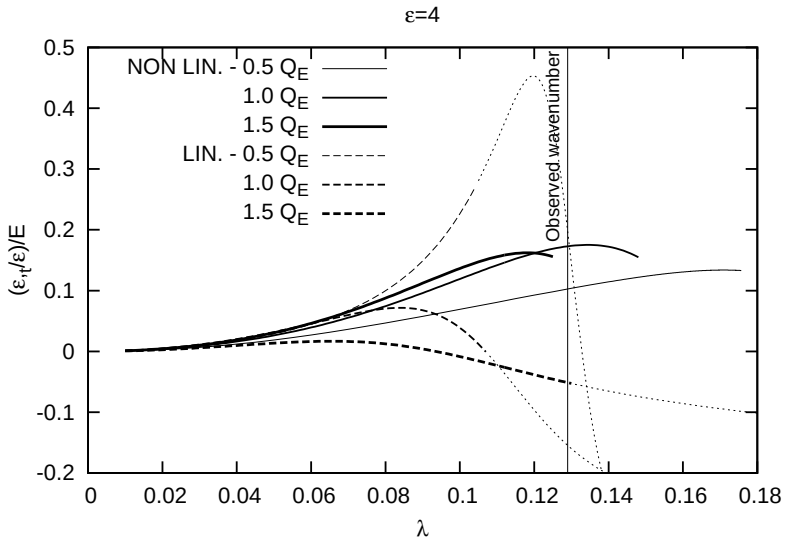

Figure 4.17: Comparison between results of the non linear model and of the linear theory: sensitivity analysis for the effect of the formative discarge Q_E. The linear model invariably underestimates the selected wavenumber; furthermore the values of wavelength nearest to the observed wavelength corresponds to a bed topography such that part of cross section would emerge.

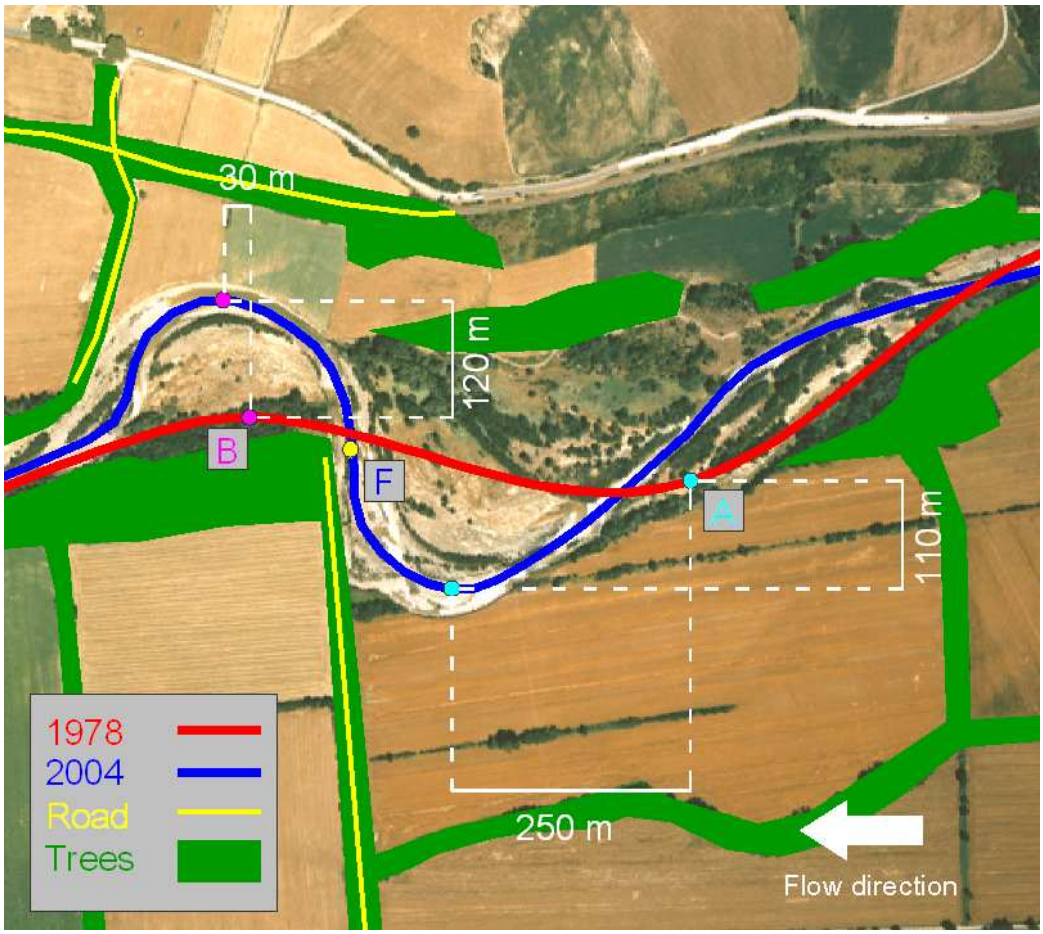

Figure 4.18: Planimetric evolution of the Cecina river from 1978 to 2004: observations.

The values of the amplification coefficient and of the migration rate provided by the non linear model appear to be consistent with field observations. In fact, referring to figure 4.18, it is possible to note the amplification and the downstream migration of both the upstream and downstream bends of the Cecina meander. One easily notes that the free amplifications of both apex point A and B are quite similar and attain values of $Y^* = 110\ m$ and $Y^* = 120\ m$, respectively. On the contrary, the migration of the downstream bend is much smaller than that of the upstream one: this is clearly due to the presence of a road and of some groups of tall trees, present since 1954 and quite distinct from shrubs and riparial vegetation which have slowed down the downstream evolution of the apex B and of the inflection point F.

We can then assume the value of $X^* = 250\ m$ as characteristic of the free downstream migration. Finally, as reported in table 4.3, it turns out that the non linear model predicts a ratio between migration and amplification rates equal to (+2.8), a value much closer to that observed in the field ($\frac{X^*}{Y^*} = +2.17$) than the value (+18.50) predicted by linear theory. Note that the value of the ratio obtained within the context of the present model is not dependent on the choice of the *dimensionless long term erosion coefficient* E, here just assumed to be constant along the entire meander.

	Non linear	*Linear*	*Observed* (2004 − 1978)
$Amplification\ rate$	+0.175	+0.072	−
$Migration\ rate$	+0.496	+1.330	−
$\frac{Migration}{Amplification}$	+2.800	+18.50	+2.17

(4.3)

4.3 Present configuration: equilibrium flow field and bed topography

In July 2007, in collaboration with a team led by Prof. Massimo Rinaldi, we have undertaken a topographic survey in order to determine the actual equilibrium bottom topography (figure 4.19) for the site of interest. From a glance at figure 4.19 it is possible to highlight immediately the presence of a deep scour located at the outer bank of the second bend, just upstream of the apex. To better analyze the results it is convenient to plot the variations of bottom elevation relative to an inclined plane characterized by the average channel slope.

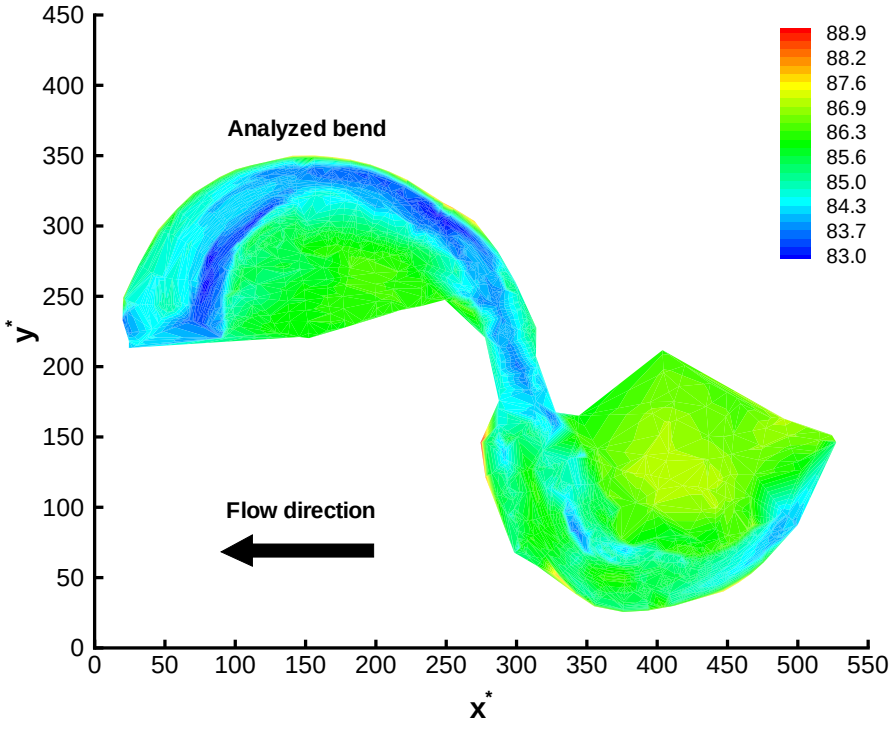

Figure 4.19: Bottom elevation (expressed in meters above m.s.l.) measured in the Cecina river reach in the survey of July 2007. Flow is from right to left.

We have firstly found the correct slope of the latter plane by best fitting the acquired data in the direction of the maximum slope. As we expected, the local longitudinal cartesian slope of the river is $i_x = 0.0023$, very close to the average slope used in the 1978 bend stability simulation and equal to the slope of the floodplain. As a first attempt we tried to perform a very rough and preliminary simulation of the bottom topography and flow field for the actual reach of the Cecina river. In fact, at this stage of development the non linear numerical code is not yet equipped to deal with non periodic planimetric configurations and with river width variations. Although in 1978 the Cecina river width was roughly constant and its planimetric configuration could be assumed to follow a sine generated curve, the latter features are not met in the present configuration (figure 4.20). With the only aim to substantiate the validity of the theoretical approach we then tried to define an average free surface width characterizing the Cecina river based on both the topographical survey and the aerial picture of 2007. In the straight reach just upstream the site of interest we estimated an average width of 20 m, slightly smaller than the value we best estimated in the curved reach, being roughly equal to $2B_u^* = 25\ m$. We then used the latter value for the following simulation. It was possible, at this point, to determine the correct elevation of the inclined plane making sure that the intersection of the latter with measured data generated an average free surface width equal to $2B_u^*$ and, consequently, a point bar nearly emerged. We then plotted the differences between the reference inclined plane and the measured data of bottom elevation (figure 4.21). To perform a simulation of flow and bed topography in the surveyed bend, we also need to estimate the formative parameters. In order to obtain the latters we evaluated the intrinsic wavenumber λ and the curvature parameter ν_0 of the meander from the aerial picture of 2007 (figure 4.20). The formative water discharge Q_u^* was finally estimated such as to generate in the model a nearly emerged point bar. The values of the relevant parameters thus obtained and used in the simulation were:

$$\begin{array}{lll} \beta_u \simeq 12.6 & \vartheta_u \simeq 0.128 & d_s \simeq 0.0077 \\ \nu_0 \simeq 0.12 & \lambda \simeq 0.1085 & \\ i_{fu} \simeq 0.00164 & & \end{array} \tag{4.4}$$

$$\begin{array}{lll} D_u^* \simeq 0.95\ m & B_u^* \simeq 25\ m & U_u^* \simeq 1.96\ m \\ Q_u^* \simeq 45\ \frac{m^3}{s} & & \end{array} \tag{4.5}$$

Figure 4.20: Comparison between the simulated wavelength and the actual planimetric configuration (from Google Earth). Flow is from right to left.

In figure 4.21 we show the comparison between the observed flow depth and the results obtained by the non linear and the linear models, respectively. We find that, consistently with measured data, the non linear theory predicts a maximum (minimum) flow depth at the outer bank (inner bank) located just downstream (upstream) the bend apex. Note that the bar is almost emerged. On the contrary, although the intensity is quite similar, the linear model predicts a phase lag of the maximum depth relative to the bend apex much larger than the non linear one, while the extension of the scour region is much larger than the measured one.

We note that, as shown in figure 4.22, the non linear model predicts a maximum depth averaged velocity located downstream of the bend apex. On the contrary, the maximum velocity predicted by the linear model is located close to the inflection point and the thread of high velocity is very elongated, reaching the next bend apex at the inner bank. Consequently, the amplification coefficient in this case is very close to zero, hence preventing the meander amplification detected in recent years. In figure 4.23 we plot the average lateral velocity. The non linear model predicts that, just upstream the bend apex, the average transversal velocity is positive (directed from the inner to the outer bank). This leads to a shift of the thread of high longitudinal velocity which is consistently located at the outer bank just downstream the bend apex. In the following table the main quantitative results are reported.

	Non linear	*Linear*	*Data*
$D_{max}\ [m]$	$+2.73$	$+2.80$	$+2.62$
D_{min}	$+0.06$	-0.85	$\simeq 0.00$
$U_{max}\ [\frac{m}{s}]$	$+2.96$	$+3.68$	$-$
U_{min}	$+0.64$	$+0.35$	$-$
$V_{max}\ [\frac{m}{s}]$	$+0.20$	$+0.31$	$-$
V_{min}	-0.20	-0.31	$-$

(4.6)

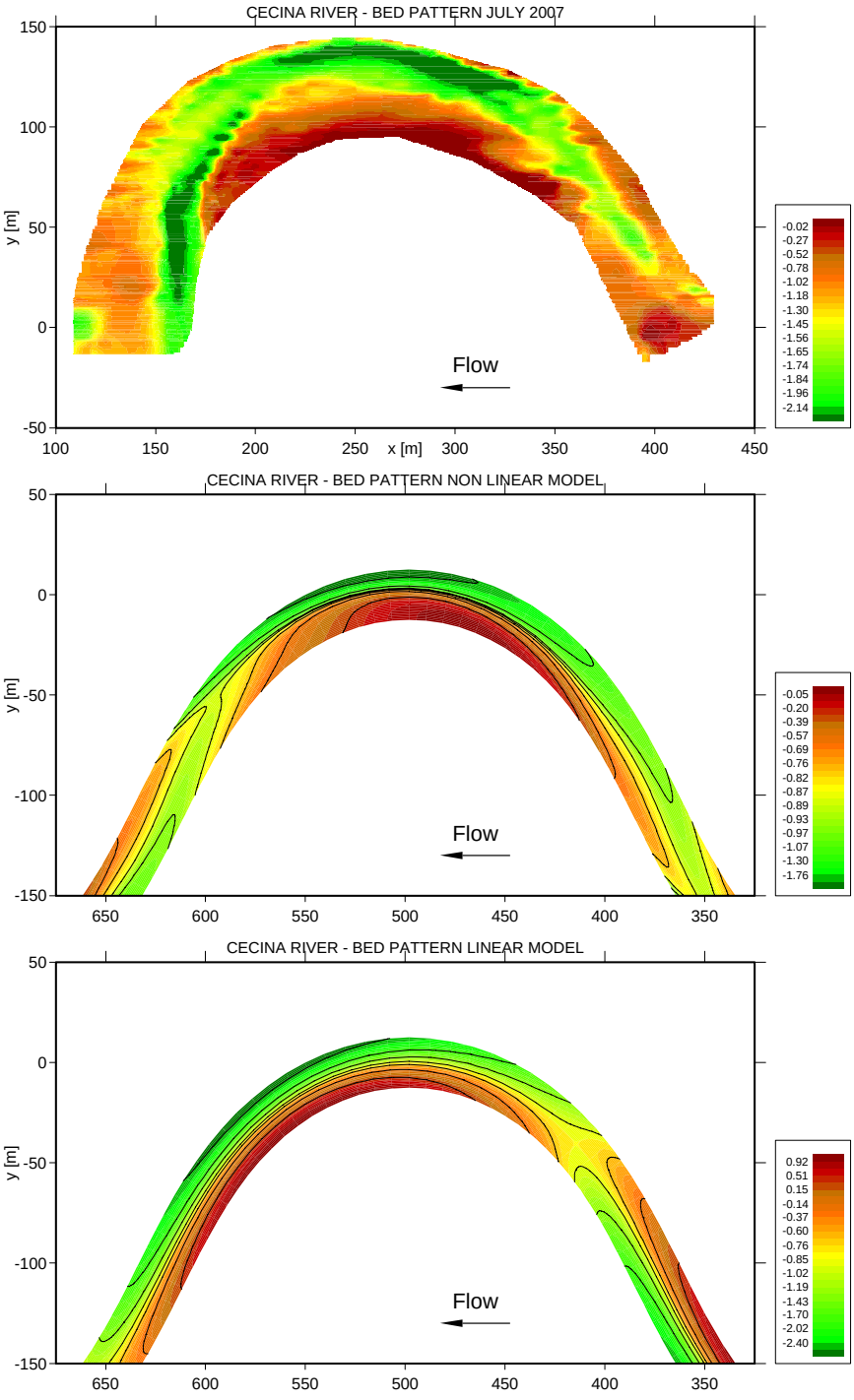

Figure 4.21: Comparison between measured values of flow depth (in meters) in the Cecina river and the values obtained using the present non linear and linear models for the 2007 planimetric configuration. Flow is from right to left.

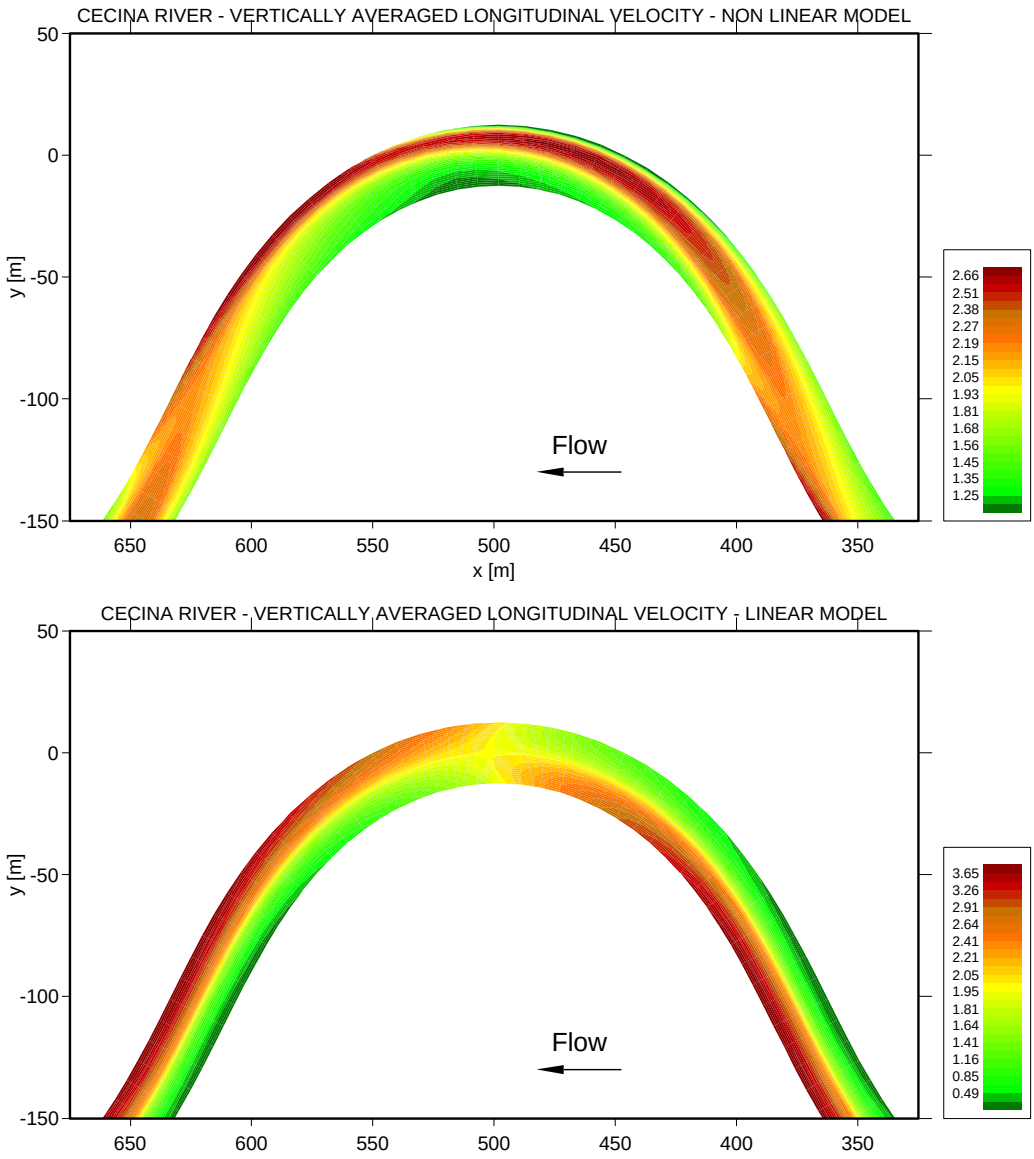

Figure 4.22: Comparison between the values of longitudinal average velocity (in meters/second) obtained using the present non linear and linear models for the 2007 planimetric configuration. Flow is from right to left.

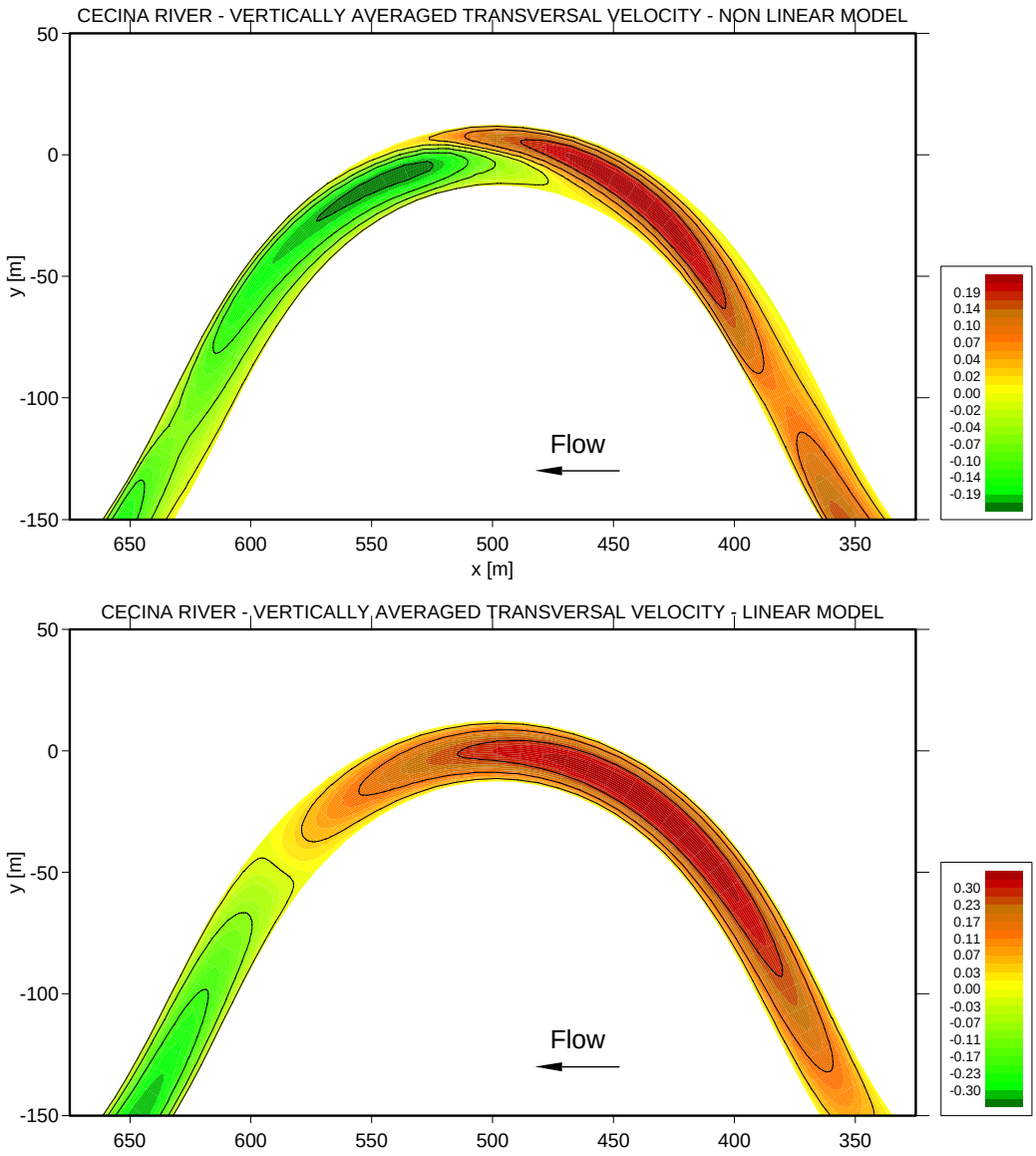

Figure 4.23: Comparison between the values of transversal average velocity (in meters/second) obtained using the present non linear and linear models for the 2007 planimetric configuration. Flow is from right to left.

Conclusions

A non linear asymptotic theory of flow and bed topography in meandering channels able to describe finite amplitude perturbations of bottom topography and account for arbitrary, yet slow, variations of channel curvature has been developed. This model appears to be a potentially useful and powerful tool for many purposes. Firstly, as shown in the present work, one can formulate a non linear bend instability theory, which predicts several characteristic features of the actual meandering process and extends results obtained by classical linear bend theories. In particular, we have found that:

- for given values of the relevant physical parameters, the bend growth rate peaks at some value of the meander wavenumber, reminiscent of (but typically larger than) the resonant value of linear stability theory: a result confirming the weakly non linear results of Seminara & Tubino (1992), consistently with field observations which show that the wavelength selected by traditional linear theories is typically larger than observed values;

- the selected wavenumber depends on the amplitude of the initial perturbation (for given value of the relevant dimensionless parameters) and, in particular, larger wavelengths (smaller wavenumbers) are associated with larger amplitudes ϵ: a feature typical of non linear waves;

- the infinite peak in the linear response at resonance is damped by non linearity: a result again confirming its weakly non linear counterpart;

- meanders are found to migrate preferentially downstream, though upstream migration is also possible, at least in principle, for relatively large values of the aspect ratio of the channel, a finding in agreement with the picture provided by the linear theory of Zolezzi & Seminara (2001);

- meanders slow down as their amplitude increases (for given value of the relevant dimensionless parameters), again a feature typical of non linear waves, driven in the present case by flow rather than geometric nonlinearities.

In conclusion, the picture offered by results obtained through the present theory seems fully satisfactory and consistent with field observations as well as previous theoretical findings. Further substantiation of the model has been achieved by comparing predictions obtained for a test case (a reach of the Cecina River, Italy) with field observations.

The availability of this model suggests a number of interesting future developments.

Firstly, the present model can be readily extended to allow also for slowly varying variations of channel width: such an extension may allow insight on the mechanism controlling the development of width oscillations correlated with channel curvature observed in nature. Moreover, the stability of the solution for flow and bed topography thus obtained may shed some light on the observed occurrence of island formation in river bends, along with the tendency of the stream to bifurcate eventually leading to chute cutoff.

A second extension of the present model can be obtained by coupling the flow field with a bank erosion law, leading to prediction of the plan form evolution of the meandering pattern accounting not only for geometric non linearity but also for flow nonlinearity, the present approach requiring a computational effort much smaller than that needed by numerical solutions of the full 3-D governing equations or their shallow water version (e.g. Mosselman (1991), Shimizu (2002) among others).

Finally, a third line of development can be readily obtained by allowing for slow temporal variations of flow and sediment supply: the morphological response of the channel to a sequence of flood events can then be investigated. Such an investigation would possibly provide a rational interpretation of the as yet loosely defined notion of 'formative discharge of an alluvial river'.

Appendix A

Linearizations

A.1 Linearization of eddy viscosity ν_t

In the present section we report the expansion procedure employed for the eddy viscosity. Starting from the definition of shear velocity in dimensionless form:

$$u_*^2 = \frac{\nu_T \sqrt{C_{fu}}}{D} u_{,\xi} \,|_{\xi_0} + O(\delta^2) \tag{A.1}$$

we expand ν_T, D, u and u_* in powers of δ:

$$u_{*0}^2 \left(1 + 2\delta \frac{u_{*1}}{u_{*0}}\right) = \frac{\nu_{T0}\sqrt{C_{fu}}}{D_0} u_{0,\xi} \,|_{\xi_0} \left[1 + \delta \left(\frac{u_{1,\xi}}{u_{0,\xi}}|_{\xi 0} - \frac{D_1}{D_0} + \frac{\nu_{T1}}{\nu_{T0}}\right)\right] \tag{A.2}$$

Hence, we find:

$$u_{*0}^2 = \frac{\nu_{T0}\sqrt{C_{fu}}}{D_0} u_{0,\xi} \,|_{\xi_0} \tag{A.3}$$

$$2\frac{u_{*1}}{u_{*0}} = \frac{u_{1,\xi}}{u_{0,\xi}}|_{\xi 0} - \frac{D_1}{D_0} + \frac{\nu_{T1}}{\nu_{T0}} \tag{A.4}$$

Expanding (1.15) we also find that:

$$\nu_{T0}\left(1 + \delta \frac{\nu_{T1}}{\nu_{T0}}\right) = \frac{\mathcal{N}(\xi)}{\sqrt{C_{fu}}} u_{*0} D_0 \left(1 + \delta \left[\frac{D_1}{D_0} + \frac{u_{*1}}{u_{*0}}\right]\right) \tag{A.5}$$

from which we obtain:

$$\nu_{T0} = \frac{\mathcal{N}(\xi)}{\sqrt{C_{fu}}} u_{*0} D_0 \tag{A.6}$$

$$\frac{\nu_{T1}}{\nu_{T0}} = \left[\frac{D_1}{D_0} + \frac{u_{*1}}{u_{*0}} \right] \tag{A.7}$$

An expression for $\frac{u_{*1}}{u_{*0}}$ is readily obtained substituting from (A.7) into (A.4):

$$\frac{u_{*1}}{u_{*0}} = \frac{u_{1,\xi}}{u_{0,\xi}}|_{\xi 0} \tag{A.8}$$

Finally, an expression for u_{*0}^2 can be obtained from (A.3) integrating (1.48) once. We find:

$$(\nu_{T0} u_{0,\xi}\,)\,|_{\xi_0} = D_0^2 \sqrt{C_{fu}} R_0 \tag{A.9}$$

hence, from (A.3), (A.9), (A.6) and (A.7) we obtain an expression for the eddy viscosity at different orders:

$$\nu_{T0} = D_0^{3/2} \mathcal{N}(\xi) \sqrt{R_0} \tag{A.10}$$

$$\frac{\nu_{T1}}{\nu_{T0}} = \frac{D_1}{D_0} + \frac{u_{1,\xi}}{u_{0,\xi}}|_{\xi 0} \tag{A.11}$$

It's important to note that equation (A.11) is not a function of ξ but depends only on the normalized conventional reference level ξ_0.

A.2 Linearization of dimensionless solid discharge ϕ

In the following section we briefly report the procedure employed to expand the dimensionless solid discharge ϕ.

Firstly, we observe that the dimensionless shear stress can be obtained by (1.20), in the form:

$$\theta = \frac{\sqrt{C_{fu}}\,(\nu_T u_{,\xi})\,|_{\xi_0}}{D(s-1)gd^*_{50}}U^*_u \;+\; O(\delta^2) = \frac{\theta_u}{\sqrt{C_{fu}}}\frac{1}{D}\,(\nu_T u_{,\xi})\,|_{\xi_0} \;+\; O(\delta^2) \tag{A.12}$$

where $\theta_u = \frac{U^{*2}_u C_{fu}}{(s-1)gd^*_{50}}$.

Hence, expanding the left side of equation (A.12) we obtain:

$$\theta = \theta_0 + \delta\ \theta_1 \tag{A.13}$$

Expanding the right side of (A.12) at order $O(\delta^0)$ we find:

$$\theta_0 = \frac{\theta_u}{\sqrt{C_{fu}}}\frac{1}{D_0}\,(\nu_{T0} u_{0,\xi})\,|_{\xi_0} \tag{A.14}$$

Using (1.48) the latter relationship may be written in the form:

$$\theta_0 = \theta_u D_0 R_0 \tag{A.15}$$

Furthermore, at order $O(\delta^1)$, the expansion of the right side of equation (A.12), after some algebra, gives:

$$\theta_1 = \frac{\theta_u}{\sqrt{C_{fu}}} \left[\frac{1}{D_0} \frac{u_{1,\xi}}{u_{0,\xi}} |_{\xi_0} \left(\nu_{T0} u_{0,\xi} \right) |_{\xi_0} + \frac{1}{D_0} \frac{\nu_{T1}}{\nu_{T0}} \left(\nu_{T0} u_{0,\xi} \right) |_{\xi_0} - \frac{D_1}{D_0^2} \left(\nu_{T0} u_{0,\xi} \right) |_{\xi_0} \right] \tag{A.16}$$

Using (1.48) and (A.11) we eventually find:

$$\frac{\theta_1}{\theta_0} = 2 \frac{u_{1,\xi}}{u_{0,\xi}} |_{\xi_0} \tag{A.17}$$

At this stage it is possible to expand the generic relation for the dimensionless solid discharge ϕ in powers of the small parameter δ using a particular bed load transport relationship. In the following we report the treatment for the classical Meyer-Peter and Müller and Parker equations.

Meyer-Peter and Müller

$$\phi = 8\,(\theta - \theta_c)^{3/2} \qquad \theta > \theta_c \tag{A.18}$$

At order $O(\delta^0)$ we find:

$$\phi_0 = 8\,(\theta_0 - \theta_c)^{3/2} \qquad \theta_0 > \theta_c \tag{A.19}$$

At order $O(\delta^1)$ we obtain:

$$\frac{\phi_1}{\phi_0} = \frac{3}{2}\frac{\theta_1}{\theta_0}\left(\frac{\theta_0}{\theta_0 - \theta_c}\right) \qquad \theta_0 > \theta_c \tag{A.20}$$

Parker

$$\phi = 0.00218\ \theta^{3/2}\ G(\zeta) \qquad \zeta = \frac{\theta}{\theta_r} \qquad \theta_r = 0.0386 \tag{A.21}$$

$$G(\zeta) \quad \begin{cases} 5474\left(1-\frac{0.853}{\zeta}\right)^{4.5} & \zeta \geq 1.59 \\ e^{14.2(\zeta-1)-9.28(\zeta-1)^2} & 1 \leq \zeta < 1.59 \\ \zeta^{14.2} & \zeta < 1 \end{cases}$$

At order $O(\delta^0)$ we find:

$$\phi_0 = 0.00218\ \theta_0\ G_0(\zeta) \qquad \zeta_0 = \frac{\theta_0}{\theta_r} \tag{A.23}$$

$$G_0(\zeta) \quad \begin{cases} 5474\left(1-\frac{0.853}{\zeta_0}\right)^{4.5} & \zeta_0 \geq 1.59 \\ e^{14.2(\zeta_0-1)-9.28(\zeta_0-1)^2} & 1 \leq \zeta_0 < 1.59 \\ \zeta_0^{14.2} & \zeta_0 < 1 \end{cases}$$

At order $O(\delta^1)$ we obtain:

$$\frac{\phi_1}{\phi_0} = \frac{G_1}{G_0}(\zeta)\ +\ \frac{3}{2}\frac{\theta_1}{\theta_0} \tag{A.24}$$

$$\frac{G_1}{G_0}(\zeta) \quad \begin{cases} \frac{4.5}{1-\frac{0.853}{\zeta_0}}\frac{0.853}{\zeta_0}\frac{\theta_1}{\theta_0} & \zeta_0 \geq 1.59 \\ \left[14.2-18.56(\zeta_0-1)\right]\zeta_0\frac{\theta_1}{\theta_0} & 1 \leq \zeta_0 < 1.59 \\ 14.2\frac{\theta_1}{\theta_0} & \zeta_0 < 1 \end{cases}$$

Appendix B

The integral criterion for bank erosion

In this section we prove the consistency of the proposed integral criterion applied in the present non linear bend theory and compare it with the local criterion employed in classical linear analyses.
Following Blondeaux & Seminara (1985), we denote by (x_a^*, y_a^*) the Cartesian coordinates of the channel axis written in the form:

$$y_a^* = \epsilon^*(t)\cos(k^* x^* - w^* t^*) \tag{B.1}$$

Normalizing equation (B.1) we obtain:

$$y_a = \epsilon(t)\cos(kx - wt) \tag{B.2}$$

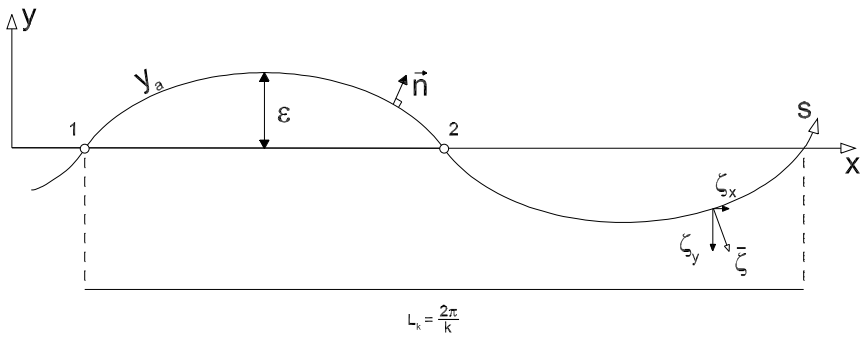

Figure B.1: Sketch illustrating channel axis and notations

Furthermore we write the dimensional curvature in the form:

$$\mathcal{C}^* = -\frac{y^{*''}}{\left[\sqrt{1+y^{*'2}}\right]^3} \tag{B.3}$$

Assuming (B.1), recalling (1.10) and substituting into (B.3) the dimensionless curvature $\mathcal{C}$ can be easily expressed as follows:

$$\mathcal{C}(x) = \frac{\frac{\epsilon k^2}{\nu_0}\sin(kx)}{\left[\sqrt{1+(\epsilon k)^2\cos^2(kx)}\right]^3} \tag{B.4}$$

Since we have scaled the radius of curvature of the channel axis by its minimum value, the maximum value of the dimensionless curvature has to attain the value $\mathcal{C} = 1$. Hence, it can be readily shown that the following relation must hold:

$$\nu_0 = \epsilon k^2 \tag{B.5}$$

At this point, it is important to note that the bank erosion vector $\vec{\zeta}$ is related to the temporal derivative of the channel axis, as sketched in figure B.2:

$$\vec{\zeta} = \vec{n}\left(\frac{\partial y_a}{\partial t}\cos\alpha\right) = \vec{n}|\vec{\zeta}| \tag{B.6}$$

Furthermore, using (B.2), we also read:

$$\mathbf{n} = (n_x, n_y) = \frac{(\epsilon k\sin(kx-wt)\ ,\ 1)}{\sqrt{1+\epsilon^2k^2\sin^2(kx-wt)}} = (\sin\alpha, \cos\alpha) \tag{B.7}$$

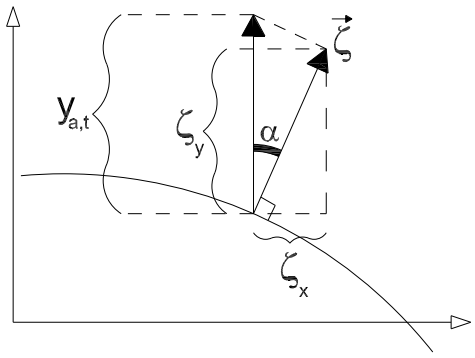

Figure B.2: Sketch illustrating the relation between $\vec{\zeta}$ and $y_{a,t}$

Hence using (B.2), (B.6) and (B.7) we readily obtain the cartesian components of the bank erosion rate:

$$\zeta_x = \frac{\epsilon k \sin(kx - wt)\left[\epsilon_{,t} k \cos(kx - wt) + \epsilon w \sin(kx - wt)\right]}{\left[\sqrt{1 + \epsilon^2 k^2 \sin^2(kx - wt)}\right]^2} \tag{B.8}$$

$$\zeta_y = \frac{\left[\epsilon_{,t} k \cos(kx - wt) + \epsilon w \sin(kx - wt)\right]}{\left[\sqrt{1 + \epsilon^2 k^2 \sin^2(kx - wt)}\right]^2} \tag{B.9}$$

Following a procedure similar to that developed by Ikeda *et al.* (1981), defining an *erosion coefficient* E, we can also write:

$$\vec{\zeta} = \vec{n}\ \left(E\left[\delta U\right]|_{n=1}\right) \tag{B.10}$$

where $\delta U|_{n=1}$ is the perturbation of the longitudinal depth averaged velocity due to secondary flow evaluated at the outer bank. Thus, if we assume a linear model for the flow field we obtain:

$$U|_{n=1} = 1 + U_1 \nu_0 \cos(kx - wt - \theta_1) \tag{B.11}$$

where θ_1 is the phase lag of velocity with respect to curvature. Substituting from (B.11) into (B.10), using (B.5) and (B.7) we find:

$$\zeta_x = \frac{\epsilon k \sin(kx - wt)\left[E\epsilon k^2 U_1 \cos(kx - wt)\cos\theta_1 + \sin(kx - wt)\sin\theta_1\right]}{\sqrt{1 + \epsilon^2 k^2 \sin^2(kx - wt)}} \tag{B.12}$$

$$\zeta_y = \frac{\left[E\epsilon k^2 U_1 \cos(kx - wt)\cos\theta_1 + \sin(kx - wt)\sin\theta_1\right]}{\sqrt{1 + \epsilon^2 k^2 \sin^2(kx - wt)}} \tag{B.13}$$

Taking advantage of the assumptions that ν_0 and ϵ be small, noting that $c = \frac{w}{k}$ and comparing (B.8 - B.9) with (B.12 - B.13) we readily find the following relations:

$$\frac{\epsilon_{,t}}{\epsilon E} = k^2 U_1 \cos\theta_1 \tag{B.14}$$

$$\frac{c}{E} = k U_1 \sin\theta_1 \tag{B.15}$$

which represent the *growth rate and the wave speed scaled by the erosion coefficient* E found within a linear context.

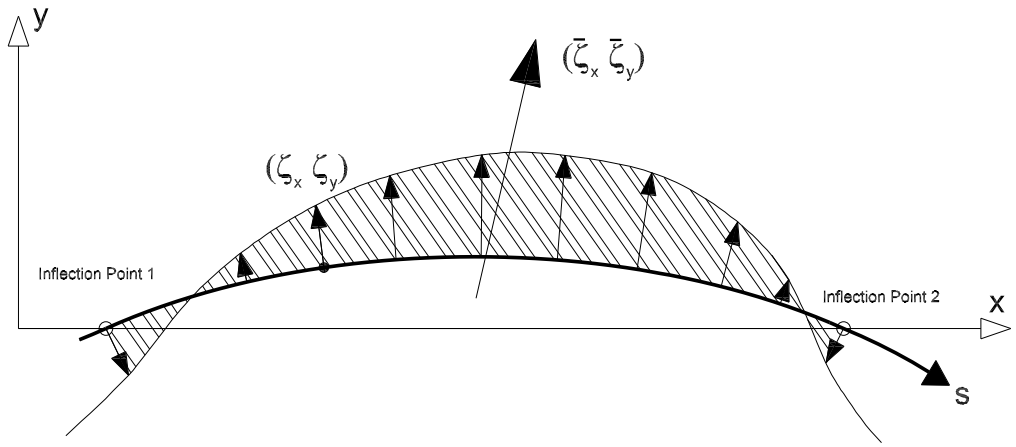

Figure B.3: Sketch illustrating the integral criterion proposed

Next we show the consistency of the integral criterion proposed. Let us evaluate the average migration vector $\left(\bar{\zeta}_x, \bar{\zeta}_y\right)$ integrating the local value of $\zeta(s)$ along the intrinsic coordinate s, between two consecutive inflection points. Taking advantage of the relation existing between cartesian and intrinsic coordinates x and s:

$$ds = \sqrt{1 + \left(\frac{\partial y}{\partial x}\right)^2}\, dx \tag{B.16}$$

and using (B.8), (B.9) according with the small amplitude ϵ of perturbation we obtain:

$$\frac{\bar{\zeta_x}}{E} = \frac{\lambda}{\pi}\int_{s_1}^{s_2} \zeta_x(s)\ ds\ = \frac{\lambda}{\pi}\int_{x_1}^{x_2} \zeta_x(x)\ dx = \frac{\lambda}{\pi}\int_{x_1}^{x_2} \left(\epsilon_{,t}\epsilon k \sin(kx-wt)\cos(kx-wt) + \epsilon^2 wk \sin^2(kx-wt)\right)\ dx \tag{B.17}$$

$$\frac{\bar{\zeta_y}}{E} = \frac{\lambda}{\pi}\int_{s_1}^{s_2} \zeta_y(s)\ ds\ = \frac{\lambda}{\pi}\int_{x_1}^{x_2} \zeta_y(x)\ dx = \frac{\lambda}{\pi}\int_{x_1}^{x_2} \left(\epsilon_{,t}\cos(kx-wt) + \epsilon w \sin(kx-wt)\right)\ dx \tag{B.18}$$

Finally, due to the fact that x_1 and x_2 represent cartesian coordinates of two consecutive inflection points, we find:

$$\frac{c}{E} = \frac{\bar{\zeta_x}}{E}\ \ \frac{2}{k\lambda\epsilon^2} \tag{B.19}$$

$$\frac{\epsilon_{,t}}{\epsilon E} = \frac{\bar{\zeta_y}}{E}\ \ \frac{k\pi}{2\epsilon\lambda} \tag{B.20}$$

The equations (B.19) and (B.20) clearly show that evaluating the normalized *wave celerity* ($\frac{c}{E}$) and the normalized *growth rate*($\frac{\epsilon_{,t}}{\epsilon E}$), in a non linear context, by integrating numerically the local value of the migration vector along the intrinsic coordinate s is a consistent procedure. It is worth noticing that $O(\frac{\bar{\zeta_x}}{E}) \sim (\nu_0^2 = \epsilon^2\lambda^4)$ and $O(\frac{\bar{\zeta_y}}{E}) \sim (\nu_0 = \epsilon\lambda^2)$ hence, the equations (B.19) and (B.20) are bounded even in the limits $\epsilon \to 0$ or $\lambda \to 0$.

Appendix C

Numerical procedure

In this section we describe the numerical resolution procedure we have followed in order to solve equation (1.81).
Let us discretize the meander into a number of N cross sections each of them characterized by P points in the transversal direction. To integrate the relation $(D_{0,n})_{j,k}$ along the cross section j, from the inner ($k = 0$) to the outer ($k = P$) bank, we need a boundary condition for the partial differential equation and a starting value for the unknown function $h_{00,\sigma}$, representing the correction of free surface slope with respect to the basic uniform flow.
Note that longitudinal derivatives appear in the integro-differential equation (1.81), hence it follows that there is the need to solve simultaneously all the N integro-differential equations (1.81) at every cross section. When the integration process is terminated on the outer bank ($k = P$) we have obtained the numerical values attained by the integral constraints (1.82) and (1.83). Hence at each cross section j we can evaluate the differences between the liquid and the solid discharges computed and the assigned values which have to be satisfied. Denoting by φ_j and ϕ_j the latter residual errors, we have to find the values of the boundary conditions in all meander sections such that the functions $\varphi_j(j = 1..N)$ and $\phi_j(j = 1..N)$ vanish:

$$\begin{aligned} \varphi_j &= \int_{-1}^{+1} D_0^{3/2} I_{F_0} dn - 2(1-\xi_u) = \varphi_j\left(D_0|_{m,0}\ ,\ h_{00,\sigma}|_m\ ,\ m = 1..N\right) \\ \phi_j &= \int_{-1}^{+1} q_{\sigma_0} dn - 2\Phi_u = \phi_j\left(D_0|_{m,0}\ ,\ h_{00,\sigma}|_m\ ,\ m = 1..N\right) \\ & \qquad\qquad [j = 1..N] \end{aligned} \tag{C.1}$$

In other words, the mathematical problem is reduced to a system of $2N$ non linear algebraic equations (φ_j , ϕ_j $-\, j = 1..N$) in $2N$ unknowns ($D_0|_{j,0}$, $h_{00,\sigma}|_j$ $-\, j = 1..N$). Therefore, the problem is well posed and can be resolved by a trial and error algorithm. Below we shortly describe the resolution procedure:

1. Firstly we start with a set of trial values of $D_0|_{j,0}$ and $h_{00,\sigma}|_j$ at each cross section j at the inner bank ($k = 0$);
   A

2. We then evaluate all the local quantities and calculate the longitudinal derivatives. With this purpose we have employed a centred scheme accurate at second order;
   A

3. Next we integrate simultaneously all the N integro-differential equations (1.81) along the transversal direction to the next point $k = 1$. This is done employing an Euler-Cauchy implicit method;
   A

4. We repeat **steps 2-3** until we reach the outer bank ($k = P$);
   B

5. It is then possible to calculate the values of the functions φ_j and ϕ_j in all the N cross sections and verify if they attain a vanishing value;
   C

6. Finally we return to **step 1**, change, by a trial and error procedure, the values of the initial conditions and repeat the procedure until at **step 5** the constraints are satisfied in every cross section;
   A

To evaluate the longitudinal derivatives at the end sections $j = 1$ and $j = N$ we impose periodicity conditions.
It is important to note that this resolution method, coupled with the analytical solution of the equations along the vertical axis, allows us to solve for both the flow field and bed topography in a very fast way. For example, if the initial conditions are "well posed", a meander discretized into $N = 108$ longitudinal cross sections and $P = 50$ points along the transversal direction, can be computed in a few seconds on a standard PC. Furthermore, vertical motion is analitycal and can be represented by any number of points without affecting computational speed, resulting into an approach many orders of magnitude faster than the fully numerical 3D solution.

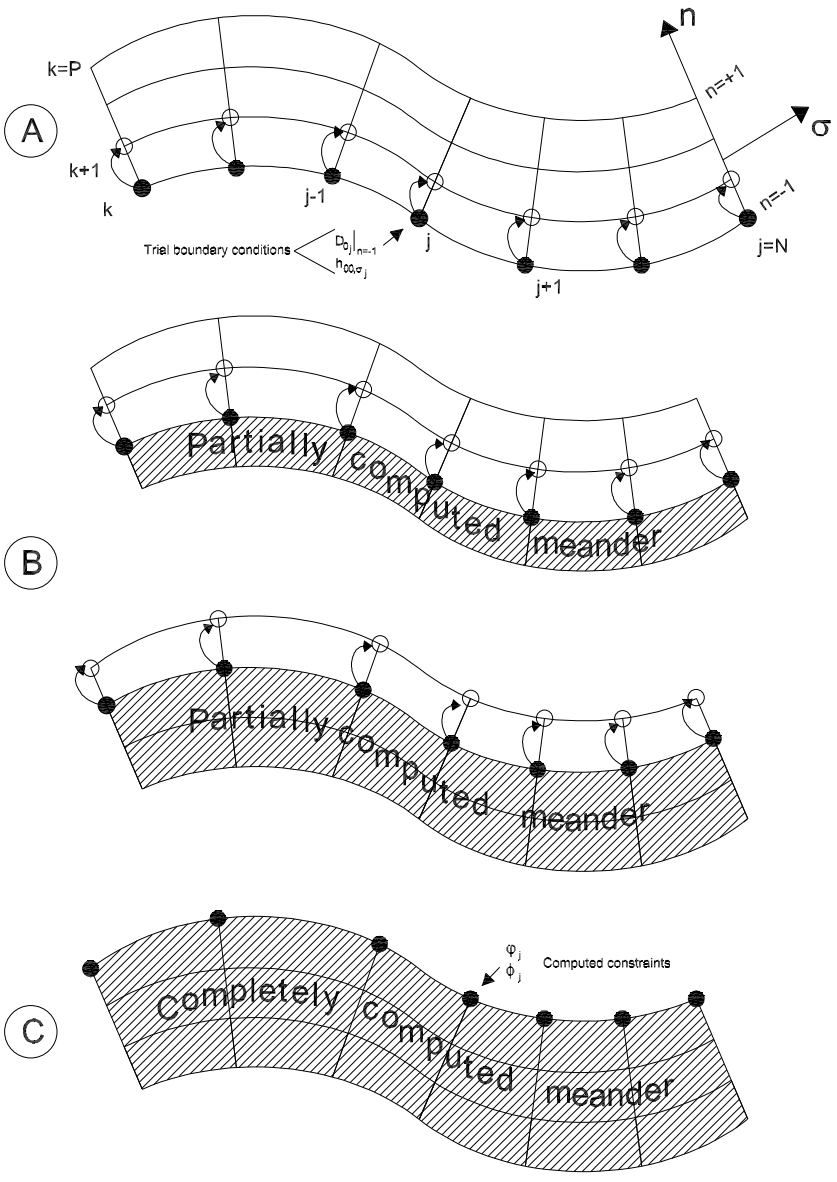

Figure C.1: Sketch illustrating the numerical procedure we have employed to obtain the bottom and the flow field along the meander

Appendix D

The mechanism responsible for the correction of free surface slope

In this section we discuss the mechanism responsible for the increase experienced by the average free surface slope relative to the equivalent straight case. At leading order assume that the uniform flat bed configuration is slightly perturbed by the effects of curvature $\mathcal{C}$ of the channel axis and by the consequent secondary flow which is proportional, say, to some curvature parameter δ. Hence, we write:

$$D_0 = 1 + \delta n \mathcal{C} \tag{D.1}$$

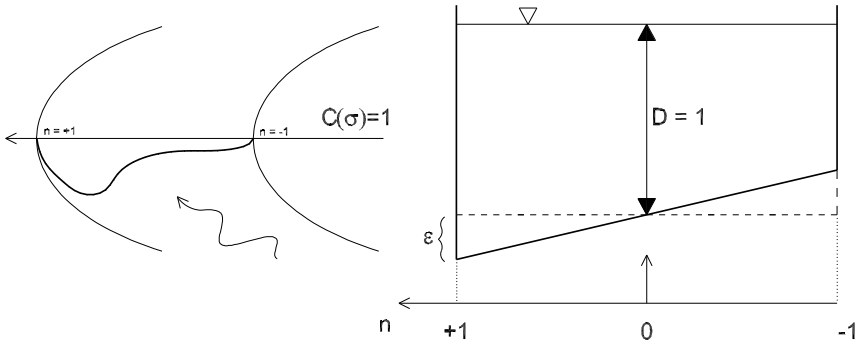

Figure D.1: Sketch illustrating bed deformation near the apex $\mathcal{C} = 1$

We then evaluate the solid discharge ϕ. The latter obviously depends on the value of the dimensionless shear stress at the bottom, which reads:

$$\theta = \theta_0 + \delta\theta_1 \tag{D.2}$$

where, referring to equations (A.15) and (A.17), θ_0 and θ_1 represent contributions due to the depth variations (which we have assumed to be proportional to the curvature parameter) and longitudinal variations of bottom velocity (which appear at first order due to convective effects).

Hence, if we assume the flow as fully developed or, in other words, if we neglect longitudinal derivatives (A.17) with (1.89), (1.95), (E.31), (E.33), (E.35) and (D.1) gives:

$$\frac{\theta_1}{\theta_0} = -n\mathcal{C}\beta_u\sqrt{C_{fu}} - \frac{3\mathcal{C}^2\gamma}{\beta_u C_{fu}}\delta + O(\delta^2) \tag{D.3}$$

with the coefficient $\gamma = \int_{\xi_0}^{1} F_0 G_1 \, d\xi$ representing the depth averaged contribution of the convective term $uv_{,n}$. It is important to note that, if we neglect the role of longitudinal derivatives, the latter integral only depends on the normalized conventional reference level ξ_0. As sketched in figure D.2 the latter term $\int_{\xi_0}^{1} uv_{,n} \, d\xi$ is positive. At A and B we note that, close to the free surface, the transversal velocity v is directed from the inner to the outer bank (positive) and is associated with a positive longitudinal velocity u greater than the one experienced near the bottom, where v is directed inwards (negative): this implies that a net transport of longitudinal momentum $\int_{\xi_0}^{1} uv \, d\xi$ occurs towards the outer bank of the cross section. Furthermore the vertical distribution of both longitudinal and transversal velocity is greater near the outer bank with respect to the inner one and this implies, following the same line of reasoning, that also the terms $\int_{\xi_0}^{1} uv_{,n} \, d\xi$ is positive. We will then show that the contribution γ has a crucial influence on the longitudinal slope of the free surface averaged over one meander wavelength.

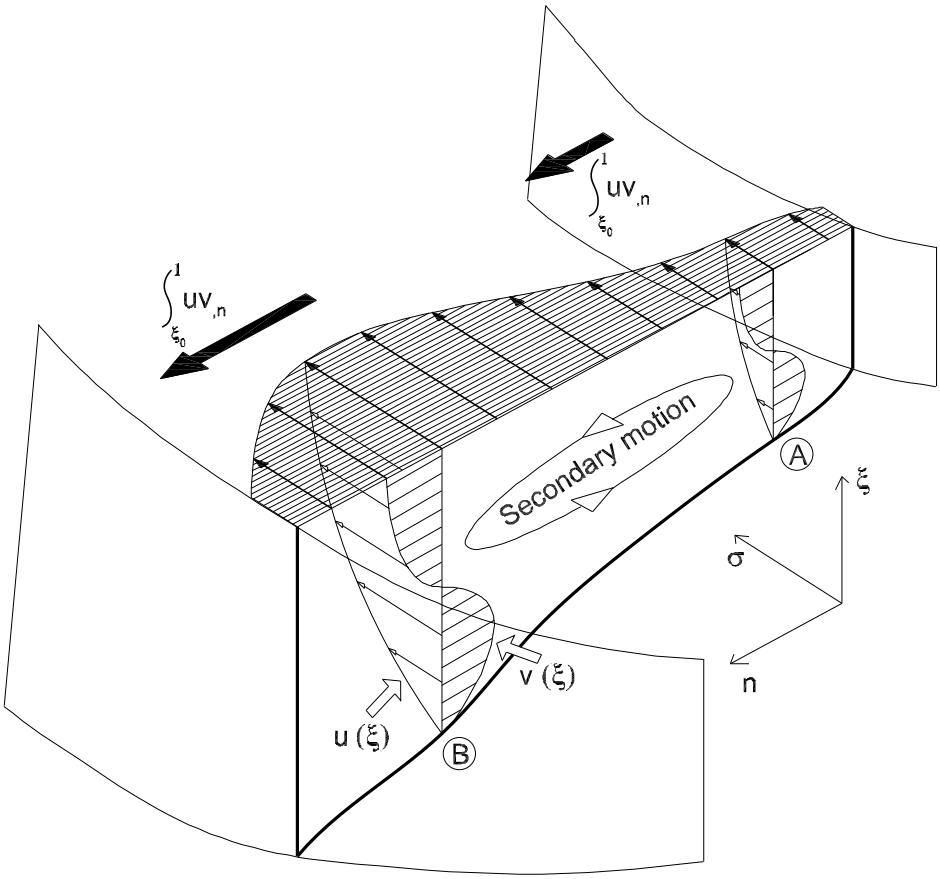

Figure D.2: Lateral transfer of longitudinal momentum

Hence, we write:

$$\theta = \theta_u R_0 \left[1 + \delta \left(n\mathcal{C} - n\mathcal{C}\beta\sqrt{C_{fu}} \right) + \delta^2 \left(-\frac{3\mathcal{C}^2\gamma}{\beta_u C_{fu}} - n^2\mathcal{C}^2\beta\sqrt{C_{fu}} \right) \right]$$

$$R_0 = 1 - \frac{h_{00,\sigma}}{\sqrt{C_{fu}}} \tag{D.4}$$

The expansion in powers of δ of the dimensionless total solid discharge Φ evaluated by means of Meyer-Peter and Müller relationship (A.18) integrated along the transversal section, after some algebra, takes the form:

$$\Phi = \int_{-1}^{1} \phi \, dn = \Phi_0 \left\{ 1 + \delta^2 \chi \right\} \tag{D.5}$$

$$\Phi_0 = 16 \left(\theta_u R_0 - \theta_c \right)^{3/2}$$

$$\chi = \chi_D + \chi_u$$

$$\chi_D = \frac{\mathcal{C}^2}{8} \left(\frac{\theta_u R_0}{\theta_u R_0 - \theta_c} \right)^2$$

$$\chi_u = \chi_{u_m} + \chi_{u_\gamma}$$

$$\chi_{u_m} = \frac{\mathcal{C}^2 \beta_u \sqrt{C_{fu}}}{8} \left(\frac{\theta_u R_0}{\theta_u R_0 - \theta_c} \right)^2 \left(\beta_u \sqrt{C_{fu}} - 2 \right) - \frac{\mathcal{C}^2 \beta_u \sqrt{C_{fu}}}{2} \left(\frac{\theta_u R_0}{\theta_u R_0 - \theta_c} \right)$$

$$\chi_{u_\gamma} = -\frac{\mathcal{C}^2 \beta_u \sqrt{C_{fu}}}{2} \left(\frac{\theta_u R_0}{\theta_u R_0 - \theta_c} \right) \frac{9\gamma}{\beta_u C_{fu}^{3/2}} \tag{D.6}$$

where Φ_0 represents the leading order total dimensionless solid discharge, χ_D is the perturbation of the latter due to depth variations and χ_u is the contribution due to convective effects. The latter can be splitted into a metric term χ_{u_m} and into a contribution generated by the transversal transport of momentum χ_{u_γ}.

At this point, neglecting changes in the free surface slope ($R_0 = 1$), the function Φ_0 collapses into the uniform flow total dimensionless solid discharge Φ_u and it turns out that the entire function χ is invariably negative within a large part of the parameter space, as reported in figure D.4.

Hence, the total solid discharge integrated in the cross section Φ is reduced with respect to Φ_u and consequently the flow has to locally increase its free surface slope ($R_0 > 1$) to compensate for the corresponding decrease of the total solid discharge. Furthermore, also note that the two contrasting effects χ_D (which increases the solid discharge) and χ_u (which decreases the solid discharge) appear at the same order of magnitude $O(\delta^2)$, hence the fact that their sum χ is negative is independent of δ.

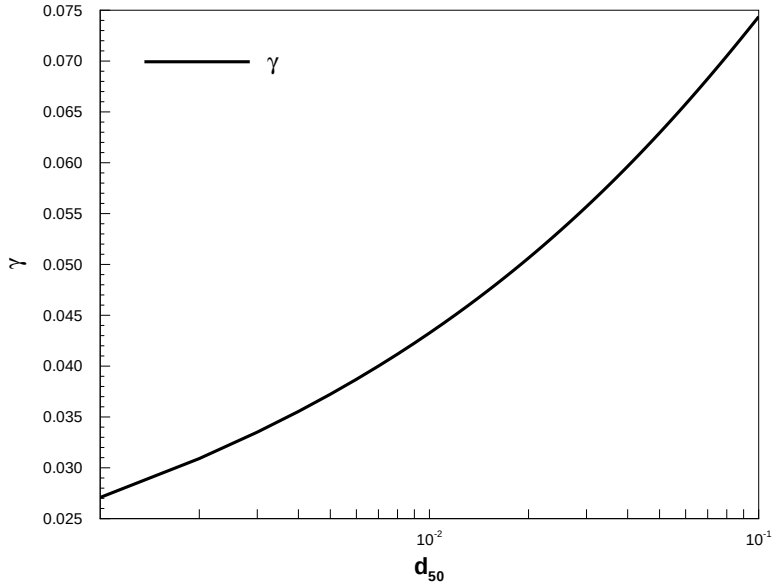

Figure D.3: Function $\gamma = \int_{\xi_0}^{1} F_0 G_1 \, d\xi$.

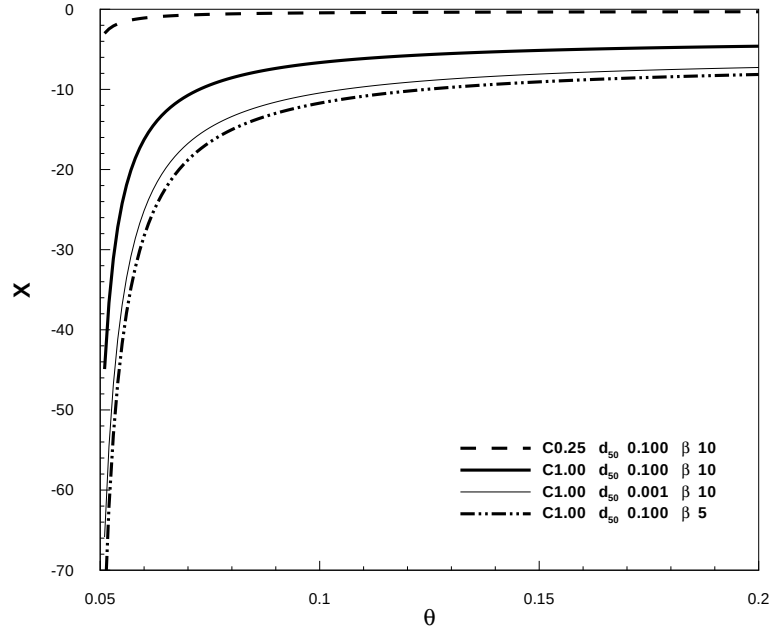

Figure D.4: Function χ.

In figure D.5 the dominant contribution for the function χ_u turns out to be given by the term χ_{u_γ} implying that the increment of the free surface slope is generated mainly by the transversal transport of momentum.

Solving in terms of the unknown R_0 the equation D.5 we obtain the local value of the free surface slope $-h_{00,\sigma}$ which would generate a solid discharge equal to the prescribed uniform flow one Φ_u. Hence, integrating the latter slopes along the entire meander we find:

$$i_f = -\frac{\lambda}{2\pi\nu_0}\int_{L=\frac{2\pi\nu_0}{\lambda}} h_{00,\sigma}d\sigma \tag{D.7}$$

where i_f represents the averaged free surface slope, obviously not dependent on λ.

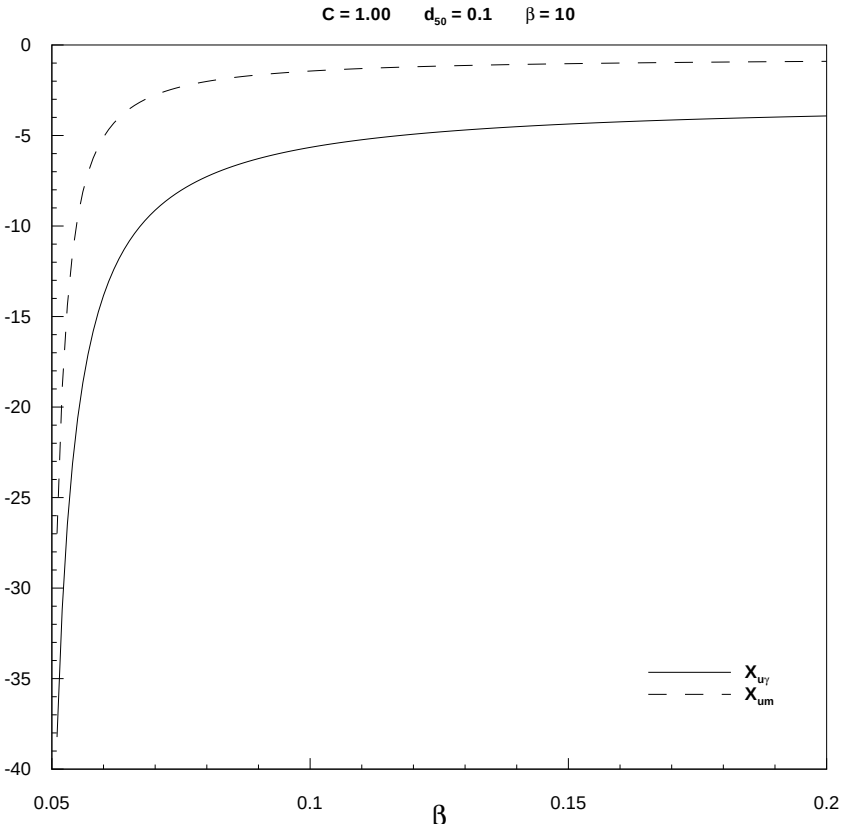

Figure D.5: Dominant effects of the transversal transport of momentum.

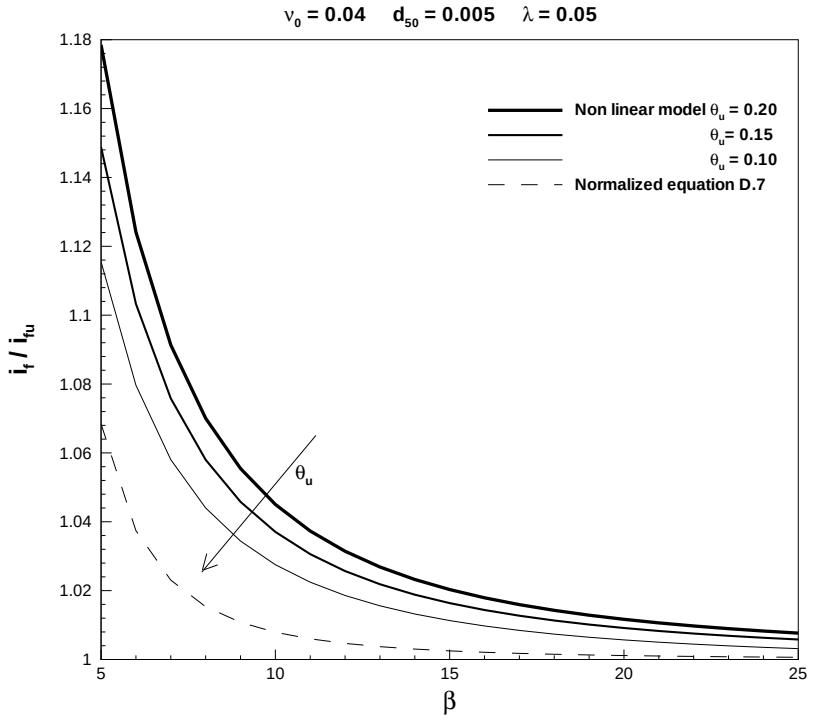

Figure D.6: Averaged meander slope i_f normalized by the uniform reference slope i_{fu}

In the figure $D.6$ the averaged free surface slope equation $D.7$, scaled by uniform flow slope, is reported and compared with the results obtained by the non linear model for different values of the shear stress parameter. The former equation does not show any appreciable changes by varying the Shields parameter, hence just one line is reported. On the contrary, the non linear plots tend to the function D.5 diminishing the value of θ_u. In fact the bed deformation, for fixed values of the parameter β, diminishes as θ_u decreases (because the mobility of the particles is reduced) getting closer to the assumption of small deformations (D.1) at the base of this simplified linear model.

Appendix E

Analytic integrals

Below we rewrite the functions f_j ($j = 0..5$) and g_j ($j = 0..8$), solutions of the ordinary differential problems (1.60, 1.92, 1.105), in a reordered and simplified way to make their numerical evaluation simpler and faster. In particular, we decompose the functions isolating terms which depend only on the normalized conventional reference level ξ_0. It's also important to note that the functions $G_j \quad [j = 1, 2]$ will be ever evaluated in the form $\mathcal{C}G_j \quad [j = 1, 2]$: in fact G_j appear ever coupled with curvature $\mathcal{C}$ in the secondary flow (1.55) and (1.98). The latter is a very important aspect from numerical point of view, avoiding numerical instability eventually due to the presence of $\mathcal{C}$ (which becomes zero at the inflection points) at denominator of equation (1.58) and (1.102).

Firstly we have to redefine the Dean's wake function $\mathcal{N}(\xi)$:

$$\mathcal{N}(\xi) = \frac{k\xi(1-\xi)}{1 + 2A\xi^2 + 3B\xi^3} = \frac{k\xi}{1 + \xi - 3B\xi^2} = k\hat{\mathcal{N}}(\xi) \tag{E.1}$$

where

$$\hat{\mathcal{N}}(\xi) = \frac{\xi}{1 + \xi - 3B\xi^2} \tag{E.2}$$

In a similar way we redefine function F_0:

$$F_0(\xi) = \frac{\sqrt{C_{fu}}}{k}\hat{F}_0 \tag{E.3}$$

where

$$\hat{F}_0(\xi) = \left[\ln\frac{\xi}{\xi_0} + A(\xi^2 - \xi_0^2) + B(\xi^3 - \xi_0^3)\right] \tag{E.4}$$

Hence, integrating once the system (1.60) for the forcing function δ_0 and using (E.1), we obtain:

$$g_{0,\xi} = \frac{\hat{N}_0}{\hat{N}} = \hat{g}_{0,\xi} \tag{E.5}$$

where $\hat{\mathcal{N}}_0 = \hat{\mathcal{N}}(\xi)|_{\xi_0}$ and $\hat{\mathcal{N}} = \hat{\mathcal{N}}(\xi)$. Furthermore integrating again (E.5) we obtain:

$$g_0 = \int_{\xi_0}^{\xi} \frac{\hat{N}_0}{\hat{N}}\, d\xi = \hat{g}_0 \tag{E.6}$$

Proceeding in a similar way with the other forcing functions δ_j $(j = 1, 2)$ of the system (1.60), after some algebra and using (E.1), (E.3), (E.5) we find:

$\boxed{g_1}$

$$\begin{aligned} g_{1,\xi} &= \tfrac{1}{k}\hat{g}_{1,\xi} + g_{0,\xi} \\ g_1 &= \tfrac{1}{k}\hat{g}_1 + g_0 \\ \hat{g}_{1,\xi} &= \tfrac{\xi-\xi_0}{\hat{N}} \\ \hat{g}_1 &= \textstyle\int \tfrac{\xi-\xi_0}{\hat{N}} \end{aligned} \tag{E.7}$$

$\boxed{g_2}$

$$\begin{aligned} g_{2,\xi} &= \tfrac{C_{fu}}{k^3}\hat{g}_{2,\xi} + g_{0,\xi} \\ g_2 &= \tfrac{C_{fu}}{k^3}\hat{g}_2 + g_0 \\ \hat{g}_{2,\xi} &= -\tfrac{1}{\hat{N}}\int \hat{F}_0^2 \\ \hat{g}_2 &= -\int\left(\tfrac{1}{\hat{N}}\int \hat{F}_0^2\right) \end{aligned} \qquad (E.8)$$

For the sake of clarity we will abbreviate the quantity $\int_{\xi_0}^{\xi} f\, d\xi$ through the notation $\int f$.

Similarly we can deal with solutions of the system (1.92):

$\boxed{f_{3,\xi}}$

$$\begin{aligned}
f_{3,\xi} &= -\tfrac{1}{k\hat{N}}\int(F_0\mathcal{C}G_1) + g_{0,\xi} \\
\int(F_0\mathcal{C}G_1) &= \mathcal{C}a_1\int(F_0 g_1) - \mathcal{C}a_1\tfrac{g_{1,\xi}}{g_{0,\xi}}|_1\int(F_0 g_0) \\
&\quad +\mathcal{C}\int(F_0 g_2) - \mathcal{C}\tfrac{g_{2,\xi}}{g_{0,\xi}}|_1\int(F_0 g_0) \\
\int(F_0 g_0) &= \tfrac{\sqrt{C_{fu}}}{k}PA_0 \\
\int(F_0 g_1) &= \tfrac{\sqrt{C_{fu}}}{k^2}PA_1 + \tfrac{\sqrt{C_{fu}}}{k}PA_0 \\
\int(F_0 g_2) &= \tfrac{C_{fu}\sqrt{C_{fu}}}{k^4}PA_2 + \tfrac{\sqrt{C_{fu}}}{k}PA_0
\end{aligned} \tag{E.9}$$

$\boxed{f_3}$

$$\begin{aligned}
f_3 &= g_0 + \tfrac{1}{k\hat{N}_0}\int(F_0\mathcal{C}G_1 g_0) - \tfrac{g_0}{k\hat{N}_0}\int(F_0\mathcal{C}G_1) \\
\int(F_0\mathcal{C}G_1 g_0) &= \mathcal{C}a_1\int(F_0 g_1 g_0) - \mathcal{C}a_1\tfrac{g_{1,\xi}}{g_{0,\xi}}|_1\int(F_0 g_0 g_0) \\
&\quad +\mathcal{C}\int(F_0 g_2 g_0) - \mathcal{C}\tfrac{g_{2,\xi}}{g_{0,\xi}}|_1\int(F_0 g_0 g_0) \\
\int(F_0 g_0 g_0) &= \tfrac{\sqrt{C_{fu}}}{k}PG_0 \\
\int(F_0 g_0 g_1) &= \tfrac{\sqrt{C_{fu}}}{k^2}PG_1 + \tfrac{\sqrt{C_{fu}}}{k}PG_0 \\
\int(F_0 g_0 g_2) &= \tfrac{C_{fu}\sqrt{C_{fu}}}{k^4}PG_2 + \tfrac{\sqrt{C_{fu}}}{k}PG_0
\end{aligned} \tag{E.9}$$

$\boxed{\int f_3}$

$$
\begin{aligned}
\int f_3 &= \int g_0 + \tfrac{1}{k\hat{N}_0} \int\int (F_0 \mathcal{C} G_1 g_0) - \tfrac{1}{k\hat{N}_0} \int (g_0 \int (F_0 \mathcal{C} G_1)) \\
\int\int (F_0 \mathcal{C} G_1 g_0) &= \mathcal{C} a_1 \tfrac{\sqrt{C_{fu}}}{k^2} IPG_1 + \mathcal{C} \tfrac{C_{fu}\sqrt{C_{fu}}}{k^4} IPG_2 \\
&\quad + IPG_0 \; d_1 \\
\int (g_0 \int (F_0 \mathcal{C} G_1)) &= \mathcal{C} a_1 \tfrac{\sqrt{C_{fu}}}{k^2} BPA_1 + \mathcal{C} \tfrac{C_{fu}\sqrt{C_{fu}}}{k^4} BPA_2 \\
&\quad + BPA_0 \; d_1 \\
d_1 &= \mathcal{C} a_1 \tfrac{\sqrt{C_{fu}}}{k} (1 - \tfrac{g_{1,\xi}}{g_{0,\xi}}|_1) + \mathcal{C} \tfrac{\sqrt{C_{fu}}}{k} (1 - \tfrac{g_{2,\xi}}{g_{0,\xi}}|_1)
\end{aligned}
\tag{E.9}
$$

$\boxed{f_{4,\xi}}$

$$\begin{aligned} f_{4,\xi} &= \tfrac{1}{k\hat{N}} F_0 \int F_0 + g_{2,\xi} \\ F_0 \int F_0 &= \tfrac{C_{fu}}{k^2} P H_0 \\ P H_0 &= \hat{F}_0 \int \hat{F}_0 \end{aligned} \tag{E.10}$$

$\boxed{f_4}$

$$\begin{aligned} f_4 &= g_2 + \int (\tfrac{F_0}{N} \int F_0) \\ \int (\tfrac{F_0}{N} \int F_0) &= \tfrac{C_{fu}}{k^3} P F_0 \end{aligned} \tag{E.11}$$

$\boxed{\int f_4}$

$$\int f_4 = \int g_2 + \tfrac{C_{fu}}{k^3} I P F_0 \tag{E.12}$$

$\boxed{f_{5,\xi}}$

$$
\begin{aligned}
f_{5,\xi} &= f_{3,\xi} + \tfrac{1}{k\hat{N}} F_0 \textstyle\int(\mathcal{C}G_1) \\
F_0 \textstyle\int(\mathcal{C}G_1) &= \mathcal{C}a_1 F_0 \textstyle\int g_1 - \mathcal{C}a_1 \tfrac{g_{1,\xi}}{g_{0,\xi}}|_1 F_0 \textstyle\int g_0 \\
&\quad + \mathcal{C}F_0 \textstyle\int g_2 - \mathcal{C}\tfrac{g_{2,\xi}}{g_{0,\xi}}|_1 F_0 \textstyle\int g_0 \\
F_0 \textstyle\int g_0 &= \tfrac{\sqrt{C_{fu}}}{k} PI_0 \\
F_0 \textstyle\int g_1 &= \tfrac{\sqrt{C_{fu}}}{k^2} PI_1 + \tfrac{\sqrt{C_{fu}}}{k} PI_0 \\
F_0 \textstyle\int g_2 &= \tfrac{C_{fu}\sqrt{C_{fu}}}{k^4} PI_2 + \tfrac{\sqrt{C_{fu}}}{k} PI_0
\end{aligned}
\qquad (E.13)
$$

$\boxed{f_5}$

$$
\begin{aligned}
f_5 &= f_3 + \textstyle\int(\tfrac{F_0}{N} \textstyle\int(\mathcal{C}G_1)) \\
\textstyle\int(\tfrac{F_0}{N} \textstyle\int(\mathcal{C}G_1)) &= \mathcal{C}a_1 \textstyle\int(\tfrac{F_0}{N} \textstyle\int g_1) - \mathcal{C}a_1 \tfrac{g_{1,\xi}}{g_{0,\xi}}|_1 \textstyle\int(\tfrac{F_0}{N} \textstyle\int g_0) \\
&\quad + \mathcal{C} \textstyle\int(\tfrac{F_0}{N} \textstyle\int g_2) - \mathcal{C}\tfrac{g_{2,\xi}}{g_{0,\xi}}|_1 \textstyle\int(\tfrac{F_0}{N} \textstyle\int g_0) \\
\textstyle\int(\tfrac{F_0}{N} \textstyle\int g_0) &= \tfrac{\sqrt{C_{fu}}}{k^2} PN_0 \\
\textstyle\int(\tfrac{F_0}{N} \textstyle\int g_1) &= \tfrac{\sqrt{C_{fu}}}{k^3} PN_1 + \tfrac{\sqrt{C_{fu}}}{k^2} PN_0 \\
\textstyle\int(\tfrac{F_0}{N} \textstyle\int g_2) &= \tfrac{C_{fu}\sqrt{C_{fu}}}{k^5} PN_2 + \tfrac{\sqrt{C_{fu}}}{k^2} PN_0
\end{aligned}
\qquad (E.14)
$$

$\boxed{\int f_5}$

$$\begin{aligned}
\int f_5 &= \int f_3 + \int\int(\tfrac{F_0}{N}\int(\mathcal{C}G_1)) \\
\int\int(\tfrac{F_0}{N}\int(\mathcal{C}G_1)) &= \mathcal{C}a_1\tfrac{\sqrt{C_{fu}}}{k^3}IPN_1 + \mathcal{C}\tfrac{C_{fu}\sqrt{C_{fu}}}{k^5}IPN_2 \\
&\quad + IPN_0\ d_2 \qquad (E.15) \\
d_2 &= \mathcal{C}a_1\tfrac{\sqrt{C_{fu}}}{k^2}(1 - \tfrac{g_{1,\xi}}{g_{0,\xi}}|_1) + \mathcal{C}\tfrac{\sqrt{C_{fu}}}{k^2}(1 - \tfrac{g_{2,\xi}}{g_{0,\xi}}|_1)
\end{aligned}$$

Hence we can deal with solutions of the system (1.105):

$\boxed{g_{3,\xi}}$

$$
\begin{aligned}
g_{3,\xi} &= g_{0,\xi} + \tfrac{1}{k\hat{N}} \int (F_0 F_1) \\
\int (F_0 F_1) &= R_1 \int (F_0 f_1) - \tfrac{1}{2} R_2 \int (F_0 f_2) - \tfrac{1}{2} R_3 \int (F_0 f_3) \\
&\quad - \tfrac{3}{2} R_2 \int (F_0 f_4) - \tfrac{5}{2} R_3 \int (F_0 f_5) - k_1 \int (F_0 f_0) \\
k_1 &= R_1 \tfrac{f_{1,\xi}}{f_{0,\xi}}|_1 - \tfrac{1}{2} R_2 \tfrac{f_{2,\xi}}{f_{0,\xi}}|_1 - \tfrac{1}{2} R_3 \tfrac{f_{3,\xi}}{f_{0,\xi}}|_1 \\
&\quad - \tfrac{3}{2} R_2 \tfrac{f_{4,\xi}}{f_{0,\xi}}|_1 - \tfrac{5}{2} R_3 \tfrac{f_{5,\xi}}{f_{0,\xi}}|_1 \\
\int (F_0 f_3) &= \tfrac{\sqrt{C_{fu}}}{k} P A_0 + \tfrac{1}{k\mathcal{N}_0} \int (F_0 \int (F_0 \mathcal{C} G_1 g_0)) \\
&\quad - \tfrac{1}{k\mathcal{N}_0} \int (F_0 g_0 \int (F_0 \mathcal{C} G_1)) \\
\int (F_0 \int (F_0 \mathcal{C} G_1 g_0)) &= \mathcal{C} a_1 \tfrac{C_{fu}}{k^3} A P G_1 + \mathcal{C} \tfrac{C_{fu}^2}{k^5} A P G_2 \\
&\quad + A P G_0 \; d_3 \\
d_3 &= \mathcal{C} a_1 \tfrac{C_{fu}}{k^2} (1 - \tfrac{g_{1,\xi}}{g_{0,\xi}}|_1) + \mathcal{C} \tfrac{C_{fu}}{k^2} (1 - \tfrac{g_{2,\xi}}{g_{0,\xi}}|_1) \\
\int (F_0 g_0 \int (F_0 \mathcal{C} G_1)) &= \mathcal{C} a_1 \tfrac{C_{fu}}{k^3} A P A_1 + \mathcal{C} \tfrac{C_{fu}^2}{k^5} A P A_2 \\
&\quad + A P A_0 \; d_3
\end{aligned}
$$

$\boxed{g_{3,\xi}}$

$$
\begin{aligned}
\int(F_0 f_4) &= \tfrac{\sqrt{C_{fu}}}{k} PA_0 + \tfrac{C_{fu}\sqrt{C_{fu}}}{k^4}(PA_2 + APF_0) \\
\int(F_0 f_5) &= \int(F_0 f_3) + \int(F_0 \int(\tfrac{F_0}{N} \int(\mathcal{C} G_1))) \\
\int(F_0 \int(\tfrac{F_0}{N} \int(\mathcal{C} G_1))) &= \mathcal{C} a_1 \tfrac{C_{fu}}{k^4} APN_1 + \mathcal{C} \tfrac{C_{fu}^2}{k^6} APN_2 \\
&\quad + APN_0 \; d_4 \\
d_4 &= \mathcal{C} a_1 \tfrac{C_{fu}}{k^3}(1 - \tfrac{g_{1,\xi}}{g_{0,\xi}}|_1) + \mathcal{C} \tfrac{C_{fu}}{k^3}(1 - \tfrac{g_{2,\xi}}{g_{0,\xi}}|_1)
\end{aligned}
\qquad (E.16)
$$

$\boxed{g_3}$

$$
\begin{aligned}
g_3 &= g_0 + \tfrac{g_0}{k\hat{N}_0}\int(F_0F_1) - \tfrac{1}{k\hat{N}_0}\int(F_0F_1g_0) \\
\int(F_0F_1g_0) &= R_1\int(F_0f_1g_0) - \tfrac{1}{2}R_2\int(F_0f_2g_0) - \tfrac{1}{2}R_3\int(F_0f_3g_0) \\
&\quad -\tfrac{3}{2}R_2\int(F_0f_4g_0) - \tfrac{5}{2}R_3\int(F_0f_5g_0) - k_1\int(F_0f_0g_0) \\
\int(F_0f_3g_0) &= \tfrac{\sqrt{C_{fu}}}{k}PG_0 + \tfrac{1}{k\hat{N}_0}\int(F_0g_0\int(F_0\mathcal{C}G_1g_0)) \\
&\quad -\tfrac{1}{k\hat{N}_0}\int(F_0g_0g_0\int(F_0\mathcal{C}G_1)) \\
\int(F_0g_0\int(F_0\mathcal{C}G_1g_0)) &= \mathcal{C}a_1\tfrac{C_{fu}}{k^3}BPG_1 + \mathcal{C}\tfrac{C_{fu}^2}{k^5}BPG_2 \\
&\quad +BPG_0\ d_3 \\
\int(F_0g_0g_0\int(F_0\mathcal{C}G_1)) &= \mathcal{C}a_1\tfrac{C_{fu}}{k^3}CPA_1 + \mathcal{C}\tfrac{C_{fu}^2}{k^5}CPA_2 \\
&\quad +CPA_0\ d_3 \\
\int(F_0f_4g_0) &= \tfrac{\sqrt{C_{fu}}}{k}PG_0 + \tfrac{C_{fu}\sqrt{C_{fu}}}{k^4}(PG_2 + KF_0) \\
\int(F_0f_5g_0) &= \int(F_0f_3g_0) + \int(F_0g_0\int(\tfrac{F_0}{N}\int(\mathcal{C}G_1))) \\
\int(F_0g_0\int(\tfrac{F_0}{N}\int(\mathcal{C}G_1))) &= \mathcal{C}a_1\tfrac{C_{fu}}{k^4}BPN_1 + \mathcal{C}\tfrac{C_{fu}^2}{k^6}BPN_2 \\
&\quad +BPN_0\ d_4
\end{aligned}
\tag{E.17}
$$

$\boxed{\int g_3}$

$$
\begin{aligned}
\int g_3 &= \int g_0 + \tfrac{1}{k\hat{N}_0}\int(g_0\int(F_0F_1)) - \tfrac{1}{k\hat{N}_0}\int\int(F_0F_1g_0)\\
\int(g_0\int(F_0F_1)) &= R_1\int(g_0\int(F_0f_1)) - \tfrac{1}{2}R_2\int(g_0\int(F_0f_2))\\
&\quad -\tfrac{1}{2}R_3\int(g_0\int(F_0f_3))\\
&\quad -\tfrac{3}{2}R_2\int(g_0\int(F_0f_4)) - \tfrac{5}{2}R_3\int(g_0\int(F_0f_5))\\
&\quad -k_1\int(g_0\int(F_0f_0))\\
\int(g_0\int(F_0f_0)) &= \tfrac{\sqrt{C_{fu}}}{k}BPA_0\\
\int(g_0\int(F_0f_1)) &= \tfrac{\sqrt{C_{fu}}}{k^2}BPA_1 + \tfrac{\sqrt{C_{fu}}}{k}BPA_0\\
\int(g_0\int(F_0f_2)) &= \tfrac{C_{fu}\sqrt{C_{fu}}}{k^4}BPA_2 + \tfrac{\sqrt{C_{fu}}}{k}BPA_0\\
\int(g_0\int(F_0f_3)) &= \tfrac{\sqrt{C_{fu}}}{k}BPA_0 + \tfrac{\mathcal{C}a_1C_{fu}}{k^4\mathcal{N}_0}(AAPG_1 - AAPA_1)\\
&\quad +\tfrac{\mathcal{C}C_{fu}^2}{k^6\mathcal{N}_0}(AAPG_2 - AAPA_2)\\
&\quad +\tfrac{d_3}{k\mathcal{N}_0}(AAPG_0 - AAPA_0)\\
\int(g_0\int(F_0f_4)) &= \tfrac{\sqrt{C_{fu}}}{k}BPA_0 + \tfrac{C_{fu}\sqrt{C_{fu}}}{k^4}(BPA_2 - AAPF_0)
\end{aligned}
$$

$\boxed{\int g_3}$

$$\begin{aligned}
\int(g_0\int(F_0f_5)) &= \int(g_0\int(F_0f_4)) + \tfrac{\mathcal{C}a_1C_{fu}}{k^4}AAPN_1 + \tfrac{\mathcal{C}C_{fu}^2}{k^6}AAPN_2 \\
&\quad + d_4AAPN_0 \\
\int\int(F_0F_1g_0) &= R_1\int\int(F_0f_1g_0) - \tfrac{1}{2}R_2\int\int(F_0f_2g_0) - \tfrac{1}{2}R_3\int\int(F_0f_3g_0) \\
&\quad - \tfrac{3}{2}R_2\int\int(F_0f_4g_0) - \tfrac{5}{2}R_3\int\int(F_0f_5g_0) - k_1\int\int(F_0f_0g_0) \\
\int\int(F_0f_0g_0) &= \tfrac{\sqrt{C_{fu}}}{k}IPG_0 \\
\int\int(F_0f_1g_0) &= \tfrac{\sqrt{C_{fu}}}{k^2}IPG_1 + \tfrac{\sqrt{C_{fu}}}{k}IPG_0 \\
\int\int(F_0f_2g_0) &= \tfrac{C_{fu}\sqrt{C_{fu}}}{k^4}IPG_2 + \tfrac{\sqrt{C_{fu}}}{k}IPG_0 \\
\int\int(F_0f_3g_0) &= \tfrac{\sqrt{C_{fu}}}{k}IPG_0 + \tfrac{1}{k\hat{N}_0}\int\int(F_0g_0\int(F_0\mathcal{C}G_1g_0)) \\
&\quad - \tfrac{1}{k\hat{N}_0}\int\int(F_0g_0g_0\int(F_0\mathcal{C}G_1))
\end{aligned}$$

$\boxed{\int g_3}$

$$\begin{aligned}
\int\int(F_0 g_0 \int(F_0 \mathcal{C} G_1 g_0)) &= \mathcal{C}a_1 \tfrac{C_{fu}}{k^3} IBPG_1 + \mathcal{C}\tfrac{C_{fu}^2}{k^5} IBPG_2 \\
&\quad + IBPG_0 d_3 \\
\int\int(F_0 g_0 g_0 \int(F_0 \mathcal{C} G_1)) &= \mathcal{C}a_1 \tfrac{C_{fu}}{k^3} ICPA_1 + \mathcal{C}\tfrac{C_{fu}^2}{k^5} ICPA_2 \\
&\quad + ICPA_0 d_3 \\
\int\int(F_0 f_4 g_0) &= \tfrac{\sqrt{C_{fu}}}{k} IPG_0 + \tfrac{C_{fu}\sqrt{C_{fu}}}{k^4}(IPG_2 + IBPF_0) \\
\int\int(F_0 f_5 g_0) &= \int\int(F_0 f_3 g_0) + \mathcal{C}a_1 \tfrac{C_{fu}}{k^4} IPN_1 + \mathcal{C}\tfrac{C_{fu}^2}{k^6} IPN_2 \\
&\quad + IBPN_0 d_4
\end{aligned} \tag{E.18}$$

$\boxed{g_{5,\xi}}$

$$
\begin{aligned}
g_{5,\xi} &= g_{0,\xi} - \tfrac{1}{k\hat{N}} \int (\mathcal{C}G_1)^2 \\
\int (\mathcal{C}G_1)^2 &= C^2 a_1^2 \int g_1^2 + C^2 \int g_2^2 + m^2 \int g_0^2 - 2Ca_1 m \int (g_0 g_1) \\
&\quad -2Cm \int (g_0 g_2) + 2C^2 a_1 \int (g_1 g_2) \\
m &= \mathcal{C}a_1 \tfrac{g_{1,\xi}}{g_{0,\xi}}|_1 + \mathcal{C}\tfrac{g_{2,\xi}}{g_{0,\xi}}|_1 \\
\int g_1 &= \tfrac{1}{k} \int \hat{g}_1 + \int g_0 \\
\int g_2 &= \tfrac{C_{fu}}{k^3} \int \hat{g}_2 + \int g_0 \\
\int g_1^2 &= \tfrac{1}{k^2} PJ_{11} + PJ_{00} + \tfrac{2}{k} PJ_{10} \\
\int g_2^2 &= \tfrac{C_{fu}^2}{k^6} PJ_{22} + PJ_{00} + 2\tfrac{C_{fu}}{k^3} PJ_{20} \\
\int (g_0 g_1) &= \tfrac{1}{k} PJ_{10} + PJ_{00} \\
\int (g_0 g_2) &= \tfrac{C_{fu}}{k^3} PJ_{20} + PJ_{00} \\
\int (g_1 g_2) &= \tfrac{C_{fu}}{k^4} PJ_{12} + \tfrac{1}{k} PJ_{10} + \tfrac{C_{fu}}{k^3} PJ_{20} + PJ_{00}
\end{aligned}
\qquad (E.19)
$$

$\boxed{g_5}$

$$
\begin{aligned}
g_5 &= g_0 - \tfrac{g_0}{k\hat{N}_0}\int(\mathcal{C}G_1)^2 + \tfrac{1}{k\hat{N}_0}\int(\mathcal{C}^2G_1^2g_0) \\
\int(\mathcal{C}^2G_1^2g_0) &= C^2a_1^2\int(g_1^2g_0) + C^2\int(g_2^2g_0) + m^2\int g_0^3 - 2Ca_1m\int(g_0^2g_1) \\
&\quad -2Cm\int(g_0^2g_2) + 2C^2a_1\int(g_0g_1g_2) \\
\int(g_1^2g_0) &= \tfrac{1}{k^2}PB_{11} + PB_{00} + \tfrac{2}{k}PB_{10} \\
\int(g_2^2g_0) &= \tfrac{C_{fu}^2}{k^6}PB_{22} + PB_{00} + 2\tfrac{C_{fu}}{k^3}PB_{20} \\
\int(g_0^3) &= PB_{00} \\
\int(g_0^2g_1) &= \tfrac{1}{k}PB_{10} + PB_{00} \\
\int(g_0^2g_2) &= \tfrac{C_{fu}}{k^3}PB_{20} + PB_{00} \\
\int(g_0g_1g_2) &= \tfrac{C_{fu}}{k^4}PB_{12} + \tfrac{1}{k}PB_{10} + \tfrac{C_{fu}}{k^3}PB_{20} + PB_{00}
\end{aligned}
\tag{E.20}
$$

$\boxed{\int g_5}$

$$
\begin{aligned}
\int g_5 &= \int g_0 - \tfrac{1}{k\hat{N}_0}\int(g_0\int(\mathcal{C}G_1)^2) + \tfrac{1}{k\hat{N}_0}\int\int(\mathcal{C}^2G_1^2g_0)\\
\int(g_0\int(\mathcal{C}G_1)^2) &= C^2a_1^2\int(g_0\int g_1^2) + C^2\int(g_0\int g_2^2) + m^2\int(g_0\int g_0^2)\\
&\quad -2Ca_1m\int(g_0\int(g_0g_1)) - 2Cm\int(g_0\int(g_0g_2))\\
&\quad +2C^2a_1\int(g_0\int(g_1g_2))\\
\int(g_0\int g_1^2) &= \tfrac{1}{k^2}APJ_{11} + APJ_{00} + \tfrac{2}{k}APJ_{10}\\
\int(g_0\int g_2^2) &= \tfrac{C_{fu}^2}{k^6}APJ_{22} + APJ_{00} + 2\tfrac{C_{fu}}{k^3}APJ_{20}\\
\int(g_0\int(g_0g_1)) &= \tfrac{1}{k}APJ_{10} + APJ_{00}\\
\int(g_0\int(g_0g_2)) &= \tfrac{C_{fu}}{k^3}APJ_{20} + APJ_{00}\\
\int(g_0\int(g_1g_2)) &= \tfrac{C_{fu}}{k^4}APJ_{12} + \tfrac{1}{k}APJ_{10} + \tfrac{C_{fu}}{k^3}APJ_{20} + APJ_{00}
\end{aligned}
$$

$\boxed{\int g_5}$

$$
\begin{aligned}
\int\int(\mathcal{C}^2 G_1^2 g_0) &= C^2 a_1^2 \int\int(g_1^2 g_0) + C^2 \int\int(g_2^2 g_0) + m^2 \int\int g_0^3 \\
&\quad -2Ca_1 m \int\int(g_0^2 g_1) - 2Cm \int\int(g_0^2 g_2) \\
&\quad +2C^2 a_1 \int\int(g_0 g_1 g_2) \\
\int\int(g_1^2 g_0) &= \tfrac{1}{k^2} IPB_{11} + IPB_{00} + \tfrac{2}{k} IPB_{10} \\
\int\int(g_2^2 g_0) &= \tfrac{C_{fu}^2}{k^6} IPB_{22} + IPB_{00} + 2\tfrac{C_{fu}}{k^3} IPB_{20} \\
\int\int(g_0^3) &= IPB_{00} \\
\int\int(g_0^2 g_1) &= \tfrac{1}{k} IPB_{10} + IPB_{00} \\
\int\int(g_0^2 g_2) &= \tfrac{C_{fu}}{k^3} IPB_{20} + IPB_{00} \\
\int\int(g_0 g_1 g_2) &= \tfrac{C_{fu}}{k^4} IPB_{12} + \tfrac{1}{k} IPB_{10} + \tfrac{C_{fu}}{k^3} IPB_{20} + IPB_{00}
\end{aligned}
\qquad (E.21)
$$

$\boxed{g_{6,\xi}}$

$$g_{6,\xi} = g_{0,\xi} + \frac{1}{k\hat{N}}\mathcal{C}G_1 \int F_0 - \frac{1}{k\hat{N}} \int (F_0 \mathcal{C} G_1) \tag{E.22}$$

$\boxed{g_6}$

$$\begin{aligned} g_6 &= g_4 + \int (\tfrac{\mathcal{C}G_1}{N} \int F_0) \\ \int (\tfrac{\mathcal{C}G_1}{N} \int F_0) &= +\mathcal{C}a_1 \tfrac{\sqrt{C_{fu}}}{k^3} PD_1 + \mathcal{C} \tfrac{C_{fu}\sqrt{C_{fu}}}{k^5} PD_2 \\ &\quad + PD_0 \; d_2 \end{aligned} \tag{E.23}$$

$\boxed{\int g_6}$

$$\begin{aligned} \int g_6 &= \int g_4 + \int \int (\tfrac{\mathcal{C}G_1}{N} \int F_0) \\ \int (\tfrac{\mathcal{C}G_1}{N} \int F_0) &= +\mathcal{C}a_1 \tfrac{\sqrt{C_{fu}}}{k^3} IPD_1 + \mathcal{C} \tfrac{C_{fu}\sqrt{C_{fu}}}{k^5} IPD_2 \\ &\quad + IPD_0 \; d_2 \end{aligned} \tag{E.24}$$

$\boxed{g_{7,\xi}}$

$$g_{7,\xi} = g_{0,\xi} + \frac{1}{k\hat{N}}\mathcal{C}G_1 \int(\mathcal{C}G_1) - \frac{1}{k\hat{N}} \int(\mathcal{C}G_1)^2 \qquad (E.25)$$

$\boxed{g_7}$

$$
\begin{aligned}
g_7 &= g_5 + \int(\tfrac{\mathcal{C}G_1}{N}\int(\mathcal{C}G_1)) \\
\int(\tfrac{\mathcal{C}G_1}{N}\int(\mathcal{C}G_1)) &= +\alpha_1[\tfrac{1}{k}PZ_{00}] \\
&\quad +\alpha_2[\tfrac{1}{k^2}(PZ_{01}+PZ_{10})+\tfrac{2}{k}PZ_{00}] \\
&\quad +\alpha_3[\tfrac{C_{fu}}{k^4}(PZ_{02}+PZ_{20})+\tfrac{2}{k}PZ_{00}] \\
&\quad +\alpha_4[\tfrac{1}{k^3}PZ_{11}+\tfrac{1}{k^2}(PZ_{01}+PZ_{10})+\tfrac{1}{k}PZ_{00}] \\
&\quad +\alpha_5[\tfrac{C_{fu}}{k^5}(PZ_{21}+PZ_{12})+\tfrac{C_{fu}}{k^4}(PZ_{02}+PZ_{20}) \\
&\quad +\tfrac{1}{k^2}(PZ_{01}+PZ_{10})+\tfrac{2}{k}PZ_{00}] \\
&\quad +\alpha_6[\tfrac{C_{fu}^2}{k^7}PZ_{22}+\tfrac{C_{fu}}{k^4}(PZ_{02}+PZ_{20})+\tfrac{1}{k}PZ_{00}
\end{aligned}
\tag{E.26}
$$

$$
\begin{aligned}
\alpha 1 &= m^2 \\
\alpha 2 &= -\mathcal{C}a_1 m \\
\alpha 3 &= -\mathcal{C}m \\
\alpha 4 &= (\mathcal{C}a_1)^2 \\
\alpha 5 &= \mathcal{C}^2 a_1 \\
\alpha 6 &= \mathcal{C}^2
\end{aligned}
$$

$\boxed{\int g_7}$

$$
\begin{aligned}
\int g_7 &= \int g_5 + \int\int (\tfrac{\mathcal{C}G_1}{N} \int (\mathcal{C}G_1)) \\
\int\int (\tfrac{\mathcal{C}G_1}{N} \int (\mathcal{C}G_1)) &= +\alpha_1 [\tfrac{1}{k} IPZ_{00}] \\
&\quad +\alpha_2 [\tfrac{1}{k^2} (IPZ_{01} + IPZ_{10}) + \tfrac{2}{k} IPZ_{00}] \\
&\quad +\alpha_3 [\tfrac{C_{fu}}{k^4} (IPZ_{02} + IPZ_{20}) + \tfrac{2}{k} IPZ_{00}] \\
&\quad +\alpha_4 [\tfrac{1}{k^3} IPZ_{11} + \tfrac{1}{k^2} (IPZ_{01} + IPZ_{10}) + \tfrac{1}{k} IPZ_{00}] \\
&\quad +\alpha_5 [\tfrac{C_{fu}}{k^5} (IPZ_{21} + IPZ_{12}) + \tfrac{C_{fu}}{k^4} (IPZ_{02} + IPZ_{20}) \\
&\quad +\tfrac{1}{k^2} (IPZ_{01} + IPZ_{10}) + \tfrac{2}{k} IPZ_{00}] \\
&\quad +\alpha_6 [\tfrac{C_{fu}^2}{k^7} IPZ_{22} + \tfrac{C_{fu}}{k^4} (IPZ_{02} + IPZ_{20}) + \tfrac{1}{k} IPZ_{00}
\end{aligned}
\tag{E.27}
$$

Finally all the functions f_j, g_j, their derivatives and integrals are decomposed into simpler parts which depend only on ξ_0 and which are simple to evaluate in an analytical form:

$$
\begin{aligned}
PA_j &= \int(\hat{F}_0\hat{g}_j) && [j=0..2]\\
PF_0 &= \int(\tfrac{\hat{F}_0}{\hat{N}}\int\hat{F}_0)\\
PG_j &= \int(\hat{F}_0\hat{g}_0\hat{g}_j) && [j=0..2]\\
PH_0 &= \hat{F}_0\int\hat{F}_0\\
PI_j &= \hat{F}_0\int\hat{g}_j && [j=0..2]\\
PJ_{ij} &= \int(\hat{g}_i\hat{g}_j) && [i,j=0..2]\\
PN_j &= \int(\tfrac{\hat{F}_0}{\hat{N}}\int\hat{g}_j) && [j=0..2]\\
APA_j &= \int(\hat{F}_0 g_0 PA_j) && [j=0..2]\\
APF_0 &= \int(\hat{F}_0 PF_0)\\
APG_j &= \int(\hat{F}_0 PG_j) && [j=0..2]\\
APN_j &= \int(\hat{F}_0 PN_j) && [j=0..2]\\
BPA_j &= \int(g_0 PA_j) && [j=0..2]\\
BPG_j &= \int(\hat{F}_0 g_0 PG_j) && [j=0..2]
\end{aligned}
$$

$$
\begin{aligned}
CPA_j &= \int(\hat{F}_0 g_0^2 PA_j) \quad [j = 0..2] \\
BPF_0 &= \int(\hat{F}_0 g_0 PF_0) \\
BPN_j &= \int(\hat{F}_0 g_0 PN_j) \quad [j = 0..2] \\
IPG_j &= \int PG_j \quad [j = 0..2] \\
IPF_0 &= \int PF_0 \\
IPN_j &= \int PN_j \quad [j = 0..2] \\
IBPG_j &= \int BPG_j \quad [j = 0..2] \\
ICPA_j &= \int CPA_j \quad [j = 0..2] \\
IBPF_0 &= \int BPF_0 \\
IBPN_j &= \int BPN_j \quad [j = 0..2] \\
AAPG_j &= \int(g_0 APG_j) \quad [j = 0..2] \\
AAPA_j &= \int(g_0 APA_j) \quad [j = 0..2] \\
AAPN_j &= \int(g_0 APN_j) \quad [j = 0..2] \\
AAPF_0 &= \int(g_0 APF_0) \\
APJ_{ij} &= \int(g_0 PJ_{ij}) \quad [i, j = 0..2] \\
PB_{ij} &= \int(g_0 \hat{g}_i \hat{g}_j) \quad [i, j = 0..2] \\
IPB_{ij} &= \int PB_{ij} \quad [i, j = 0..2]
\end{aligned}
$$

$$
\begin{aligned}
PD_j &= \int(\tfrac{\hat{g}_j}{\hat{N}} \int \hat{F}_0) \quad [j = 0..2] \\
IPD_j &= \int PD_j \qquad [j = 0..2] \\
PZ_{ij} &= \int(\tfrac{\hat{g}_i}{\hat{N}} \int \hat{g}_j) \quad [i, j = 0..2] \\
IPZ_{ij} &= \int PZ_{ij} \qquad [i, j = 0..2]
\end{aligned}
$$

Taking advantage of previous relations we proceed to simplify further the terms $\frac{F_{1j,\xi}}{F_{0,\xi}}|_{\xi_0}$ $(j = 1..5)$ in the evaluation of function $\frac{u_{1,\xi}}{u_{0,\xi}}|_{\xi_0}$ (1.95).

Firstly, integrating once the system (1.51), we obtain an useful relationship for $F_{0,\xi}$:

$$F_{0,\xi} = \frac{\sqrt{C_{fu}\,(1-\xi)}}{N} \tag{E.29}$$

Hence using (1.91), (1.92), (E.29) and (E.7) we find:

$$F_{11,\xi}|_{\xi_0} \;=\; 1 - \frac{f_{1,\xi}}{f_{0,\xi}}|_1 \;=\; \frac{\xi_0 - 1}{N_0} \tag{E.30}$$

$$\frac{F_{11,\xi}}{F_{0,\xi}}|_{\xi_0} \;=\; -\,\frac{1}{\sqrt{C_{fu}}} \tag{E.31}$$

Similarly we obtain:

$$\frac{F_{12,\xi}}{F_{0,\xi}}|_{\xi_0} \;=\; \frac{\int_{\xi_0}^1 F_0^2\; d\xi}{\sqrt{C_{fu}}\,(1-\xi_0)} \tag{E.32}$$

$$\frac{F_{13,\xi}}{F_{0,\xi}}|_{\xi_0} \;=\; \frac{\int_{\xi_0}^1 F_0 \mathcal{C} G_1\; d\xi}{\sqrt{C_{fu}}\,(1-\xi_0)} \tag{E.33}$$

$$\frac{F_{14,\xi}}{F_{0,\xi}}|_{\xi_0} \;=\; -\;\frac{F_0|_1}{\sqrt{C_{fu}}} + \frac{F_{12,\xi}|_{\xi_0}}{F_{0,\xi}|_{\xi_0}} \tag{E.34}$$

$$\frac{F_{15,\xi}}{F_{0,\xi}}|_{\xi_0} = \;-\;\frac{F_0|_1 \;\int_{\xi_0}^{1} \mathcal{C}G_1 \; d\xi}{\sqrt{C_{fu}}\,(1-\xi_0)} + \frac{F_{13,\xi}|_{\xi_0}}{F_{0,\xi}|_{\xi_0}} \tag{E.35}$$

Bibliography

Blondeaux, P. & Seminara, G. 1985 A unified bar-bend theory of river meanders. *J. Fluid Mech.* **157**, 449–470.

Camporeale, C. & Ridolfi, L. 2006 Convective nature of the planimetric instability in meandering river dynamics. *Phys. Rev. E* **73** (026311), 1–8.

Howard, A. D. & Knutson, T.R. 1984 Sufficient conditions for river meandering: A simulation approach. *Water Resour. Res.* **20** (11), 1659–1667.

Ikeda, S., Parker, G. & Sawai, K. 1981 Bend theory of river meanders. part 1. linear development. *J. Fluid Mech.* **112**, 363–377.

Imran, J. & Parker, G. 1999 A nonlinear model of flow in meandering submarine and subaerial channels. *J. Fluid Mech.* **400**, 295–331.

Jager, H.R.A. 2003 Modelling planform changes of braided rivers. PhD thesis, University of Twente.

Kevorkian, J. & Cole, J.D. 1981 *Perturbation methods in applied mathematics*. Springer.

Kovacs, A. & Parker, G. 1994 A new vectorial bedload formulation and its application to the time evolution of straight river channels. *J. Fluid Mech.* **267**, 153–183.

Langbein, W.B. & Leopold, L.B. 1966 River meanders: theory of minimum variance. *U.S. Geol. Survey* **422-H**, prof. Paper.

Mosselman, E. 1991 Modelling of river morphology with non-orthogonal horizontal curvilinear coordinates. *Communications on Hydraulic and Geotechnical Engineering* **91**, delft University of Technology, Delft, NL.

Nanson, G.C. & Hickin, E.J. 1983 Channel migration and incision on the beatton river. *J.Hydr.Engng* **109**, 327–337.

Nelson, J.M. & Smith, J.D. 1989 Evolution and stability of erodible channel beds. In *River Meandering* (ed. S. Ikeda & G. Parker), pp. 321–377. Washington, D.C.: AGU, Water Resources Monograph 12.

Parker, G. 1978*a* Self-formed straight rivers with equilibrium banks and mobile bed. part 1. the sand-silt river. *J. Fluid Mech.* **89**, 109–125.

Parker, G. 1978*b* Self-formed straight rivers with equilibrium banks and mobile bed. part 2. the gravel river. *J. Fluid Mech.* **89**, 127–146.

Parker, G. 1984 Lateral bed load transport on side slopes. *J. Hydraul. Engng. ASCE* **110(HY2)**, 197–199.

Parker, G. 1990 Surface-based bedload transport relation for gravel rivers. *J. Hydraul. Res.* **28** (4), 417–436.

Pizzuto, E.J. & Meckelnburg, J.S. 1989 Evaluation of a linear bank erosion equation. *Water Resour. Res.* **25**, 1005–1013.

Repetto, R., Tubino, M. & Paola, C. 2002 Planimetric instability of channels with variable width. *J. Fluid. Mech.* **457**, 79–109.

Romanelli, L. Rossi, Rinaldi, M., Darby, S.E., Luppi, L. & Nardi, L. 2004 Monitoring and modelling river bank processes: a new methodological approach. In *River Flow 2004* (ed. M. Greco, A. Carravetta & R. Dalla Morte), , vol. 2, pp. 993–998. A.A. Balkema.

Seminara, G. 2006 Meanders. *J. Fluid Mech.* **554**, 271–297.

Seminara, G. & Solari, L. 1998 Finite amplitude bed deformations in totally and partially transporting wide chanel bends. *Water Resour. Res.* **34** (6), 1585–1598.

Seminara, G., Solari, L. & Parker, G. 2003 Bed load at low shields stress on arbitrarily sloping beds: failure of the bagnold hypothesis. *Water Resour. Res.* **38** (11), 31–1/31–6.

Seminara, G. & Tubino, M. 1992 Weakly nonlinear theory of regular meanders. *J. Fluid Mech.* **244**, 257–288.

Shields, I. A. 1936 Anwendung der ahnlichkeitmechanik und der turbulenzforschung auf die gescheibebewegung. *Mitt. Preuss Ver.-Anst., Berlin, Germany* **26**.

Shimizu, Y. 2002 A method for simultaneous computation of bed and bank deformation of a river. In *River Flow 2002*, , vol. 2, pp. 793–801.

Sun, T., Meakin, P., T.Jøssang & K.Schwarz 1996 A simulation model for meandering rivers. *Water Resources Research* **32**, 2937–2954.

Talmon, A. M., Struiksma, N. & Mierlo, M.C.L.M. Van 1995 Laboratory measurements of the sediment transport on transverse alluvial-bed slopes. *J. Hydraul. Res.* **33**, 495–517.

Zolezzi, G. & Seminara, G. 2001 Downstream and upstream influence in river meandering. Part 1. General theory and application to overdeepening. *J. Fluid Mech.* **438**, 183–211.